E-ISSN: 2148-6247

Turkish Journal of PHARMACEUTICAL SCIENCES

An Official Journal of the Turkish Pharmacists' Association, Academy of Pharmacy

Volume: 23 Issue: 2 April 2026

www.turkjps.org

Emerging Sources Citation Index · PubMed Central · PubMed · Scopus · TR Dizin

galenos Publishing House

Turkish Journal of
PHARMACEUTICAL SCIENCES

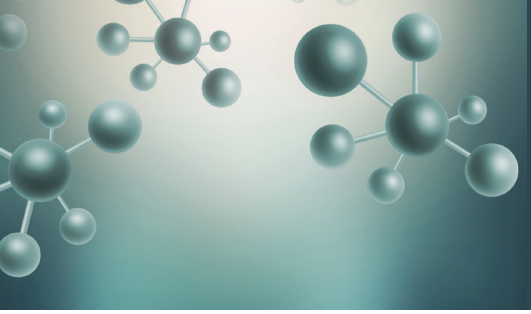

Turkish Journal of
PHARMACEUTICAL SCIENCES

Editorial Board

Turkish Journal of
PHARMACEUTICAL SCIENCES

Advisory Board

Turkish Journal of
PHARMACEUTICAL SCIENCES

Please refer to the journal's webpage (https://www.turkjps.org/) for "Editorial Policy" and "Instructions to Authors".

The editorial and publication process of the **Turkish Journal of Pharmaceutical Sciences** are shaped in accordance with the guidelines of ICMJE, WAME, CSE, COPE, EASE, and NISO. The Turkish Journal of Pharmaceutical Sciences is indexed in **PubMed, PubMed Central, Thomson Reuters / Emerging Sources Citation Index, Scopus, ULAKBİM, Türkiye Citation Index, Embase, EBSCO Host, Türk Medline, Cabi, CNKI.**

The journal is published online.

Owner: Turkish Pharmacists' Association, Academy of Pharmacy

Responsible Manager: Kutay DEMİRKAN

galenos yayınevi

Publisher Contact
Address: Molla Gürani Mah. Kaçamak Sk. No: 21/1
34093 İstanbul, Türkiye
Phone: +90 (530) 177 30 97
E-mail: info@galenos.com.tr/yayin@galenos.com.tr
Web: www.galenos.com.tr | **Publisher Certificate Number:** 14521

Publication Date: September 2026
E-ISSN: 2148-6247
International scientific journal published bimonthly.

Turkish Journal of
PHARMACEUTICAL SCIENCES

CONTENTS

Original Articles

Turk J Pharm Sci 2026;23(2):56-64
DOI: 10.4274/tjps.galenos.2026.59852

ORIGINAL ARTICLE

Antimutagenic and Antigenotoxic Effects of *Ruscus aculeatus* L. Rhizomes and Roots

Gülşah ESEN[1], Dilan TALU[2], Hananeh KORDBACHEH[3], Etil GÜZELMERİÇ[4], Muhammed HAMİTOĞLU[1], Hasan KIRMIZIBEKMEZ[4]

[1]Yeditepe University Faculty of Pharmacy, Department of Toxicology, İstanbul, Türkiye
[2]Yeditepe University Faculty of Pharmacy, İstanbul, Türkiye
[3]Eastern Mediterranean University Faculty of Pharmacy, Famagusta, Northern Cyprus
[4]Yeditepe University Faculty of Pharmacy, Department of Pharmacognosy, İstanbul, Türkiye

ABSTRACT

Objectives: *Ruscus aculeatus* L. (butcher's broom) is widely used for its medicinal virtues, mainly attributed to steroidal saponins such as ruscogenin and neoruscogenin glycosides. Despite its long-standing use, data on its genotoxicity and safety remain limited. The present study aimed to assess the potential antimutagenic and antigenotoxic effects of extracts prepared from the underground parts of *R. aculeatus*.

Materials and Methods: Ethanolic (EtOH) extract and decoction (aqueous extract) were prepared from the underground parts of *R. aculeatus*. Ames, micronucleus (MN), and comet assays were conducted to evaluate (anti)mutagenic and (anti)genotoxic effects. The quantification of ruscogenins in the acid-hydrolyzed extract was performed using high-performance liquid chromatography (HPLC) to standardise the plant material.

Results: Total ruscogenin and neoruscogenin content was calculated as 0.71% in the plant material by HPLC analyses. Neither the ethanolic nor the aqueous extract exhibited mutagenicity, while the EtOH extract showed marked antimutagenic activity at the highest concentration in the Ames test. Likewise, no genotoxicity was observed in either of the investigated extracts in the Micronucleus and Comet assays. EtOH extract exhibited antigenotoxic activity in the micronucleus assay, whereas the aqueous extract (decoction) provided no significant protection. The comet assay revealed no antigenotoxic activity for either the EtOH extract or the decoction. Overall, the underground parts of *R. aculeatus* displayed neither intrinsic mutagenicity nor genotoxicity, whereas the EtOH extract exhibited selective genoprotective effects.

Conclusion: The EtOH extract showed remarkable antimutagenic and antigenotoxic effects. This study constitutes the first report on the genoprotective and antimutagenic effects of *R. aculeatus*. From a toxicological perspective, the use of the underground parts of *R. aculeatus* is considered safe.

Keywords: Butcher's broom, ames, micronucleus, comet, HPLC

INTRODUCTION

Türkiye, located at the intersection of three continents, harbors high botanical diversity, with over 11,000 identified taxa, including 3,649 endemic species.[1,2] This richness is largely attributed to the country's diverse edaphic, geological, and topographical conditions. The genus Ruscus (Asparagaceae) is represented in Türkiye by four species, of which *Ruscus aculeatus* L., commonly known as butcher's broom, is widespread in coastal forests. It is a small evergreen shrub, reaching up to 80 cm in height and characterized by spiny cladodes and bright red fruits. Its rhizomes, functioning as underground storage organs, give rise to adventitious roots. Each year, buds located between

***Correspondence:** hkirmizibekmez@yeditepe.edu.tr, **ORCID-ID:** orcid.org/0000-0002-6118-8225

Received: 29.12.2025 **Accepted:** 27.06.2026 **Epub:** 21.07.2026 **Publication Date:** 01.09.2026

Cite this article as: Esen G, Talu D, Kordbacheh H, Güzelmeriç E, Hamitoğlu M, Kırmızıbekmez H. Antimutagenic and antigenotoxic effects of *Ruscus aculeatus* L. rhizomes and roots. Turk J Pharm Sci. 2026;23(2):56-64

the nodes and internodes on the rhizomes produce shoots that typically mature within one growing season.[3] The underground parts of *R. aculeatus* consist of rhizomes and roots, which are rich in steroidal saponins, particularly glycosides of ruscogenin and neoruscogenin.[4] In accordance with this phytochemical profile, the European Pharmacopoeia defines "Rusci rhizome" as the dried, entire or cut underground organs of *R. aculeatus* and requires that they contain not less than 1% steroidal sapogenins, calculated as the sum of ruscogenin and neoruscogenin.[5] The aerial parts of *R. aculeatus* contain saponins, flavonoids (such as apigenin, quercetin, and kaempferol derivatives), and a variety of phenolic acids, mainly p-coumaric acid.[6,7] In the berries of *R. aculeatus*, anthocyanins, especially pelargonidin derivatives, were detected.[8]

Traditionally, the rhizomes of *R. aculeatus* have been widely used in ethnomedicine across various cultures. In Türkiye, infusions of the fruits are administered orally to treat hemorrhoids, whereas decoctions of the underground parts are used to remove kidney stones and alleviate eczema.[9,10] In Palestinian folk medicine, the underground parts are applied topically to treat skin diseases.[11] In Italy, decoctions prepared from the rhizomes have traditionally been used for the management of warts and chilblains.[12] Apart from its traditional use, *R. aculeatus* has been the subject of numerous studies investigating its antioxidant, anti-inflammatory, and anticancer activities.[6] Mimaki et al.[13] investigated the cytotoxic potential of saponins isolated from the underground parts of *R. aculeatus* in human promyelocytic leukemia HL-60 cells using the MTT assay. Among the isolated compounds, a furostanol saponin bearing a diglycoside moiety acylated with a (2S,3S)-2-hydroxy-3-methylpentanoic acid and an acetyl group, as well as its corresponding spirostanol saponin, exhibited pronounced cytotoxic activity, with IC_{50} values of approximately 3.5 and 3.0 µg/mL, respectively.[13] Zhao et al.[14] showed that ruscogenin exerts anti-apoptotic effects against lipopolysaccharide-induced pulmonary endothelial apoptosis by suppressing TLR4/MyD88/NF-κB signaling, suggesting that it could be a promising therapeutic agent for acute lung injury. In addition to the pharmacological activities previously investigated, its venotonic and vasoprotective properties have attracted particular attention, leading to the development of formulations to treat chronic venous insufficiency and hemorrhoids. Phenolic compounds and spirostanol saponins isolated from a methanolic extract of the underground parts of *R. aculeatus* were evaluated for their ability to inhibit thrombin-induced hyperpermeability in human microvascular endothelial cells and were compared with the aglycone neoruscogenin. Neoruscogenin exerted a mild concentration-dependent effect, reducing hyperpermeability to 71.8% at 100 µM. The highest activities were observed at 10 µM for the spirostanol saponins deglucoruscin and ruscin, and for esculin, resulting in reductions in thrombin-induced hyperpermeability to 41.9%, 42.6%, and 53.3%, respectively. These findings support the anti-edematous and vasoprotective role of *R. aculeatus* in chronic venous disorders.[15]

Despite the widespread use of *R. aculeatus* in both traditional and contemporary medicine, there are currently no reports on its potential genoprotective properties, including antimutagenic and antigenotoxic activities. Moreover, the European Medicines Agency 2018 report on the preclinical safety of *R. aculeatus* rhizome indicates that the available data address only general aspects of safety and that the lack of genotoxicity studies prevents a comprehensive safety evaluation.[16] Therefore, this study aimed to assess the potential (anti)mutagenic and (anti) genotoxic effects of the underground parts of *R. aculeatus*, addressing a gap in the literature. In addition, the plant material investigated in this study was standardized for ruscogenin and neoruscogenin using the HPLC method described in the European Pharmacopoeia.[5]

MATERIALS AND METHODS

Chemicals and solvents

HPLC-grade acetonitrile was purchased from Merck (Darmstadt, Germany). Analytical-grade methanol, dichloromethane and n-butanol were obtained from Sigma-Aldrich (Steinheim, Germany), while ethanol (EtOH) and hydrochloric acid (37%) were supplied by IsoLab (Eschau, Germany). Potassium hydroxide was also purchased from Sigma-Aldrich (Steinheim, Germany). A standard mixture containing ruscogenin and neoruscogenin in a ratio of 3:7 (w/w) was obtained from Bionorm (İzmir, Türkiye). *Salmonella typhimurium* strains and the post-mitochondrial fraction (S9) prepared from rat liver were supplied by Moltox Molecular Toxicology, Inc. (NC, USA). 2-aminofluorene was obtained from Merck (Hohenbrunn, Germany), and nutrient broth was supplied by Hi Media Laboratories Ltd. (Mumbai, India). Histidine was provided by Fluka (USA). Ethics committee approval and patient informed consent were not required for this study.

Plant material

The underground parts (roots and rhizomes) of *R. aculeatus* were collected in November 2023 in Şile, İstanbul, Türkiye (coordinates: 41.07624° N, 29.32419° E). The plant material was identified by Prof. Dr. Hasan Kırmızıbekmez, and the herbarium specimen (YEF 23014) has been deposited in the Herbarium of the Yeditepe University Faculty of Pharmacy, Department of Pharmacognosy, İstanbul, Türkiye.

Extraction of the plant material

To prepare the ethanolic (EtOH) extract, 50 g of dried and powdered plant material was macerated in 500 mL of ethanol overnight and then extracted at 45 °C for 4 h. After filtration, the solvent was removed under reduced pressure, and the resulting residue was dispersed in distilled water and then lyophilized (yield: 10.0%).

For the decoction, 50 g of dried and coarsely powdered plant material was mixed with 500 mL of distilled water, and the mixture was gradually heated to boiling. The mixture was then simmered over low heat for 30 min, filtered while hot, and lyophilized (yield: 10.4%).

The acid-hydrolyzed extract was prepared according to the European Pharmacopoeia to liberate aglycones.[5] The powdered herbal drug (2.000 g) was mixed with a solvent mixture (75 mL)

consisting of ethanol and distilled water (4:1, v/v) and potassium hydroxide (0.2 g), then extracted under a reflux condenser for 4 h. After cooling, the mixture was filtered into a 100 mL volumetric flask. The residue was rinsed with anhydrous ethanol (3 × 10 mL), and the rinsings were combined with the filtrate. The volume was then adjusted to 100 mL with anhydrous ethanol. Subsequently, a 25 mL aliquot of this solution was transferred to a round-bottom flask and evaporated to dryness under reduced pressure. The residue was dissolved in n-butanol (10 mL), followed by the addition of hydrochloric acid (3 mL) and distilled water (8 mL). The mixture was hydrolyzed under a reflux condenser for 1 h, and then cooled and transferred to a 100 mL volumetric flask. The round-bottom flask was rinsed with methanol (3 × 20 mL); the rinsings were combined, and the final volume was adjusted to 100 mL with methanol.

Thin-layer chromatography (TLC) analysis

TLC was performed on the EtOH extract and decoction to obtain preliminary compositional information and evaluate the presence of the sapogenins ruscogenin and neoruscogenin. The standard solution containing ruscogenin and neoruscogenin at a concentration of 2 mg/mL was used as the reference solution.

The sample test and the standard solutions were first applied to a silica gel plate and developed using dichloromethane-methanol-distilled water (80:20:2, v/v/v) as a mobile phase. After development, plates were derivatized with vanillin reagent, dried at 100–105 °C for 2 minutes, and evaluated under UV (366 nm) and white light.

High-performance liquid chromatography (HPLC) analysis

The Agilent 1260 Infinity HPLC system (Darmstadt, Germany) was used for the quantitative evaluation of ruscogenin and neoruscogenin in the sample test solutions. In accordance with the European Pharmacopoeia, the chromatographic separation of ruscogenin and neoruscogenin was achieved on a reverse-phase Agilent Zorbax Extend C_{18} column (4.6 mm x 250 mm, 5-µm particle size) using mobile phases A (distilled water) and B (acetonitrile). The mobile phase gradient was programmed as follows: 60% B (0–25 min), 60–100% B (25--27 min), 100% B (27–37 min). The flow rate was set to 1.2 mL/min, the injection volume was 20 µL, and detection was performed at 203 nm. Peaks were identified by comparing the retention times (t_R) of ruscogenin and neoruscogenin obtained from HPLC chromatograms of the standard solution (0.05 mg/mL) and sample test solutions. The percentage content of total sapogenins (ruscogenin and neoruscogenin) in the sample test solution was calculated using the following equation:

$$[(A_1 \times m_2 \times 4 \times p_1) / (A_2 \times m_1)] + [(A_3 \times m_2 \times 4 \times p_2) / (A_4 \times m_1)]$$

A_1 is the area of the peak belong to ruscogenin in the sample test solution obtained with the HPLC chromatogram. A_2 is the area of the peak of ruscogenin in the reference solution. A_3 is the area of the peak belong to neoruscogenin in the sample test solution obtained with the HPLC chromatogram. A_4 is the area of the peak of neoruscogenin in the reference solution. m_1 is the mass of the herbal drug in the test solution. m_2 is the mass of the ruscogenins in reference solution. p is the percentage content of ruscogenin and neoruscogenin.

Ames mutagenicity/antimutagenicity assay

Stock solutions of the EtOH and aqueous extracts were prepared by dissolving 150 mg of each in 1.5 mL of dimethyl sulfoxide (DMSO), followed by serial dilutions to obtain final concentrations of 10, 100, 1000, and 5000 µg/plate. *Salmonella typhimurium* strains were cultured at 37 °C and 120 rpm for 12–16 h to reach 1–2 × 10^9 cells/mL.

For the Ames assay, 0.05 mL of test sample, 0.5 mL of phosphate buffer (–S9) or S9 mix (+S9), and 0.1 mL of bacterial culture were mixed with top agar containing histidine–biotin (0.05 mM) and poured onto MGA plates. Plates were incubated at 37 °C for 48 h, after which the revertant colonies were counted and compared with controls. Antimutagenicity was evaluated by co-treating samples with standard mutagens in the presence or absence of S9 and was expressed as the percentage inhibition of revertant formation.[17]

Genotoxicity/antigenotoxicity assays

Cell culture and sample preparation

CHO cells (ATCC; CCL61) were cultured at 37 °C with 5% CO_2. The extract stock solutions (200 mg/mL in DMSO) were diluted in medium to final concentrations of 10, 50, 100, and 200 µg/mL.

Dose selection

Cytotoxicity was determined by MTT assay after a 24 h exposure, followed by a 3 h MTT incubation. Formazan crystals were solubilized in isopropanol and the absorbance was measured to calculate cell viability.

Micronucleus (MN) assay

The MN assay was carried out in an accredited laboratory (TÜRKAK TS EN ISO/IEC 17025, No: AB-1764-T) following the procedure described by Helvacioglu et al.[18] CHO-K1 cells (2 × 10^9 cells/well) were seeded in 6-well plates and treated with the extracts for 24 h. DMSO (0.5%) and EMS (6 mM) served as the negative and positive controls, respectively. After exposure, cells were incubated with cytochalasin B (2.4 µg/mL), then subjected to hypotonic treatment in 0.07 M KCl, fixed with methanol:acetic acid (3:1), and stained with 5% Giemsa solution. A total of 1,000 binucleated cells per group were analyzed microscopically (Zeiss Primo Star, 40×). MN frequency (MN%) and nuclear division index were determined using established formulas.[18]

Comet assay

CHO-K1 cells (3 × 10^9 cells/well) were seeded into 6-well plates, pre-incubated for 24 h, and then exposed to different extract concentrations. DMSO (0.5%) and EMS (5 mM) were used as negative and positive controls. Following 4 h of treatment, cells were harvested, mixed with low-melting-point agarose, applied to pre-coated slides, lysed, electrophoresed, and fixed. DNA was stained with ethidium bromide and observed under a fluorescence microscope (Carl Zeiss AG, Oberkochen, Germany). Tail parameters were evaluated using Bs 200

Pro software, with 100 nucleoids scored per treatment. DNA damage was expressed as the percentage of DNA in the tail.[18]

Antigenotoxic properties of the extracts were further assessed by co-treatment with EMS (6 mM for the MN assay and 5 mM for the comet assay). Exposure times were 24 h and 4 h, respectively, and the protective effects were evaluated following the same procedures.

Statistical analysis

Statistical analyses were performed using GraphPad Prism version 7.0 (GraphPad Software, La Jolla, CA, USA). Statistical significance was set at $p \leq 0.05$. Depending on the data distribution and experimental design, comparisons were performed using Student's t-test or the Kruskal-Wallis test. For the Ames test, Dunnett's multiple comparison test was used to compare treatment groups with the spontaneous control.

RESULTS

Chemical profiling of the R. aculeatus underground parts

The extracts prepared from the underground parts of *R. aculeatus* were evaluated for their antimutagenic and antigenotoxic potential using two extraction approaches. An acid hydrolysis step was applied to estimate the amounts of steroidal sapogenins, ruscogenin, and neoruscogenin. To perform chemical fingerprinting and check for the presence of reference compounds in the extracts, TLC analysis was performed. TLC chromatograms of the EtOH and aqueous extracts showed no bands co-migrating with the standards (ruscogenin/neoruscogenin mixture). By contrast, the acid hydrolyzed extract displayed distinct bands at the expected retardation factor (R_F) values for ruscogenin/neoruscogenin (data not shown), indicating liberation of the aglycones upon hydrolysis. Phytochemically, these patterns are consistent with ruscogenin/neoruscogenin being present predominantly as glycosidic forms (saponins) in the native matrix; decoction and, to a lesser extent, EtOH extraction under the conditions used yielded extracts largely depleted of free aglycones.

Further analyses were conducted with HPLC. As shown in Figure 1, the retention times (t_R) of neoruscogenin and ruscogenin were approximately 16.97 and 21.42 min, respectively. Peak identities were confirmed based on retention times. The EtOH extract (10 mg/mL) showed the presence of neoruscogenin, whereas ruscogenin was not observed (Figure 2). In contrast, the extract prepared by decoction (5 mg/mL) showed no peaks corresponding to either of the sapogenins (Figure 3). However, the acid-hydrolyzed extract contained detectable peaks for both neoruscogenin and ruscogenin (Figure 4), confirming that acid hydrolysis liberates sapogenins from saponins, as expected.

According to the pharmacopoeial (European Pharmacopoeia) specifications, the minimum required content of total sapogenins (neoruscogenin and ruscogenin) is 1%.[5] Based on the HPLC analysis of the acid-hydrolyzed extract, the total

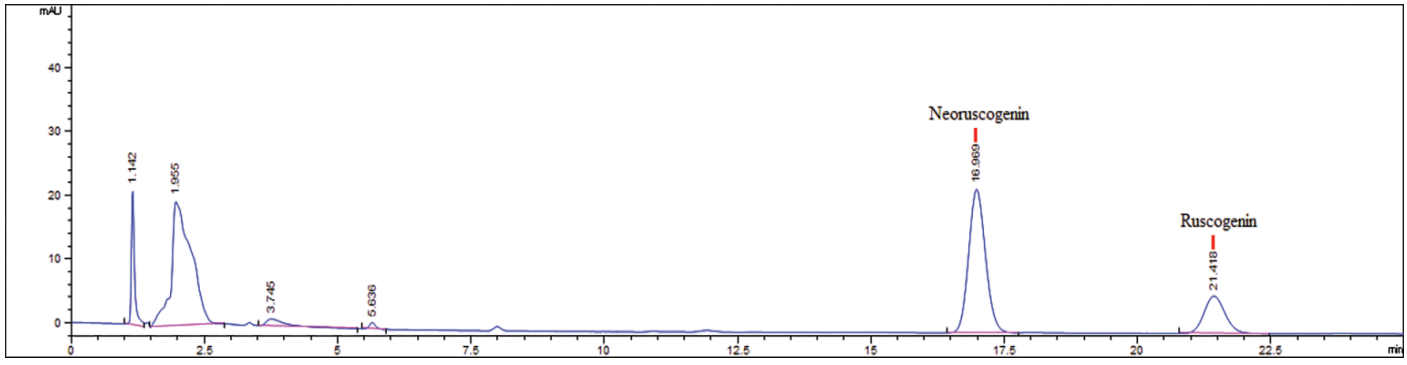

Figure 1. HPLC chromatogram of neoruscogenin and ruscogenin at 203 nm.
HPLC, high-performance liquid chromatography.

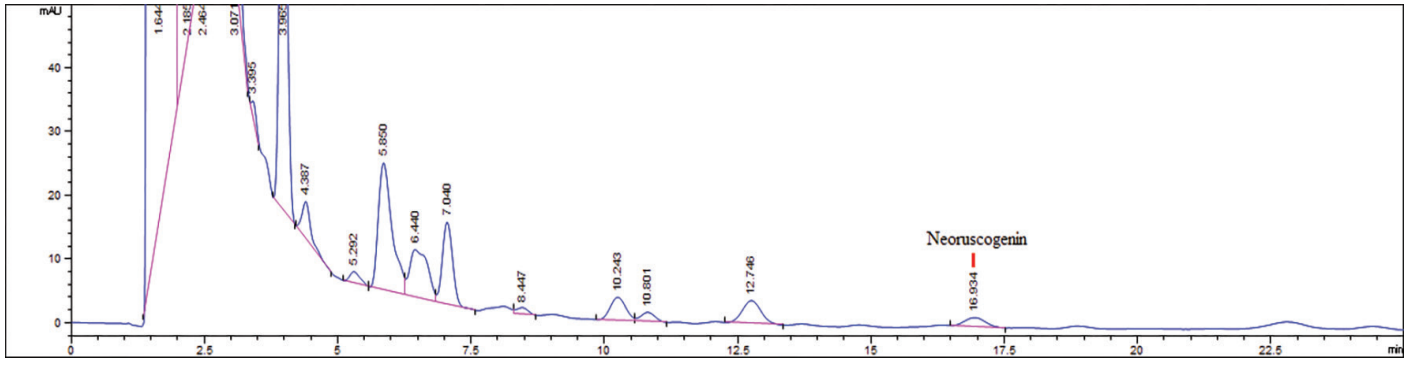

Figure 2. HPLC chromatogram of EtOH extract of *R. aculetaus* (10 mg/mL) at 203 nm.
EtOH, ethanolic; HPLC, high-performance liquid chromatography.

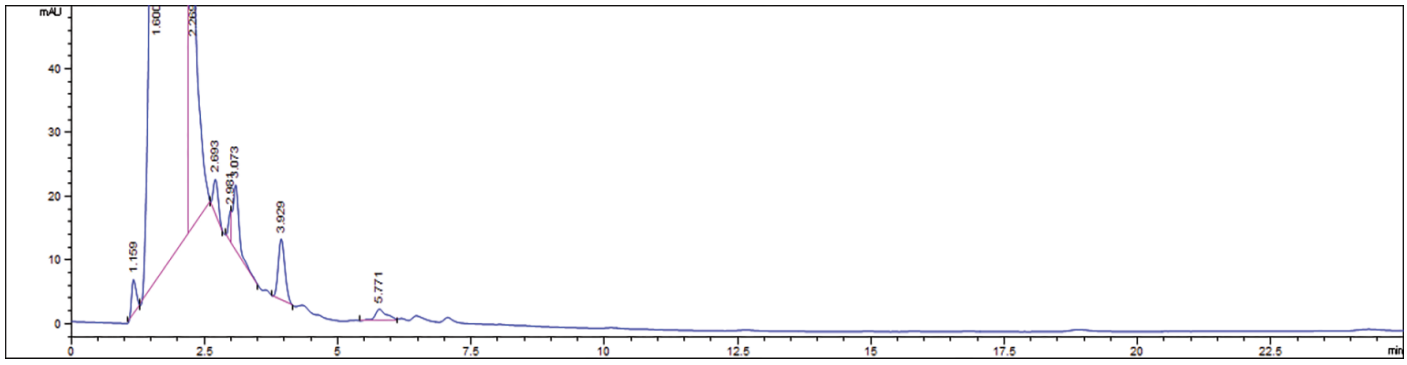

Figure 3. HPLC chromatogram of decoction of *R. aculeatus* (5 mg/mL) at 203 nm.
HPLC, high-performance liquid chromatography; *R. aculeatus*, *Ruscus aculeatus*.

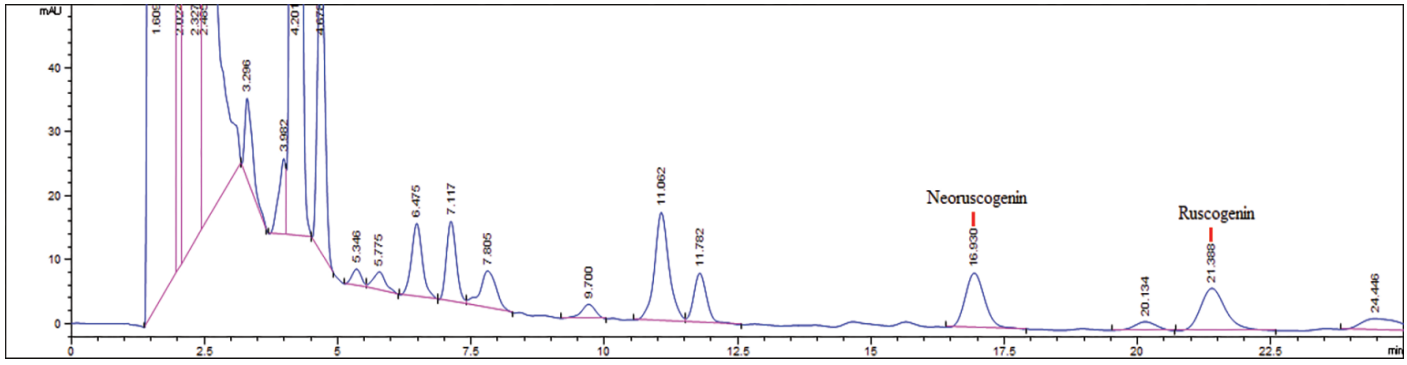

Figure 4. HPLC chromatogram of acid hydrolyzed extract of *R. aculeatus* at 203 nm.
HPLC, high-performance liquid chromatography; *R. aculeatus*, *Ruscus aculeatus*.

sapogenin content was 0.71%. As previously noted, HPLC analysis revealed no detectable sapogenin peaks in the extract prepared by decoction and only a minor peak in the EtOH extract, whereas clear peaks were observed following acid hydrolysis. These findings indicate that sapogenins are predominantly present in the raw material as glycosides, and hydrolysis is essential to meet pharmacopoeial compliance. Therefore, EP indicates an acid hydrolysis reaction prior to HPLC analysis.

Mutagenicity/antimutagenicity and genotoxicity/antigenotoxicity

The mutagenicity of the EtOH extract and decoction prepared from the underground parts of *R. aculeatus* was assessed in *Salmonella typhimurium* strains TA98 and TA100, and the mutagenic index (MI) was defined as (revertants in treated plates)/(revertants in the negative control). MI values remained < 2 for all tested concentrations, indicating the absence of a mutagenic effect.[19]

Consistent with these findings, the MN assay showed no significant increase in frequency of micronuclei (Figure 5), and the alkaline comet assay in CHO cells showed no significant change in % tail DNA relative to the negative control (Figure 6). Taken together, these results indicate that neither the EtOH extract nor the decoction exhibits mutagenic or genotoxic effects under the conditions tested, supporting the safety of *R. aculeatus* preparations in the context of traditional use and potential therapeutic applications.

Antimutagenic and antigenotoxic activities of the EtOH extract and the decoction from the underground parts of *R. aculeatus* were evaluated against known mutagenic/genotoxic agents. At the highest doses tested in the Ames assay (5000 µg/plate), the EtOH extract produced a marked inhibition of S9 activated mutagenicity in both Salmonella strains, meeting the criterion for strong antimutagenic activity (≥ 40% inhibition; Figure 7).

In the MN assay, EMS-induced increases in MN/1000 BN were significantly reduced by the EtOH extract ($p < 0.01$), demonstrating a clearer dose-dependent effect at 100–200 µg/mL, whereas the decoction produced no significant protection (Figure 8). In contrast, comet assay readouts (% tail DNA) did not differ significantly from the positive control for either extract, despite a downward trend at higher EtOH extract concentrations that was not statistically significant ($p > 0.05$) (Figure 9).

Taken together, these data suggest that, while the EtOH extract exhibits robust antimutagenic activity and antigenotoxic effects detectable at the chromosomal level (MN), it does not measurably protect against direct DNA strand breaks under the comet assay conditions used, whereas the decoction shows no detectable protection in either system.

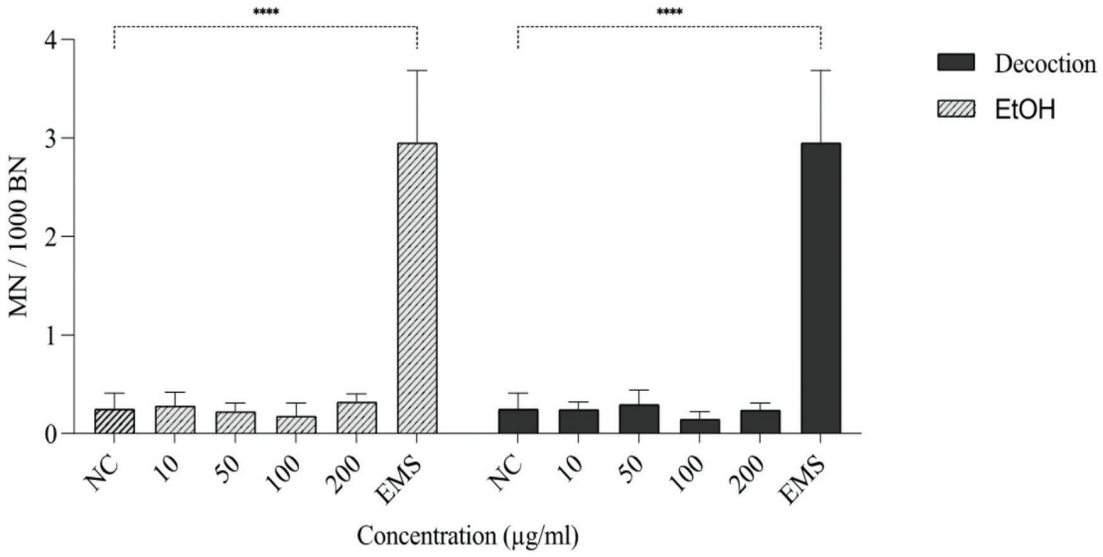

Figure 5. Cytokinesis-block MN assay results. The data represent the mean ± standard deviation from three independent experiments. Statistical analysis was performed using a one-way ANOVA followed by Dunnett's post-hoc test. ****$p < 0.0001$. The concentration of EMS used as a positive control was 6 mM.

ANOVA, analysis of variance; EMS, ethyl methanesulfonate; MN, micronucleus; NC: negative control.

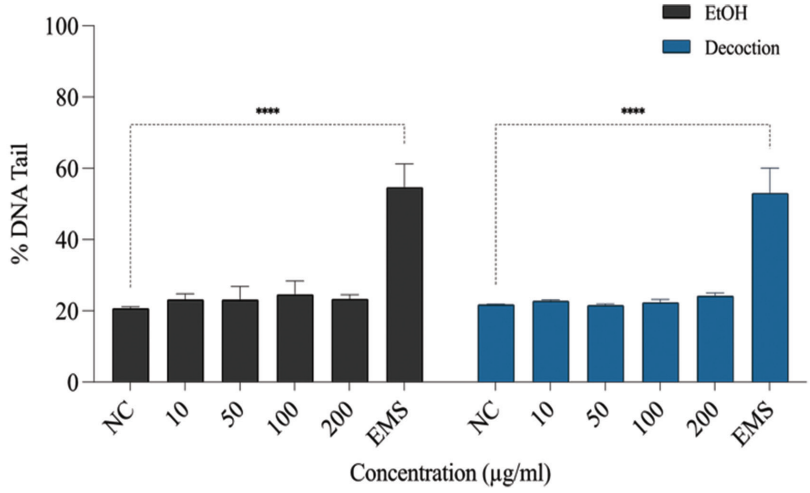

Figure 6. Comet assay results (% DNA in tail) in CHO cells. The data represent the mean ± standard deviation from three independent experiments. Statistical analysis was performed using one-way ANOVA followed by Dunnett's post-hoc test. ****$p < 0.0001$. The concentration of EMS used as a positive control was 5 mM.

ANOVA, analysis of variance; CHO: Chinese hamster ovary; EMS, ethyl methanesulfonate; EtOH, ethanol; MN, micronucleus; NC: negative control.

DISCUSSION

According to the HPLC findings, the acid-hydrolyzed extract exhibited markedly higher ruscogenin and neoruscogenin levels than the non-hydrolyzed extracts, as expected. Consistent with these results, Vlase et al.[20] reported that quantification of total ruscogenin and neoruscogenin (present mainly as saponins and only in small amounts as free aglycones) required a hydrolysis step achieved by heating samples with sulfuric acid, followed by extraction of the liberated sapogenins into an organic solvent. Comparable variability in sapogenin content has also been reported in the literature. Ozer et al.[21] determined the total sapogenin content of the underground parts of *R. aculeatus* collected from eighteen different locations in the Marmara region (Türkiye) using the HPLC method described in the European Pharmacopoeia, reporting values ranging from 0.5% to 1.5%, which were also in line with our findings. Similarly, Vlase et al.[20] reported ruscogenin and neoruscogenin contents of 0.020% and 0.046%, respectively, in roots of *R. aculeatus* collected in Romania in May by LC–MS/MS. In another study,

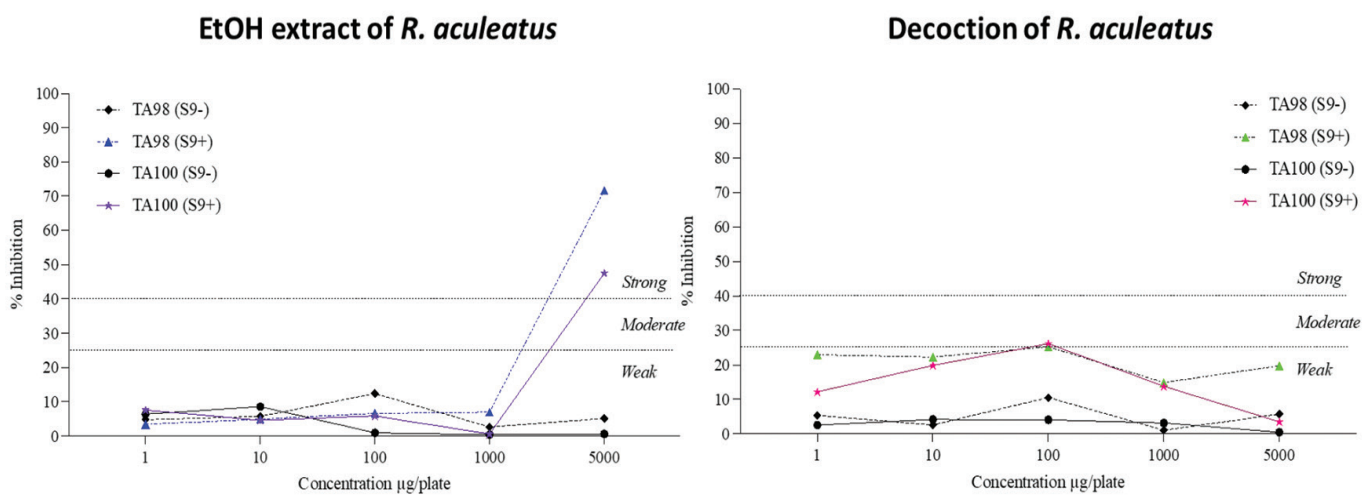

Figure 7. Antimutagenicity results of EtOH extract and decoction.
EtOH, ethanolic; *R. aculeatus, Ruscus aculeatus.*

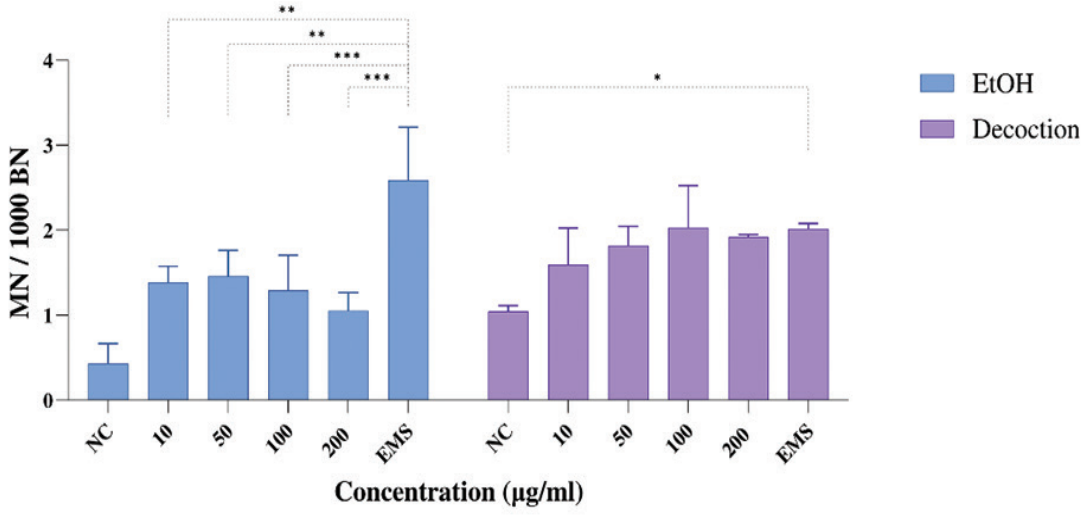

Figure 8. Cytokinesis-block MN assay results for antigenotoxicity assessment for extracts. The data represent the mean ± standard deviation from three independent experiments. Statistical analysis was performed using one-way ANOVA followed by Dunnett's post-hoc test. Comparisons were made between the positive control group and each treatment group. Statistical significance is indicated by asterisks: not significant ($p > 0.05$), *$p < 0.05$, **$p < 0.01$, ***$p < 0.001$, ****$p < 0.0001$. The concentration of EMS used as a positive control was 6 mM.
ANOVA, analysis of variance; EMS, ethyl methanesulfonate; EtOH, ethanol; MN, micronucleus; NC: negative control.

Güvenç et al.[22] analyzed Ruscus taxa collected from different regions and seasons in Türkiye using ultra-performance liquid chromatography and reported free ruscogenin contents between 0.05% and 0.22%; however, following acid hydrolysis, total ruscogenin levels increased to between 0.7% and 1.5%. Collectively, these findings suggest that both analytical methodology and raw material variability, including collection site and season, play a critical role in determining sapogenin content.

Regarding the results of antimutagenic and antigenotoxic assays, the lack of antimutagenic and antigenotoxic activity of the decoction may be explained by its abundance of polysaccharides, resulting in relatively lower amounts of potential bioactive molecules (i.e., steroidal saponins and phenolic metabolites) compared with the EtOH extract. In line with our toxicological results, Verschaeve et al.[23] reported that aqueous leaf and fruit extracts of *Ruscus hypophyllum* L. exhibited no genotoxicity in the bacterial Vitotox test and induced effects only at high concentrations in the Comet assay performed on human C3A hepatocytes.

The phytochemical and toxicological studies were performed on plant material collected from only one location. Thus, the

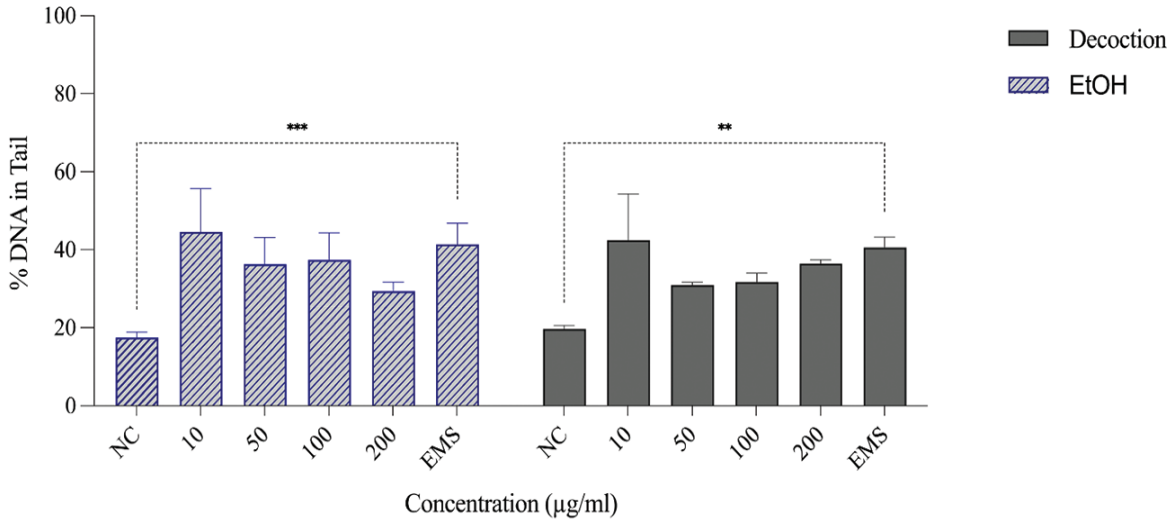

Figure 9. Comet assay results for the extracts (% DNA in tail) in CHO cells. The data represent the mean ± standard deviation from three independent experiments. Statistical analysis was performed using one-way ANOVA followed by Dunnett's post-hoc test. Comparisons were made between the positive control group and each treatment group. Statistical significance is indicated by asterisks: not significant ($p > 0.05$),*$p < 0.05$, **$p < 0.01$, ***$p < 0.001$, ****$p < 0.0001$. The concentration of EMS used as a positive control was 6 mM.

ANOVA, analysis of variance; CHO: Chinese hamster ovary; EMS, ethyl methanesulfonate; EtOH, ethanol; MN, micronucleus; NC: negative control.

results cannot be extrapolated to all *R. aculeatus* specimens that grow wild in the flora of Türkiye.

CONCLUSION

This study constitutes the first report on the genoprotective and antimutagenic effects of *R. aculeatus* extracts. The plant material was also standardized for sapogenin content. The findings of this study will shed light on further comprehensive safety profile studies on *R. aculeatus*. Furthermore, the cancer chemopreventive potential of *R. aculeatus* extracts warrants attention. Besides, different extraction methods, such as Ultrasound-Assisted Extraction, Soxhlet Extraction, Pressurized Liquid Extraction, and Microwave-Assisted Extraction, can be used to prepare extracts and compare their bioactivities in future studies.

Ethics

Ethics Committee Approval: There is not required for ethical approval.

Informed Consent: There is not required for informed consent.

Acknowledgements

The authors wish to thank Prof. Dr. Erdal BEDİR (Department of Bioengineering, İzmir Institute of Technology, İzmir, Türkiye; Bionorm) for kindly providing standard mixture containing ruscogenin and neoruscogenin.

Footnotes

Authorship Contributions

Concept: M.H., H.K., Design: E.G., M.H., H.K., Data Collection or Processing: G.E., D.T., H.Ko., E.G., M.H., Analysis or Interpretation: G.E., D.T., H.Ko., E.G., M.H., Literature Search: G.E., D.T., E.G., H.K., Writing: G.E., E.G., M.H., H.K.

Conflict of Interest: Hasan KIRMIZIBEKMEZ, the author of this article, is a member of the advisory board of the Turkish Journal of Pharmaceutical Sciences. However, he was not involved in any stage of the editorial review or decision-making process for this manuscript.

Financial Disclosure: TÜBİTAK under 2209-A University Students Research Projects Support Program (project no: 1919B012323297).

REFERENCES

1. Güner A, Aslan S, Ekim T, Vural M, Babaç MT. Türkiye Bitkileri Listesi (Damarlı Bitkiler). İstanbul: Nezahat Gökyiğit Botanik Bahçesi ve Flora Araştırmaları Derneği Yayını; 2012.
2. Davis PH, Mill RR, Tan K. Flora of Turkey and the East Aegean Islands. Edinburgh: Edinburgh University Press; 1988.
3. Kebeli F, Çelikel FG. Ruscus species distributed in Türkiye. J AARI. 2024;34:68-76.
4. Özçınar Ö, Tağ Ö, Yusufoğlu H, Kıvçak B, Bedir E. Biotransformation of neoruscogenin by the endophytic fungus Alternaria eureka. J Nat Prod. 2018;81:1357-1367.
5. European Directorate for the Quality of Medicines & HealthCare. Rusci rhizoma. In: European Pharmacopoeia. 11th ed. Strasbourg: Council of Europe; 2023. Available from: https://www.edqm.eu

6. Pacuła W, Sowa I, Feldo M, Graczyk F, Patryn R, Wójciak M. Current insights into the phytochemistry and pharmacological properties of *Ruscus aculeatus*. Molecules. 2025;30:4417.

7. Luís A, Domingues F, Duarte AP. Bioactive compounds, RP-HPLC analysis of phenolics, and antioxidant activity of some Portuguese shrub species extracts. Nat Prod Commun. 2011;6:1863-1872.

8. Longo L, Vasapollo G. Determination of anthocyanins in *Ruscus aculeatus* L. berries. J Agric Food Chem. 2005;53:475-479.

9. Emre G, Doğan A, Haznedaroğlu MZ, Şenkardeş İ, Ülger M, Satıroğlu A, Emmez BC, Tugay O. An ethnobotanical study of medicinal plants in Mersin (Turkey). Front Pharmacol. 2021;12:664500.

10. Tuzlacı E, Aymaz PE. Turkish folk medicinal plants, part IV: Gönen (Balıkesir). Fitoterapia. 2021;2:323-343.

11. Ali-Shtayeh MS, Yaghmour RMR, Faidi YR, Salem K, Al-Nuri MA. Antimicrobial activity of 20 plants used in folkloric medicine in the Palestinian area. J. Ethnopharmacol. 1998;60:265-271.

12. Guarrera PM. Traditional phytotherapy in Central Italy (Marche, Abruzzo, and Latium). Fitoterapia. 2005;76:1-25.

13. Mimaki Y, Kuroda M, Kameyama A, Yokosuka A, Sashida Y. New steroidal constituents of the underground parts of *Ruscus aculeatus* and their cytostatic activity on HL-60 cells. Chem Pharm Bull. 1998;46:298-303.

14. Zhao J, He B, Seshadri VD, Xu S. Anticancer effect of ruscogenin in B(a)P-induced lung cancer in mice via modulation of proinflammatory cytokines and mitochondrial enzymes. Appl Biochem Biotechnol. 2022;194:5862-5877.

15. Barbič M, Willer EA, Rothenhöfer M, Heilmann J, Fürst R, Jürgenliemk G. Spirostanol saponins and esculin from Rusci rhizoma reduce the thrombin-induced hyperpermeability of endothelial cells. Phytochemistry. 2013;90:106-113.

16. European Medicines Agency. European Union herbal monograph on *Ruscus aculeatus* L., rhizoma. Amsterdam: European Medicines Agency; 2018. Available from: https://www.ema.europa.eu/en/documents/herbal-monograph/european-union-herbal-monograph-ruscus-aculeatus-l-rhizoma-revision-1_en.pdf

17. Guzelmeric E, Sipahi H, Ozhan Y, Hamitoglu M, Helvacioglu S, Duz G, Akyildiz IE, Kadioglu Yaman B, Hazar M, Aydin Dilsiz SA, Aydin A, Yesilada E. Comprehensive estrogenic/anti-estrogenic, anticancer, mutagenic/anti-mutagenic, and genotoxic/anti-genotoxic activity studies on chemically characterized black poplar and Eurasian aspen propolis types. J Pharm Biomed Anal. 2023;226:115241.

18. Helvacioglu S, Charehsaz M, Bankoglu EE, Stopper H, Aydin A. The ameliorative effect of rosmarinic acid and epigallocatechin gallate against doxorubicin-induced genotoxicity. Drug Chem Toxicol. 2024;47:1087-1099.

19. Levy DD, Zeiger E, Escobar PA, Hakura A, van der Leede BM, Kato M, Moore MM, Sugiyama K. Recommended criteria for the evaluation of bacterial mutagenicity data (Ames test). Mutat Res Genet Toxicol Environ Mutagen. 2019;848:403074.

20. Vlase L, Kiss B, Balica G, Tas M, Crisan G, Leucuta SE. High-throughput LC/MS/MS analysis of ruscogenin and neoruscogenin in *Ruscus aculeatus* L. J AOAC Int. 2009;92:1055-1059.

21. Ozer G, Guzelmeric E, Sezgin G, Ozyurek E, Arslan A, Sezik E, Yesilada E. Comparative determination of ruscogenins content in Butcher's Broom rhizome samples gathered from the populations grown in different soil conditions in the Marmara Region and attempts for pilot field cultivation of rhizomes. J Chem Metrol. 2018;12:79-88.

22. Güvenç A, Şatır E, Coşkun M. Determination of ruscogenin in Turkish Ruscus L. species by UPLC. Chromatographia. 2007;66:141-145.

23. Verschaeve L, Edziri H, Anthonissen R, Boujnah D, Skhiri F, Aouni M, Mastouri M. In vitro toxicity and genotoxic activity of aqueous leaf and fruit extracts of Ruscus hypophyllum L. Acta Physiol Plant. 2017;39:206.

Turk J Pharm Sci 2026;23(2):65-74
DOI: 10.4274/tjps.galenos.2026.68256

ORIGINAL ARTICLE

Plasma Concentrations of Amyloid-β Peptides, BACE-1, and Tau Proteins in Alzheimer's Disease

Nejla YILDIRIM[1], Naile Merve GÜVEN AKSU[1,2], Başak Özlem PERK[1], Benay CAN EKE[2]*

[1]Ankara University, Graduate School of Health Sciences, Ankara, Türkiye
[2]Ankara University Faculty of Pharmacy, Department of Pharmaceutical Toxicology, Ankara, Türkiye

ABSTRACT

Objectives: The aim of this study was to compare, using ELISA, plasma levels of amyloid beta (Aβ)40, Aβ42, beta-site amyloid precursor protein cleaving enzyme 1 (BACE-1), total tau (t-tau), and phosphorylated tau (p-tau), as well as the Aβ42/Aβ40 ratio, between patients with Alzheimer's disease (AD) and healthy controls, and to evaluate their diagnostic performance in relation to demographic and lifestyle factors.

Materials and Methods: This study is a single-center, cross-sectional, case-control study. Twenty-four individuals diagnosed with AD and 37 healthy volunteers included in the study. Alongside the analysis of plasma samples obtained from the participants, demographic data were analyzed to assess the potential influence of lifestyle and environmental factors on disease development.

Results: Analysis of the case data showed that increasing age was a risk factor for AD, higher education level was associated with an increased risk of AD, and tea consumption was inversely associated with AD. While age is a well-known risk factor, both the increased risk of AD associated with higher education and the relatively protective effect of tea consumption against AD are supported by the literature. Evaluation of the levels of Aβ40, Aβ42, BACE-1, t-tau, and p-tau and of the Aβ42/Aβ40 ratio revealed no significant differences between the patient and control groups. Additionally, Aβ40, Aβ42, BACE-1 showed correlations in both the control and Alzheimer's groups, whereas t-tau did not.

Conclusion: None of the investigated plasma biomarkers (Aβ40, Aβ42, BACE-1, t-tau, p-tau, and the Aβ42/Aβ40 ratio) discriminated Alzheimer's patients from healthy controls, with all receiver operating characteristic area under the curve values below 0.62. These findings indicate that in this cohort, plasma levels of these individual markers did not provide diagnostic value; larger longitudinal studies including cerebrospinal fluid comparisons and multi-marker panels are needed.

Keywords: Alzheimer's disease, amyloid beta, BACE-1, tau, ELISA

INTRODUCTION

Alzheimer's disease (AD), which emerges with advancing age, is a progressive neurodegenerative disorder characterized by memory loss and cognitive decline.[1] The disease was first described by Dr. Alois Alzheimer in 1906.[2] Changes in brain biomarker levels can be detected years before clinical symptoms appear.[3]

The pathophysiology of AD involves complex mechanisms at the genetic, molecular, and cellular levels, and interacts with both the central and peripheral immune systems.[4] According to the World Health Organization, AD accounts for approximately 60–70% of dementia cases and affects around 55 million people worldwide.[5] The disease ranks among the leading causes of death in elderly populations, particularly in developed countries.[1]

The AT(N) classification system, proposed by the National Institute on Aging and the Alzheimer's Association in 2018, defines AD based on biomarkers, categorizing disease stages according to amyloid (A), tau (T), and neurodegeneration (N)

***Correspondence:** eke@pharmacy.ankara.edu.tr, **ORCID-ID:** orcid.org/0000-0001-9817-9034

Received: 29.09.2025 **Accepted:** 16.07.2026 **Epub:** 05.08.2026 **Publication Date:** 01.09.2026

Cite this article as: Yıldırım N, Güven Aksu NM, Perk BÖ, Can Eke B. Plasma concentrations of amyloid-β peptides, BACE-1, and tau proteins in Alzheimer's disease. Turk J Pharm Sci. 2026;23(2):65-74

markers. Recently, plasma-based biomarkers have shown promising diagnostic potential.[6]

AD can be divided into two groups according to age of onset: early-onset (< 65 years) and late-onset (≥ 65 years). Early-onset AD is associated with genetic mutations in the Presenilin 1, Presenilin 2, and amyloid precursor protein (*APP*) genes, whereas late-onset AD is linked to the APOE ε4 allele. Clinical staging categorizes patients into three groups: cognitively normal, mild cognitive impairment, and dementia.[5]

Various hypotheses have been proposed to explain the neuropathological basis of AD. The most widely recognized hypothesis is the amyloid cascade hypothesis, in which cleavage of the APP by beta-site amyloid precursor protein cleaving enzyme 1 (BACE-1) follows the amyloidogenic pathway to produce Aβ peptides, mainly Aβ40 and Aβ42. The Aβ42 isoform, considered the most toxic, leads to neuronal loss through accumulation of plaques, oligomers, and fibrils.[7]

The second important mechanism underlying AD's formation is tau pathology, which involves hyperphosphorylation of the microtubule-stabilizing tau protein and results in the formation of neurofibrillary tangles that contribute to neuronal degeneration. There is a synergistic interaction between tau and Aβ pathologies, with Aβ promoting mechanisms that trigger tau's conversion into its toxic form.[8]

Glutamate-mediated excitotoxicity, driven by excessive activation of NMDA receptors, causes intracellular calcium accumulation, leading to neuronal death and plays a role in AD pathogenesis.[9]

The initial breakthrough in understanding AD came in the 1970s with the demonstration of deficiencies in choline acetyltransferase activity in the brains of Alzheimer's patients, which were attributed to cholinergic deficits. Recognition of acetylcholine's role in memory and learning led to the cholinergic hypothesis of AD, which inspired therapeutic strategies aimed at enhancing cholinergic function. Cholinergic depletion is considered a late feature of the neurodegenerative cascade.[10]

In AD development, non-modifiable risk factors include age, genetic predisposition, sex, and Down syndrome, while modifiable risk factors encompass educational level, marital status, cognitive stimulation, history of head trauma, lifestyle factors (alcohol and tobacco use), metabolic disorders (type II diabetes, dyslipidemia, obesity, cerebrovascular diseases, hypertension), immunological and inflammatory factors, pathogenic infections, metal exposure, and pesticides. Additionally, factors that negatively impact quality of life, such as stress, depression, and insufficient sleep, have been shown in case-control studies to significantly influence AD risk.[11,12]

In this study, quantitative measurements of disease-associated proteins in plasma samples from patients with AD and healthy controls were performed using ELISA. Correlation analyses among these proteins were conducted to evaluate the diagnostic potential of plasma-based biomarkers.

MATERIALS AND METHODS

This was a single-center, cross-sectional case-control study comparing plasma biomarker concentrations between clinically diagnosed AD patients and cognitively healthy controls, who were recruited over the same study period.

This study was approved by the Ethics Committee on Ankara University (decision no: İ3-148-20, date: 12.10.2020).

A total of 24 patients aged 65 and older diagnosed with AD by specialist clinicians in fully equipped hospitals were included in the study; the group comprised 5 males (21%) and 19 females (79%). Diagnoses were established based on the criteria of the National Institute of Neurological and Communicative Disorders and Stroke and the Alzheimer's Disease and Related Disorders Association and on clinical interviews using the Structured Clinical Interview for Diagnostic and Statistical Manual of Mental Disorders, fourth edition (DSM-IV) axis I disorders, conducted in accordance with the DSM-IV of the American Psychiatric Association. The diagnosis of AD was definitively confirmed through review of patient records, including official diagnostic reports, and, when necessary, by contacting the institutions that issued the reports or the diagnosing specialists. Only patients with confirmed diagnoses were included in the study.

Legal guardians of the patients were informed about the study, and written consent was obtained. The patient group consisted of residents of a nursing home who had been diagnosed with AD by specialized physicians at fully equipped hospitals.

The control group included 37 individuals aged 65 and older, comprising 18 males (49%) and 19 females (51%), all of whom had no diagnosis of AD or other forms of dementia or cognitive impairment. Informed consent was obtained from all control participants, who were recruited from hospitals and health centers.

Exclusion criteria for both groups included individuals under 65 years of age; those for whom blood sampling was contraindicated due to coagulation disorders or anemia; individuals diagnosed with other types of dementia; and those with significant comorbidities (e.g., cancer) that could potentially affect the results.

Blood sample collection and plasma preparation

Venous blood samples (10 mL) were collected from all volunteers into tubes containing ethylenediaminetetraacetic acid.

Samples from both patient and control groups were centrifuged at 2500 rpm for 10 minutes to separate plasma.

Plasma samples were stored at -80 °C. Before analysis, samples were brought to room temperature, and analyses were performed according to the kit instructions. The plasma samples were thawed at room temperature on the day of analysis. To avoid the impact of multiple freeze–thaw cycles, only aliquots that had not been previously thawed were used in this study.

Concentrations of Aβ40, Aβ42, BACE-1, total tau (t-tau), and phosphorylated tau (p-tau) in plasma were measured and evaluated using ELISA.

The following ELISA kits and equipment were used in this study:

Nepenthe human β-site APP cleaving enzyme 1 ELISA kit (catalog number: NE010080201, production site: Gebze-Kocaeli/Türkiye)

Nepenthe human t-tau proteins ELISA kit (catalog number: NE010133301, production site: Gebze-Kocaeli/Türkiye)

Assay genie human phospho tau (P181) ELISA Kit (catalog number: HUFI03189

Nepenthe human amyloid beta peptide 1-42 ELISA kit (catalog number: NE010126401, production site: Gebze-Kocaeli/Türkiye)

Nepenthe human amyloid beta peptide 1-42 ELISA kit (catalog number: NE010123001, production site: Gebze-Kocaeli/Türkiye), and a microplate reader equipped with a 450 ± 10 nm wavelength filter. Analyses were performed in duplicate. Laboratory personnel were blinded.

Preparation of kits

Each kit was prepared and used according to the manufacturer's instructions.

Demographic data

Relationships between AD and various demographic factors, including patient age, education level, employment history, comorbidities, medication use, history of head trauma, smoking and alcohol consumption, frequency of tea and coffee intake, dietary habits, frequency of exercise, disease stage, family history of Alzheimer's, and place of residence were evaluated.

Statistical analysis

The distribution of continuous variables and the homogeneity of variances were assessed using the Shapiro–Wilk and Levene's tests, respectively. As the assumptions of parametric tests were not met, continuous variables were summarized using the median (25^{th}–75^{th} percentiles) and compared between groups using the Mann–Whitney U test. Correlations among continuous variables were assessed using Spearman's rank correlation coefficient. Categorical variables were presented as counts and percentages and compared using the continuity-corrected χ^2 test, Fisher's exact test, or the Fisher–Freeman–Halton test, as appropriate for the expected cell frequencies. Where multiple pairwise comparisons were performed, a Bonferroni correction was applied.

Candidate predictors with univariate $p < 0.10$ were entered into a multivariable logistic regression model. Exercise was excluded due to quasi-complete separation, and tea and coffee consumption were entered in separate models due to their conceptual overlap. Variance inflation factors were calculated to assess multicollinearity, and all values remained below 2.5. Considering the modest events-per-variable ratio, a sensitivity analysis was performed using Firth penalized (bias-reduced) logistic regression. The direction, magnitude, and statistical significance of all predictors were preserved, supporting the stability of the model.

To address the age difference between groups, biomarker comparisons were performed using a rank-based ANCOVA. In this approach, biomarker values and age were rank-transformed, and the biomarker rank was regressed on group with age rank as a covariate. This is the non-parametric analogue of an age-adjusted Mann–Whitney U test and is appropriate for the non-normal distributions observed in these data.

All analyses were performed using IBM SPSS Statistics version 25 (IBM Corporation, Armonk, NY, USA). Two-sided *p*-values were considered statistically significant unless otherwise specified.

RESULTS

This study demonstrated that the Alzheimer's and control groups were similar in demographic, clinical, and comorbid conditions; however, some demographic factors, such as age, gender, and education level, may be associated with AD, as shown in Table 1.

Association of lifestyle habits with AD

Table 2 shows the lifestyle habits of individuals diagnosed with AD (n = 24) compared with those of healthy controls (n = 37).

A statistically significant difference between groups was found with respect to smoking history ($p = 0.010$). While 78.3% of the Alzheimer's group reported never smoking, the rate in the control group was 40.5%. Current smokers were found only in the control group.

There was no history of alcohol consumption in the Alzheimer's group, whereas 29.7% of controls reported such a history; this difference was not statistically significant ($p = 0.149$).

A significant difference in coffee consumption between groups was observed ($p < 0.001$). In the Alzheimer's group, 73.9% reported consuming only one cup of coffee daily, whereas in the control group consumption was more frequent and varied: 27% consumed one cup and 21.6% consumed two cups per day.

Tea consumption also differed significantly ($p < 0.001$) between the control and Alzheimer's groups. While 91.3% of the Alzheimer's group consumed only one cup of tea per day, 64.9% of the control group consumed three or more cups per day.

No significant difference in dietary habits was detected between the groups ($p = 0.389$).

A significant difference in regular exercise habits was found ($p < 0.001$). All individuals in the Alzheimer's group reported engaging in regular exercise during the past year. In contrast, 40.5% of the control group reported no exercise, while only 32.4% reported exercising regularly for over one year.

Clinical characteristics specific to the Alzheimer's group

The disease duration among the 24 individuals diagnosed with AD varied (Table 3), with a median of 4 years (range: 0–10 years). When examining the disease stages, 29.2% were in the early stage, 37.5% were in the moderate stage, and 33.3% were in the advanced stage.

A family history of Alzheimer's was present in 12.5% cases. Among these, 8.3% reported a similar disease history in their spouse, while 4.2% reported it in their sibling. The majority of participants (79.2%) had no family history of Alzheimer's, and 8.3% did not provide information on this matter.

Table 1. Demographic and clinical characteristics of cases by groups.

Characteristic	Control (n = 37)	Alzheimer (n = 24)	*p*-value
Age (years)*	70.0 (66.0–75.0)	83.0 (73.5–88.0)	< 0.001[a]
Gender			0.055[b]
- Female	19 (51.4%)	19 (79.2%)	
- Male	18 (48.6%)	5 (20.8%)	
Education level			0.074[c]
- Illiterate	7 (20.0%)	1 (4.2%)	
- Primary school	14 (40.0%)	7 (29.2%)	
- Middle school	3 (8.6%)	2 (8.3%)	
- High school	2 (5.7%)	7 (29.2%)	
- Associate degree	0 (0.0%)	1 (4.2%)	
- Bachelor's degree	9 (25.7%)	6 (25.0%)	
Work history			0.938[b]
- No	13 (37.1%)	10 (41.7%)	
- Yes	22 (62.9%)	14 (58.3%)	
Comorbidities			
- Hypertension	14 (37.8%)	14 (58.3%)	0.191[b]
- Heart diseases	20 (54.1%)	8 (33.3%)	0.186[b]
- Diabetes mellitus	10 (27.0%)	6 (25.0%)	> 0.999[b]
- Hyperlipidemia	3 (8.1%)	3 (12.5%)	0.672[d]
- COPD	5 (13.5%)	1 (4.2%)	0.388[d]
- Asthma	4 (10.8%)	0 (0.0%)	0.147[d]
Medication use			0.635[b]
- None	3 (8.8%)	1 (4.2%)	
- Yes	31 (91.2%)	23 (95.8%)	
History of head trauma	5 (13.5%)	0 (0.0%)	0.146[d]

*Descriptive statistics are expressed as median (25th percentile–75th percentile)
[a]Mann–Whitney U test; [b]Continuity corrected χ^2 test; [c]Fisher–Freeman–Halton test; [d]Fisher's exact test; COPD, chronic obstructive pulmonary disease.

Table 2. Frequency distribution of smoking and alcohol history, tea and coffee consumption, dietary, and exercise habits by groups.

Variable	Control (n = 37)	Alzheimer (n = 24)	*p*-value
Smoking history			0.010[a]
- Never	15 (40.5%)[A]	18 (78.3%)[A]	
- Former smoker	18 (48.6%)	5 (21.7%)	
- Current smoker	4 (10.8%)	0 (0.0%)	
Alcohol history			0.149[b]
- None	32 (88.9%)	23 (100%)	
- Yes	4 (11.1%)	0 (0.0%)	
Coffee consumption			< 0.001[a]
- None	8 (21.6%)	5 (21.7%)	
- Occasionally	14 (37.8%)[B]	1 (4.3%)[B]	
- 1 cup/day	10 (27.0%)[C]	17 (73.9%)[C]	
- 2 cups/day	5 (13.5%)	0 (0.0%)	
Tea drinking habit			< 0.001[a]
- None	1 (2.7%)	0 (0.0%)	
- 1 cup/day	3 (8.1%)[C]	21 (91.3%)[C]	
- 2 cups/day	9 (24.3%)	2 (8.7%)	
- ≥ 3 cups/day	24 (64.9%[C]	0 (0.0%)[C]	
Dietary habit			0.389[a]
- Vegetable-based	22 (61.1%)	12 (52.2%)	
- Meat-based	11 (30.6%)	6 (26.1%)	
- Balanced	3 (8.3%)	5 (21.7%)	
Regular exercise			< 0.001[a]
- No	15 (40.5%)[A]	0 (0.0%)[A]	
- < 1 year	8 (21.6%)[C]	12 (100%)[C]	
- 1 year	2 (5.4%)	0 (0.0%)	
- > 1 year	12 (32.4%)[D]	0 (0.0%)[D]	

[a]Fisher–Freeman–Halton test; [b]Fisher's exact test.
[A]Significant difference between groups (p = 0.010); [B]Significant difference (p = 0.009); [C]Significant difference (p < 0.001); [D]Significant difference (p = 0.024).

Regarding the place of residence prior to diagnosis, most individuals with Alzheimer's (79.2%) lived in urban centers, 12.5% resided in other settlements, and 8.3% did not specify their residence.

Biomarker levels

In Table 4, levels of Aβ40, Aβ42, BACE-1, t-tau, and p-tau were compared between individuals with AD and the control group; no statistically significant differences were found (p > 0.05).

Aβ40 levels were measured at medians of 1492.00 ng/L [interquartile range (IQR): 965.75–1749.50] in the control group and 1224.50 ng/L (IQR: 884.63–1818.25) in the Alzheimer's group; the difference was not significant (p = 0.535).

Aβ42 levels were 84.70 ng/L (IQR: 72.20–100.77) in the control group and 80.24 ng/L (IQR: 69.75–105.89) in the Alzheimer's group (p = 0.859).

BACE-1 levels were slightly lower in the Alzheimer's group (median 4.41 ng/mL, IQR: 3.95–6.10) than in the control group (median 5.19 ng/mL, IQR: 4.30–6.24); however this difference was not statistically significant (p = 0.226).

Table 3. Other clinical findings of cases in the Alzheimer's group.

Variable	n = 24
Disease duration (years)*	4 (0–10)
Disease stage	
- Early	7 (29.2%)
- Moderate	9 (37.5%)
- Advanced	8 (33.3%)
Family history of Alzheimer's	
- No	19 (79.2%)
- Yes	3 (12.5%)
- Not specified	2 (8.3%)
If yes, relationship	
- Spouse	2 (8.3%)
- Sibling	1 (4.2%)
Place of residence before diagnosis	
- Urban	19 (79.2%)
- Other	3 (12.5%)
- Not specified	2 (8.3%)

*Descriptive statistics are presented as median (minimum-maximum) values.

T-tau levels were measured at 197.38 ng/L (IQR: 177.38–324.39) in the Alzheimer's group and 261.44 ng/L (IQR: 195.32–323.51) in the control group, with no significant difference (p = 0.138).

P-tau levels were 29.49 pg/mL (IQR: 15.33–59.12) in the Alzheimer's group and 25.38 pg/mL (IQR: 14.62–52.18) in the control group (p = 0.585).

The Aβ42/Aβ40 ratio was calculated for each participant and compared between groups. The median (IQR) ratio was 0.064 (0.051–0.084) in the control group and 0.070 (0.058–0.088) in the Alzheimer's group; this difference was not statistically significant (Mann–Whitney U, p = 0.159).

Receiver operating characteristic (ROC) analysis results

The discriminatory ability of biomarkers to distinguish Alzheimer's patients from the control group (Table 5) was evaluated using ROC analysis. The area under the curve (AUC) values and 95% confidence intervals (CIs) obtained from the ROC analysis are presented below:

The AUC value for Aβ40 (0.547; 95% CI: 0.398–0.697) was not significant for diagnostic discrimination (p = 0.535).

The Aβ42 AUC was 0.514 (95% CI: 0.363–0.664), indicating weak, not statistically significant discriminatory power (p = 0.859).

The AUC for BACE-1 level was 0.592 (95% CI: 0.440–0.745), which did not reach statistical significance (p = 0.226).

T-tau showed an AUC of 0.613 (95% CI: 0.458–0.768), demonstrating limited diagnostic discrimination (p = 0.138).

The AUC value for p-tau was 0.542 (95% CI: 0.392–0.691), indicating poor diagnostic discrimination (p = 0.585).

ROC analysis yielded an AUC of 0.608 (95% CI 0.469–0.744; p = 0.159); the 95% CI included the chance line. The direction of the numerical difference was opposite to that commonly reported in the literature, in which a decreased plasma Aβ42/Aβ40 ratio is expected in AD. This discordance is addressed in the discussion.

None of the biomarkers showed strong discrimination for the diagnosis of AD; their AUC values were not significantly high.

Multivariable logistic regression analysis results

In the multivariable logistic regression analysis, as shown in Table 6, factors potentially effective in distinguishing between control and Alzheimer's groups were evaluated simultaneously. Age, education level, and tea consumption habits were found to be statistically significant.

Age showed a significant positive association with Alzheimer's diagnosis [odds ratip (OR) = 1.256; 95% CI: 1.027–1.536; p = 0.026]. Each additional year of age increased the odds of an Alzheimer's diagnosis by approximately 25%.

Education level was significantly associated with Alzheimer's (OR = 2.101; 95% CI: 1.050–4.202; p = 0.036). Higher educational attainment was associated with an increased risk of an Alzheimer's diagnosis.

Tea- drinking habit was inversely and significantly associated with AD (OR = 0.094; 95% CI: 0.020–0.452; p = 0.003). This finding indicates that individuals who consume tea have a lower likelihood of being diagnosed with AD.

Table 4. Protein levels in control and Alzheimer's groups.

Biomarker	Control (n = 37) (median, IQR)	Alzheimer (n = 24) (median, IQR)	p-value[a]
Aβ40 (ng/L)	1492.00 (965.75–1749.50)	1224.50 (884.63–1818.25)	0.535
Aβ42 (ng/L)	84.70 (72.20–100.77)	80.24 (69.75–105.89)	0.859
BACE-1 (ng/mL)	5.19 (4.30–6.24)	4.41 (3.95–6.10)	0.226
t-tau (ng/L)	261.44 (195.32–323.51)	197.38 (177.38–324.39)	0.138
p-tau (pg/mL)	25.38 (14.62–52.18)	29.49 (15.33–59.12)	0.585
Aβ42/Aβ40 ratio	0.064 (0.051–0.084)	0.070 (0.058–0.088)	0.159

[a]Mann-Whitney U test; IQR, interquartile range; BACE-1, beta-site amyloid precursor protein cleaving enzyme 1; t-tau, total tau; p-tau, phosphorylated tau. Descriptive statistics are presented as median (25^{th}-75^{th} percentile).

However, female sex (OR = 2.021; p = 0.704) and a history of smoking (OR = 0.404; p = 0.528) were not significantly associated with Alzheimer's diagnosis.

Correlation analysis among proteins

Spearman correlation analysis was performed on all participants in the study group (n = 61) to evaluate the relationships among Aβ40, Aβ42, BACE-1, t-tau, and p-tau protein levels (Table 7).

Aβ40 levels showed statistically significant positive correlations with Aβ42 (r = 0.640; $p < 0.001$), BACE-1 (r = 0.543; $p < 0.001$), and t-tau (r = 0.695; $p < 0.001$).

Table 5. ROC analysis results of protein measurements for differentiating control and Alzheimer's groups.

Biomarker	AUC	95% CI	*p*-value
Aβ40 (ng/L)	0.547	0.398–0.697	0.535
Aβ42 (ng/L)	0.514	0.363–0.664	0.859
BACE-1 (ng/mL)	0.592	0.440–0.745	0.226
t-tau (ng/L)	0.613	0.458–0.768	0.138
p-tau (pg/mL)	0.542	0.392–0.691	0.585
Aβ42/Aβ40	0.608	0.469–0.744	0.159

ROC, receiver operating characteristic; AUC, area under the curve; CI, confidence interval; BACE-1, beta-site amyloid precursor protein cleaving enzyme 1; t-tau, total tau; p-tau, phosphorylated tau.

Table 6. Multivariable logistic regression analysis results: investigating the combined effects of potential predictors in differentiating control and Alzheimer's groups.

Variable	OR	95% CI	Wald	*p*-value
Age	1.256	1.027–1.536	4.929	**0.026**
Female sex factor	2.021	0.053–76.636	0.144	0.704
Education level	2.101	1.050–4.202	4.404	**0.036**
Smoking history	0.404	0.024–6.756	0.398	0.528
Tea drinking habit	0.094	0.020–0.452	8.721	**0.003**

OR, odds ratio; CI, confidence interval.

Table 7. Correlation coefficients and significance levels among protein measurements in all subjects.

	Aβ42	BACE-1	t-tau	p-tau
Aβ40	0.640	0.543	0.695	0.084
p-value[a]	< 0.001	< 0.001	< 0.001	0.518
Aβ42		0.696	0.775	0.120
p-value[a]		< 0.001	< 0.001	0.355
BACE-1			0.798	0.080
p-value[a]			< 0.001	0.542
t-tau				0.001
p-value[a]				0.999

[a]Spearman's rank correlation test was used; BACE-1, beta-site amyloid precursor protein cleaving enzyme 1; t-tau, total tau; p-tau, phosphorylated tau.

No significant correlation was found between Aβ40 and p-tau levels (r = 0.084; p = 0,518).

Aβ42 exhibited strong positive correlations with BACE-1 (r = 0.696; $p < 0.001$) and t-tau (r = 0.775; $p < 0.001$), while its correlation with p-tau was weak and statistically non-significant (r = 0.120; p = 0.355).

BACE-1 showed a strong and statistically significant correlation with t-tau (r = 0.798; $p < 0.001$), but no significant correlation with p-tau (r = 0.080; p = 0.542).

The correlation coefficient between t-tau and p-tau levels was near zero (r = 0.001; p = 0.999), indicating no statistically significant relationship between these variables.

DISCUSSION

The primary aim of this study was to investigate Aβ40, Aβ42, BACE-1, t-tau, and p-tau levels in patients with AD and healthy controls; however, no statistically significant differences were detected between the groups. Although Aβ40 and Aβ42 levels showed the expected decreasing trend in the Alzheimer's group, these differences did not reach statistical significance.[13]

BACE-1 levels were lower in the AD group. BACE-1 is an important enzyme involved in the conversion of APP to Aβ peptides; some studies have reported increased activity of this enzyme in AD.[14]

The lower BACE-1 levels observed in this study may be due to variability related to sample size or biological differences among individuals. Analysis of tau protein showed that t-tau levels were higher in the control group. Generally, t-tau and p-tau levels are expected to increase in AD due to neuronal damage. However, p-tau levels did not differ significantly between groups in this study. This may be explained by disease stage heterogeneity, timing of biomarker measurement, or the evaluation of plasma rather than cerebrospinal fluid (CSF) levels.[15]

In this study, the measured biomarkers did not differ significantly between the Alzheimer's and control groups. These findings indicate the limited diagnostic value of current biomarkers and highlight the need for larger-scale longitudinal studies including CSF/plasma correlation analyses.

The discriminative power of Aβ40, Aβ42, BACE-1, t-tau, and p-tau levels in the diagnosis of AD, as well as the Aβ42/Aβ40 ratio, was evaluated using ROC analysis. The AUC values for all biomarkers were below 0.6 (AUC of Aβ42/Aβ40 ratio was 0.608 and AUC of t-tau is 0.613 these results do not demonstrate a significant discriminatory performance). Generally, tests with AUC values close to 0.5 have only chance-level discriminatory ability. Specifically, the AUC values for Aβ42 and Aβ40 were 0.514 and 0.547, respectively, indicating insufficient diagnostic value to distinguish AD. Although BACE-1 had a relatively higher AUC of 0.592 compared with other biomarkers, it did not reach statistical significance. The highest AUC was observed for t-tau at 0.613; however, the CI was wide, and statistical significance was not achieved. This suggests that t-tau alone is inadequate for diagnosis and should be evaluated alongside

other parameters. P-tau also demonstrated poor discriminatory ability, with an AUC of 0.542.

The plasma Aβ42/Aβ40 ratio did not differ significantly between AD patients and controls, and its direction of effect was opposite to that observed in larger cohorts using ultrasensitive plasma assays. This observation should be interpreted with caution: conventional ELISA has limited sensitivity at the low plasma Aβ42 concentrations present in peripheral blood, and the performance of the ratio in plasma has been shown to depend strongly on the analytical platform used. Our null and directionally reversed finding should not, therefore, be taken as evidence against the utility of the ratio; rather, it supports the need for larger, prospectively designed studies using ultrasensitive platforms (e.g., Simoa, IP-MS) to establish the diagnostic value of this ratio.

Finally, correlations among Aβ40, Aβ42, BACE-1, t-tau, and p-tau protein levels were investigated, revealing positive associations among some biomarkers.

The high correlation coefficients observed between Aβ40-Aβ42, Aβ42-BACE-1, and BACE-1-t-tau suggest that these proteins participate in shared biological processes underlying the pathophysiology of AD. The correlation between Aβ peptides, which are generated by cleavage of APP, and BACE-1, which plays a key role in this process, supports the interconnected nature of these biochemical pathways.[16]

Similarly, the significant correlations detected between Aβ peptide levels and t-tau indicate that amyloid accumulation may be associated with neuronal degeneration. These findings imply that AD could be conceptualized as a spectrum involving both amyloid and tau pathologies.[17]

In contrast, the lack of significant correlations between p-tau levels and other proteins is noteworthy. Notably, the absence of a correlation between t-tau and p-tau suggests that these two markers may reflect distinct pathological processes. The formation of p-tau via hyperphosphorylation may represent a regulatory mechanism independent of t-tau levels. Overall, the correlation analyses reveal substantial interactions among Alzheimer's biomarkers but also indicate that certain markers, such as p-tau, may behave more independently. This underscores the importance of carefully selecting combinations of diagnostic and prognostic biomarkers.[18]

The use of ELISA kits from different manufacturers to assess distinct biomarkers represents a methodological limitation of the present study. Using a particular kit for p-tau measurement, while other brand kits were used for the remaining analytes, may increase the risk of inter-assay variability due to differences in calibration standards, assay sensitivity, and potential cross-reactivity between platforms. This may limit the direct comparability of absolute biomarker concentrations across assays. Therefore, the results should be interpreted with consideration of this methodological heterogeneity.

The central finding of this study is that none of the five plasma biomarkers (Aβ40, Aβ42, BACE-1, t-tau, p-tau) nor the Aβ42/Aβ40 ratio showed a statistically significant difference between AD patients and healthy controls. ROC analyses yielded AUC values between 0.51 and 0.61, and all 95% CIs included the chance line (AUC = 0.50). These results should not be interpreted as marginal or promising; the rank-biserial effect sizes were uniformly small ($r \leq 0.19$), indicating that the underlying group separation on these plasma measures was limited in magnitude, even in the absence of statistical significance.

Large-scale studies conducted worldwide have shown that the plasma Aβ42/Aβ40 ratio correlates with CSF biomarkers and neuroimaging biomarkers in early-stage AD.[19]

Although there is general consensus regarding the association of CSF Aβ levels with AD, studies evaluating peripheral Aβ biomarkers in plasma have shown conflicting results. Some studies have reported no relationship between plasma Aβ levels and AD,[20-22] while others have revealed relationships in opposite directions.[23] However, recent studies involving well-characterized large participant populations have shown that a lower plasma Aβ42/40 ratio is consistently associated with an increased risk of incident AD.[24-26]

Although CSF analysis and positron emission tomography imaging are widely utilized in the diagnosis of AD and are considered highly accurate, these methods have certain limitations. For instance, they may impose a substantial economic burden, involve invasive procedures, and require complex organization. Therefore, the aim in both the present study and similar studies conducted worldwide is to develop approaches that enable early diagnosis of AD using plasma-based biomarkers.

In this study, multivariate analysis identified age and educational level as significant predictors of AD. The marked increase in the likelihood of receiving an AD diagnosis with advancing age reflects the strong association between the disease and age-related neurodegenerative processes, consistent with findings frequently reported in the literature.

The findings of this study revealed that the risk of AD increases with higher educational attainment. However, the literature suggests that increased education strengthens "cognitive reserve", thereby reducing the risk of AD.[27] The divergent finding observed in our study may be attributable to changes in working conditions associated with higher education, increased exposure to stressors, a sedentary lifestyle, and the adverse effects of urbanization. Moreover, improved access to healthcare services among individuals with higher educational levels, leading to more frequent diagnosis of AD, may represent another possible explanation.[28]

The strong association between age and AD is consistent with existing literature showing that AD risk increases with advancing age. Although female sex is known as a risk factor for AD,[29,30] the lack of statistically meaningful results regarding sex differences in our study is understandable due to the uneven distribution of genders in the Alzheimer's group (19 females vs. 5 males).

Further studies are needed to clarify the impact of comorbidities and a history of head trauma on AD.[31]

The significantly lower smoking rate in the Alzheimer's group, compared to controls, may be related to lifestyle changes associated with disease progression, such as reduced ability to live independently and increased supervision. It is also possible that smoking cessation or a forgotten smoking history among AD patients contributed to this finding. The effects of smoking on AD have long been debated because nicotine's potentially protective effects may be offset by the harmful effects of the many toxic chemicals in tobacco.[32]

Alcohol consumption history was not obtained for the Alzheimer's group, possibly due to caregiver-imposed restrictions or the patients' inability to recall previous habits. Although a higher rate of alcohol use was noted in the control group, this difference was not statistically significant. Moreover, the role of alcohol in AD risk remains controversial, depending on the quantity and type of alcohol consumed.[33]

A statistically significant difference was found between groups in coffee consumption ($p < 0.001$). This difference may be due to fewer participants in the Alzheimer's group reporting occasional coffee consumption ($p = 0.009$), whereas a higher proportion reported consuming one cup daily. Overall, coffee consumption was more prevalent in the Alzheimer's group. The cognitive effects of caffeine-containing beverages, such as coffee, remain controversial in the literature.[34] Larger prospective studies are needed to draw firmer conclusions.

One of the most noteworthy findings of this study is the protective effect of tea consumption against AD. Individuals who consumed tea had significantly lower odds of developing AD. This protective association may be explained by antioxidants present in tea (e.g., catechins and flavonoids), the neuroprotective effects of tea, and the positive influence of caffeine on synaptic plasticity.[35] However, it should be emphasized that this finding represents an association rather than causation. Further prospective and biochemically supported studies are required to clarify the underlying mechanisms.

While the literature suggests a protective effect of the Mediterranean diet on AD,[36] no significant difference was detected between groups in terms of dietary habits in our study. Given the long-term impact of diet on AD risk, it is plausible that the Alzheimer's group's inability to accurately recall past dietary habits influenced this result.

Notably, all individuals in the Alzheimer's group reported engaging in exercise in recent years. However, this may be explained by the perception of low-intensity activities, such as daily short walks, as "exercise." In contrast, a significant proportion of the control group reported not exercising, which warrants careful consideration when interpreting results for the Alzheimer's group. This finding contradicts the majority of the literature reporting the protective effects of physical exercise on AD.[37]

Lifestyle variables were collected by self-report or caregiver report. In a cohort with documented cognitive impairment, these data are susceptible to recall and perception biases (for example, daily short walks reported as "regular exercise"), which may explain the paradoxical finding that 100% of AD patients reported exercising in recent years.

A family history of AD was reported at only 12.5%, suggesting a limited genetic predisposition in the sample. However, this prevalence may not reflect the true rate due to patients' inability to provide accurate information and to incomplete anamnesis obtained from relatives. Although genetic predisposition is recognized as a significant risk factor in AD, community-based studies have also shown that the disease can develop in individuals without a family history.[38]

The high proportion of individuals living in urban centers prior to diagnosis (79.2%) suggests potential environmental effects of urban living on AD. However, this finding may primarily reflect demographic characteristics of the sample, such as easier access to healthcare services and a higher likelihood of diagnosis in urban areas. Lower diagnosis rates in rural regions may be related to limited disease awareness or restricted access to healthcare services.[39]

These findings indicate a heterogeneous nature of AD in terms of disease progression, familial history, and environmental factors. Supporting these clinical data with larger samples and longer follow-up periods will contribute to a better understanding of individual and environmental determinants of the disease.

Study limitations

This study has certain limitations. First, the sample size was relatively small (a total of 61 participants: 24 patients with AD and 37 healthy controls), which may limit the statistical power and generalizability of the findings. Obtaining the required sample from patients is ethically constrained, resulting in "disease stage heterogeneity" within the patient group. As a single-center study, it does not allow comparisons across different geographical regions or sociocultural backgrounds. The cross-sectional design further restricts the ability to establish causal relationships. Moreover, potential confounding variables such as lifestyle factors, dietary habits, and genetic predispositions could not be fully controlled. Given the limited number of studies measuring the proteins investigated in our study using ELISA with different commercial kits, the extent to which inter-assay (kit/brand-related) variability may influence the comparability of results remains uncertain, and the results should therefore be interpreted with caution.

A sensitivity analysis indicated that the present sample was adequately powered to detect moderate or larger between-group differences (rank-biserial $r \geq 0.36$) for each plasma biomarker under a Mann–Whitney U framework, but not small effects ($r < 0.36$). The observed effects were small ($r = 0.02$–0.19), consistent with limited separation between groups in plasma amyloid and tau measurements in this cohort. Detecting effects of this magnitude would require considerably larger cohorts of several hundred participants per group, which is difficult to achieve in a single-center study of a frail, elderly AD population. These findings are therefore presented as hypothesis-generating.

Lifestyle variables were collected via self- or caregiver report. Their susceptibility to recall and perception biases in a cognitively impaired cohort (e.g., daily short walks reported as "regular exercise") limits the interpretability of the data.

Although the present findings do not demonstrate strong diagnostic performance, the investigated biomarkers may still contribute to future biomarker-guided therapeutic strategies and patient stratification approaches in AD.

CONCLUSION

In this case-control study, plasma levels of Aβ40, Aβ42, BACE-1, t-tau, p-tau , and the Aβ42/Aβ40 ratio did not differ between AD patients and healthy controls, and none of these markers, alone or as a ratio, demonstrated adequate discriminative power (all AUCs below 0.62).These null findings should not be interpreted as evidence that plasma biomarkers lack clinical value in general; rather, they likely reflect the limitations of a single-center design and modest sample size, heterogeneity in disease stage, and the known lower sensitivity of plasma assays compared with CSF for detecting amyloid and tau pathology.

Ethics

Ethics Committee Approval: This study was approved by the Ethics Committee on Ankara University (decision no: İ3-148-20, date: 12.10.2020).

Informed Consent: Legal guardians of the patients were informed about the study, and written consent was obtained. The patient group consisted of residents of a nursing home who had been diagnosed with AD by specialized physicians at fully equipped hospitals.

Footnotes

Authorship Contributions

Surgical and Medical Practices: N.M.G.A., B.Ö.P., B.C.E., Concept: N.Y., B.C.E., Design: N.Y., B.C.E., Data Collection or Processing: N.Y., N.M.G.A., B.C.E., Analysis or Interpretation: N.Y., B.C.E., Literature Search: N.Y., B.E., Writing: N.Y., B.C.E.

Conflict of Interest: The authors declare no conflicts of interest.

Financial Disclosure: This research was supported by the 21L0237005 project number of Ankara University Scientific Research Projects Coordination Office.

REFERENCES

1. Uddin MS, Kabir MT, Tewari D, Mamun AA, Mathew B, Aleya L, Ashraf GM. Revisiting the role of brain and peripheral Aβ in the pathogenesis of Alzheimer's disease. J Neurol Sci. 2020;416:116974.
2. Mendez MF. Early-onset Alzheimer disease. Neurologic clinics. 2017;35:263-81.
3. Jia J, Ning Y, Chen M, Wang S, Yang H, Li F, Ding J, Li Y, Zhao B, Lyu J, Yang S, Yan X, Wang Y, Qin W, Wang Q, Li Y, Zhang J, Liang F, Liao Z, Wang S. Biomarker changes during 20 years preceding Alzheimer's disease. N Engl J Med. 2024;390:712-722.
4. Gouilly D, Rafiq M, Nogueira L, Salabert AS, Payoux P, Péran P, Pariente J. Beyond the amyloid cascade: an update of Alzheimer's disease pathophysiology. Rev Neurol (Paris). 2023;179:812-830.
5. Seath P, Macedo-Orrego LE, Velayudhan L. Clinical characteristics of early-onset versus late-onset Alzheimer's disease: a systematic review and meta-analysis. Int Psychogeriatr. 2024;36:1093-1109.
6. Jack CR Jr, Andrews JS, Beach TG, Buracchio T, Dunn B, Graf A, Hansson O, Ho C, Jagust W, McDade E, Molinuevo JL, Okonkwo OC, Pani L, Rafii MS, Scheltens P, Siemers E, Snyder HM, Sperling R, Teunissen CE, Carrillo MC. Revised criteria for diagnosis and staging of Alzheimer's disease: Alzheimer's Association Workgroup. Alzheimers Dement. 2024;20:5143-5169.
7. Orobets KS, Karamyshev AL. Amyloid precursor protein and Alzheimer's disease. Int J Mol Sci. 2023;24:14794.
8. Mudher A, Colin M, Dujardin S, Medina M, Dewachter I, Alavi Naini SM, Mandelkow EM, Mandelkow E, Buée L, Goedert M, Brion JP. What is the evidence that tau pathology spreads through prion-like propagation? Acta Neuropathol Commun. 2017;5:99.
9. Srivastava S, Ahmad R, Khare SK. Alzheimer's disease and its treatment by different approaches: a review. Eur J Med Chem. 2021;216:113320.
10. Briggs R, Kennelly SP, O'Neill D. Drug treatments in Alzheimer's disease. Clin Med (Lond). 2016;16:247-253.
11. Passeri E, Elkhoury K, Morsink M, Broersen K, Linder M, Tamayol A, Malaplate C, Yen FT, Arab-Tehrany E. Alzheimer's disease: treatment strategies and their limitations. Int J Mol Sci. 2022;23:13954.
12. Wilson RS, Arnold SE, Schneider JA, Kelly JF, Tang Y, Bennett DA. Chronic psychological distress and risk of Alzheimer's disease in old age. Neuroepidemiology. 2006;27:143-153.
13. Rissman RA, Langford O, Raman R, Donohue MC, Abdel-Latif S, Meyer MR, Wente-Roth T, Kirmess KM, Ngolab J, Winston CN, Jimenez-Maggiora G, Rafii MS, Sachdev P, West T, Yarasheski KE, Braunstein JB, Irizarry M, Johnson KA, Aisen PS, Sperling RA; AHEAD 3-45 Study team. Plasma Aβ42/Aβ40 and phospho-tau217 concentration ratios increase the accuracy of amyloid PET classification in preclinical Alzheimer's disease. Alzheimers Dement. 2024;20:1214-1224.
14. Wu G, Sankaranarayanan S, Wong J, Tugusheva K, Michener MS, Shi X, Cook JJ, Simon AJ, Savage MJ. Characterization of plasma β-secretase (BACE1) activity and soluble amyloid precursor proteins as potential biomarkers for Alzheimer's disease. J Neurosci Res. 2012;90:2247-2258.
15. Stevenson-Hoare J, Heslegrave A, Leonenko G, Fathalla D, Bellou E, Luckcuck L, Marshall R, Sims R, Morgan BP, Hardy J, de Strooper B, Williams J, Zetterberg H, Escott-Price V. Plasma biomarkers and genetics in the diagnosis and prediction of Alzheimer's disease. Brain. 2023;146:690-699.
16. Hampel H, Vassar R, De Strooper B, Hardy J, Willem M, Singh N, Zhou J, Yan R, Vanmechelen E, De Vos A, Nisticò R, Corbo M, Imbimbo BP, Streffer J, Voytyuk I, Timmers M, Tahami Monfared AA, Irizarry M, Albala B, Koyama A, Watanabe N, Kimura T, Yarenis L, Lista S, Kramer L, Vergallo A. The β-secretase BACE1 in Alzheimer's disease. Biol Psychiatry. 2021;89:745-756.
17. Karran E, De Strooper B. The amyloid hypothesis in Alzheimer disease: new insights from new therapeutics. Nat Rev Drug Discov. 2022;21:306-318.
18. Rawat P, Sehar U, Bisht J, Selman A, Culberson J, Reddy PH. Phosphorylated tau in Alzheimer's disease and other tauopathies. Int J Mol Sci. 2022;23:12841.
19. Pérez-Grijalba V, Romero J, Pesini P, Sarasa L, Monleón I, San-José I, Arbizu J, Martínez-Lage P, Munuera J, Ruiz A, Tárraga L, Boada M, Sarasa M. Plasma Aβ42/40 ratio detects early stages of Alzheimer's

disease and correlates with CSF and neuroimaging biomarkers in the AB255 study. J Prev Alzheimers Dis. 2019;6:34-41.

20. Hansson O, Zetterberg H, Vanmechelen E, Vanderstichele H, Andreasson U, Londos E, Wallin A, Minthon L, Blennow K. Evaluation of plasma Abeta(40) and Abeta(42) as predictors of conversion to Alzheimer's disease in patients with mild cognitive impairment. Neurobiol Aging. 2010;31:357-367.
21. Lopez OL, Kuller LH, Mehta PD, Becker JT, Gach HM, Sweet RA, Chang YF, Tracy R, DeKosky ST. Plasma amyloid levels and the risk of AD in normal subjects in the cardiovascular health study. Neurology. 2008;70:1664-1671.
22. Lövheim H, Elgh F, Johansson A, Zetterberg H, Blennow K, Hallmans G, Eriksson S. Plasma concentrations of free amyloid β cannot predict the development of Alzheimer's disease. Alzheimers Dement. 2017;13:778-782.
23. Mehta PD, Pirttila T, Patrick BA, Barshatzky M, Mehta SP. Amyloid beta protein 1-40 and 1-42 levels in matched cerebrospinal fluid and plasma from patients with Alzheimer disease. Neurosci Lett. 2001;304:102-106.
24. Chouraki V, Beiser A, Younkin L, Preis SR, Weinstein G, Hansson O, Skoog I, Lambert JC, Au R, Launer L, Wolf PA, Younkin S, Seshadri S. Plasma amyloid-β and risk of Alzheimer's disease in the Framingham Heart Study. Alzheimers Dement. 2015;11:249-57.e1.
25. Graff-Radford NR, Crook JE, Lucas J, Boeve BF, Knopman DS, Ivnik RJ, Smith GE, Younkin LH, Petersen RC, Younkin SG. Association of low plasma Abeta42/Abeta40 ratios with increased imminent risk for mild cognitive impairment and Alzheimer disease. Arch Neurol. 2007;64:354-362. Erratum in: Arch Neurol. 2007;64:1246.
26. Lambert JC, Schraen-Maschke S, Richard F, Fievet N, Rouaud O, Berr C, Dartigues JF, Tzourio C, Alpérovitch A, Buée L, Amouyel P. Association of plasma amyloid beta with risk of dementia: the prospective Three-City Study. Neurology. 2009;73:847-853.
27. Rosselli M, Uribe IV, Ahne E, Shihadeh L. Culture, ethnicity, and level of education in Alzheimer's disease. Neurotherapeutics. 2022;19:26-54.
28. Seyedsalehi A, Warrier V, Bethlehem RAI, Perry BI, Burgess S, Murray GK. Educational attainment, structural brain reserve and Alzheimer's disease: a mendelian randomization analysis. Brain. 2023;146:2059-2074.
29. Nebel RA, Aggarwal NT, Barnes LL, Gallagher A, Goldstein JM, Kantarci K, Mallampalli MP, Mormino EC, Scott L, Yu WH, Maki PM, Mielke MM. Understanding the impact of sex and gender in Alzheimer's disease: a call to action. Alzheimers Dement. 2018;14:1171-1183.
30. Riedel BC, Thompson PM, Brinton RD. Age, APOE and sex: triad of risk of Alzheimer's disease. J Steroid Biochem Mol Biol. 2016;160:134-147.
31. Mckee AC, Daneshvar DH. The neuropathology of traumatic brain injury. Handb Clin Neurol. 2015;127:45-66.
32. Wang Q, Du W, Wang H, Geng P, Sun Y, Zhang J, Wang W, Jin X. Nicotine's effect on cognition, a friend or foe? Prog Neuropsychopharmacol Biol Psychiatry. 2023;124:110723.
33. Peng B, Yang Q, B Joshi R, Liu Y, Akbar M, Song BJ, Zhou S, Wang X. Role of alcohol drinking in Alzheimer's disease, Parkinson's Disease, and amyotrophic lateral sclerosis. Int J Mol Sci. 2020;21:2316.
34. Nila IS, Villagra Moran VM, Khan ZA, Hong Y. Effect of daily coffee consumption on the risk of Alzheimer's disease: a systematic review and meta-analysis. J Lifestyle Med. 2023;13:83-89.
35. Ide K, Matsuoka N, Yamada H, Furushima D, Kawakami K. Effects of tea catechins on Alzheimer's disease: recent updates and perspectives. Molecules. 2018;23:2357.
36. Stefaniak O, Dobrzyńska M, Drzymała-Czyż S, Przysławski J. Diet in the prevention of Alzheimer's disease: current knowledge and future research requirements. Nutrients. 2022;14:4564.
37. De la Rosa A, Olaso-Gonzalez G, Arc-Chagnaud C, Millan F, Salvador-Pascual A, García-Lucerga C, Blasco-Lafarga C, Garcia-Dominguez E, Carretero A, Correas AG, Viña J, Gomez-Cabrera MC. Physical exercise in the prevention and treatment of Alzheimer's disease. J Sport Health Sci. 2020;9:394-404.
38. Karch CM, Cruchaga C, Goate AM. Alzheimer's disease genetics: from the bench to the clinic. Neuron. 2014;83:11-26.
39. Karmarkar AM, Roy I, Lane T, Shaibi S, Baldwin JA, Kumar A. Home health services for minorities in urban and rural areas with Alzheimer's and related dementia. Home Health Care Serv Q. 2023;42:265-281.

Turk J Pharm Sci 2026;23(2):75-84
DOI: 10.4274/tjps.galenos.2026.27927

ORIGINAL ARTICLE

Establishment and Validation of a Stability-Indicating RP-HPLC Protocol for Mavacamten in Oral Capsule Preparations

Pratibha Atul DAROI[1]*, Pranjali PATIL[1], Vijay MUNIPALLI[2], Bhushan SONAWANE[2]

[1]LSHGCT's Gahlot Institute of Pharmacy, Department of Pharmaceutical Quality Assurance, Koparkhairne, Navi Mumbai, Maharashtra, India
[2]Central Drugs Testing Laboratory, Zonal FDA Bhavan, Department of Analytical Research and Development Mumbai, Maharashtra, India

ABSTRACT

Objectives: Mavacamten (MYK-461), approved for hypertrophic cardiomyopathy, is a cardiac myosin inhibitor. At present, no pharmacopoeial method for its quantification has been reported. Our study was designed to establish a validated stability-indicating reverse-phase high-performance liquid chromatography method to quantify MYK-461 in its capsule formulation.

Materials and Methods: For chromatographic separation, an Inertsil ODS-3V C18 column (250 × 4.6 mm, 5 µm) with the mobile phase of 0.1% trifluoroacetic acid and acetonitrile (50:50 v/v) was used. The flow rate (1.0 mL/min), column temperature (35 ˚C), injection volume (10 µL), total run time (10 minutes), and detection wavelength (269 nm) were applied.

Results: The validated method showed precision, accuracy, and robustness, with relative standard deviation < 2% and recovery of 100.5%. Linearity was observed over the range 5–75 µg/mL (r = 0.9994). We achieved a clear, well-resolved separation of MYK-461 from impurities, with estimated limit of detection (1.58 µg/mL) and limit of quantification (4.8 µg/mL). In forced degradation studies, we observed the highest degradation under acidic conditions (10.37%), while minimal degradation under photolytic (0.93%), thermal (1.66 %), oxidative (2.56%), and alkaline (4.19%) conditions.

Conclusion: The developed method is precise and reliable, and offers a practical tool for routine quality control and future research, while emphasising the need for controlled storage conditions to ensure long-term drug integrity.

Keywords: Forced degradation, mavacamten, cardiomyopathy, RP-HPLC, validation

INTRODUCTION

Cardiomyopathies represent a diverse array of myocardial anomalies denoted by structural and functional impairments without having overt coronary artery disease, hypertension, valve dysfunction, or structural malformation at birth.[1-3] Advances in genetic and molecular diagnostics have revealed that many forms of cardiomyopathy, including hypertrophic, dilated, and arrhythmogenic types, are frequently associated with pathogenic gene variants affecting sarcomere or desmosomal proteins.[4] Recent studies have also emphasised the role of inflammation, autoimmunity, and metabolic deregulation in the pathogenesis and progression of these conditions, offering novel targets for precision therapy.[5-8] International Union of Pure and Applied Chemistry of mavacamten is 6-{[(1S)-1-phenylethyl] amino}-3-propane-2-yl-1H-pyrimidine-2,4-dione, as depicted in Figure 1.

Mavacamten got FDA approval in April 2022 for managing symptomatic obstructive hypertrophic cardiomyopathy (HCM), thus offering a unique treatment option for adults with obstructive HCM under New York Heart Association (NYHA) class II-III.[9,10]

***Correspondence:** pratibhadaroi@gmail.com, **ORCID-ID:** orcid.org/0000-0002-2481-4960

Received: 20.08.2025 **Accepted:** 18.08.2026 **Publication Date:** 01.09.2026

Cite this article as: Daroi PA, Patil P, Munipalli V, Sonawane B. Establishment and validation of a stability-indicating RP-HPLC protocol for mavacamten in oral capsule preparations. Turk J Pharm Sci. 2026;23(2):75-84

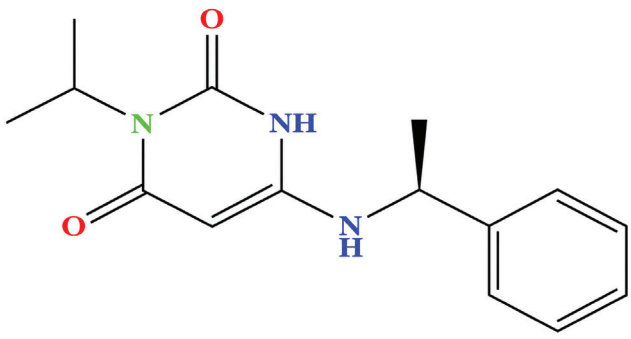

Figure 1. Mavacamten structure.

HCM is marked by abnormal thickening of the myocardial wall, which increases the propensity for severe arrhythmias and transient cardiac arrest. This condition typically stems from excessive thickening of the wall of the left ventricle, which compromises cardiac output. In cases of symptomatic obstructive HCM, mavacamten has become a game-changing treatment.[11] Mavacamten binds reversibly to cardiac β-myosin heavy chain, a motor protein involved in cardiac muscle contraction. It inhibits myosin ATPase activity, reducing excessive ATP-driven cross-bridge formation between actin and myosin. In HCM, hypercontractility results in left ventricular outflow tract (LVOT) obstruction.[12] Mavacamten inhibits cross-bridging between actin and myosin filaments, thus normalising contractile force without overly compromising systolic function. By reducing myocardial tension, it promotes ventricular relaxation and lowers the LVOT gradient, resulting in improved diastolic filling. Eventually, all these mechanisms result in decreased cardiac hypertrophy, improved exercise capacity, and reduced risk of symptoms associated with obstructive HCM.[13] The most common side effects reported with mavacamten during the clinical studies are dizziness and fainting.[14] The MOA of mavacamten is unique, and it differs from that of drugs like β-blockers as well as calcium channel blockers, commonly employed to treat HCM cases.[15] Mavacamten has demonstrated significant clinical benefits in reducing symptoms, improving exercise tolerance, and reversing heart muscle thickening in patients with obstructive HCM. However, it requires close monitoring, as it may temporarily reduce cardiac function. Precise and reliable analytical methods are essential to ensure proper dosing, effectiveness, and safety in clinical use.

Being a pioneering cardiac myosin inhibitor of its kind, mavacamten is approved on five continents for the treatment of HCM in individuals classified under NYHA class II or III, aiming to modulate cardiac efficiency and alleviate symptoms.[16] To the best of our knowledge, no reverse-phase chromatographic techniques for mavacamten have been reported in the literature, nor has there been an analytical method documented in any pharmacopoeia. To address this need, we developed a stability-indicating reverse-phase high-performance liquid chromatography (RP-HPLC) method that can be reliably used to quantify mavacamten in capsules. This method was subsequently validated under the ICH Q2 (R1) standards.

It has been increasingly emphasized that ensuring the intrinsic stability and degradation behaviour of pharmaceutical compounds is important. Forced degradation (FD) studies were undertaken to serve this objective, as they are critical to pharmacological efficacy and safety of the product under investigation. Stress testing and FD investigation underscored the stability-indicating nature of the developed method, focusing on the predominant degradation pathways, notably acid-induced hydrolysis. Our study provides a rapid chromatographic technique that caters to both advanced clinical studies and routine quality assurance testing.

MATERIALS AND METHODS

Reagents and chemicals

A certified reference standard of mavacamten (purity: 99.74%) and a bulk drug sample were obtained from the Central Drug Testing Laboratory, Mumbai, India. Commercial capsule formulations containing mavacamten (CAMZYOS®, in strengths equivalent to 2.5, 5, and 10 mg), manufactured by Bristol-Myers Squibb, were used in method development and validation studies.

Chromatographic analyses were performed using acetonitrile of HPLC grade (purity ≥ 99.9%). Trifluoroacetic acid, triethylamine, and potassium dihydrogen phosphate of analytical reagent grade (purity ≥ 99.0%) were sourced from Rankem, India. High-purity water generated through a Milli-Q® water purification system (18.2 MΩ·cm resistivity) was employed for the preparation of mobile phase components, standard solutions, sample solutions, and all subsequent dilutions. All reagents and solvents were used as received without further purification.

Instruments

For chromatographic analysis of mavacamten, a Dionex Ultimate 3000 HPLC system from Thermo Scientific was used. Because the UV/VIS detector was compatible with the chromophoric groups of mavacamten, it was used with an adjustable wavelength selection, allowing sensitive detection at 269 nm.

Methodology

Preparation of a mobile phase

A mobile phase comprising acetonitrile and 0.1% (v/v) trifluoroacetic acid (50:50, v/v) was prepared. The 0.1% trifluoroacetic acid solution was obtained by diluting 1.0 mL of trifluoroacetic acid to 1000 mL with HPLC-grade purified water. The resulting mobile phase was filtered through a 0.45 µm membrane filter, sonicated, and degassed before chromatographic analysis.

Preparation of the sample solution from formulated capsules

To obtain a 50 µg/mL concentration, 5 mg of mavacamten was dissolved in the same diluent, and the solution was diluted to 100 mL to prepare the sample solution. The solution was then passed through 0.45 µm membranes and sonicated for 10 minutes to ensure complete solubility and to avoid particle interference.

Preparation for the standard and calibration curve solution

The intermediate stock solution of 100 μg/mL was prepared. For this purpose, a 10-mg mavacamten reference standard was accurately weighed and dissolved in a diluent in a volumetric flask to obtain a final volume of 100 mL. By utilising a 70:30% v/v ratio of acetonitrile-water as the diluent, 5 mL of a 100 μg/mL intermediate solution was diluted to 10 mL to produce the standard solution with a concentration of 50 μg/mL. A 100 μg/mL stock solution was used for calibration and subsequent dilutions. Mavacamten standard solutions at concentrations between 5 and 75 μg/mL were prepared and added to the system. A calibration curve established the relationship between the analyte content and the detector response, enabling evaluation of the method's linearity.

Chromatographic conditions

The UV spectrophotometer was used to perform spectral scanning between 200 and 400 nm of a standard solution of mavacamten (50 μg/mL). UV detection revealed an absorption peak (λ_{max}) at 269 nm. Separation was achieved on an Inertsil ODS-3V C18 column (250 × 4.6 mm, 5 μm) at 35 °C, employing an isocratic mobile phase with a 50:50 v/v composition of 0.1% trifluoroacetic acid added to acetonitrile. To reduce carryover, ensure mobile phase integrity, and maintain constant chromatographic performance, an autosampler with a fixed-volume loop and integrated needle rinse was used to add a 10 μL injection. Flow uniformity and baseline stability of the detector were achieved using degassing devices. A Millipore filtration system with 0.45 μm membrane filters was used to remove particulate matter.

Validation

System suitability

Key chromatographic variables such as peak area, number of theoretical plates, tailing factor, and retention time were assessed by 6 consequetive injections of standard mavacamten solution (50 μg/mL).

Specificity

The chromatograms of the blank, the mavacamten sample, and the standard were recorded and evaluated for the presence of interfering or impurity peaks.

Linearity, limit of detection (LOD) and limit of quantification (LOQ)

Standard solutions of mavacamten in the concentration range of 5–75 μg/mL were prepared and injected into the HPLC system. A calibration curve was constructed by plotting peak area against analyte concentration to evaluate the linearity of the developed method.

Linearity was assessed using least-squares linear regression analysis. The slope, intercept, and correlation coefficient (r) were obtained from the regression equation. The limits of detection and quantification were estimated using the standard deviation (SD) of the response (σ) and the slope of the calibration curve (S), according to the following equations: LOD = 3.3σ/S, LOQ = 10σ/S.

Accuracy

Using the standard addition method, sample solutions were spiked at 4 levels, viz., 100%, 110%, 120%, and 130%, and the mean recovery (%) was assessed. Solutions at concentrations of 50 μg/mL, 55 μg/mL, 60 μg/mL, and 65 μg/mL were prepared. Accuracy was evaluated using a recovery study, and the results were expressed as percent recovery.

Precision

The precision of the developed RP-HPLC method was evaluated in terms of repeatability (intraday precision) and intermediate precision (interday precision).

Intraday precision was assessed by analysing six replicate preparations of mavacamten at a concentration of 50 μg/mL across three time points on the same day: morning (10:00 AM), afternoon (1:00 PM), and evening (4:00 PM). The assay values obtained at each time point were used to determine the mean, SD, and percentage relative SD (RSD %).

Intermediate precision was evaluated by analysing six replicate preparations of mavacamten (50 μg/mL) on two different days by different analysts under the same chromatographic conditions. The assay results obtained on each day were statistically evaluated in terms of mean assay, SD, and RSD %.

The precision of the method was expressed as the percentage relative SD (RSD %), and values not exceeding 2.0% were considered acceptable.

Robustness

Robustness was evaluated to assess the influence of small, deliberate changes in chromatographic conditions. Variations were introduced in the detection wavelength (± 2 nm), flow rate (± 0.2 mL/min), column temperature (± 2 °C), and mobile phase composition (± 2%, v/v). The influence of these changes on the assay results was evaluated by calculating the assay percentage and RSD %.

Content uniformity analysis of mavacamten capsules

The developed method was applied to determine the content uniformity of mavacamten capsules available in 2.5 mg, 5 mg, and 10 mg dosage strengths to assess the consistency of drug distribution among individual dosage units. Sample solutions (50 μg/mL) were prepared using a diluent of acetonitrile: water (70:30 v/v) by precisely diluting each dosage strength to final volumes of 50 mL (2.5 mg), 100 mL (5 mg), and 200 mL (10 mg).

FD studies

FD studies were performed under acidic, alkaline, oxidative, thermal, and photolytic stress conditions to evaluate the stability-indicating capability of the developed RP-HPLC method. For acidic degradation, 1.0 mL of the standard stock solution was mixed with 1.0 mL of 0.1 M hydrochloric acid, and the mixture was maintained under the specified stress conditions. Following the degradation period, the solution was neutralised with an equivalent volume of 0.1 M sodium hydroxide and then diluted to 10 mL with a diluent consisting of acetonitrile and water (70:30 v/v).

For alkaline degradation, 1.0 mL of the standard stock solution was treated with 1.0 mL of 0.1 M sodium hydroxide. After completion of the stress exposure period, the solution was neutralised using an equivalent volume of 0.1 M hydrochloric acid and diluted to 10 mL with the diluent.

Oxidative degradation was carried out by treating the standard stock solution with 3% (v/v) hydrogen peroxide and maintaining the mixture under prescribed conditions before dilution. Thermal degradation studies were performed by exposing the standard solution to 60 °C in a hot air oven for 24 h. For photolytic degradation, the standard solution was exposed to ultraviolet radiation at 254 nm in a UV chamber for 24 h.

After completion of the respective stress treatments, all samples were appropriately diluted with the diluent, filtered through a 0.45 µm membrane filter, and analysed using the developed RP-HPLC method.

Statistical analysis

Data acquisition and chromatographic processing were performed using the Chromeleon™ Chromatography Data System (version 7.2.6, Thermo Fisher Scientific, USA). Statistical calculations were performed using Microsoft Excel (version 2021; Microsoft Corporation, Redmond, WA, USA).

Ethical approval and informed consent

Ethics committee approval and informed consent were not required for this study, as the research involved only the development and validation of an analytical method for pharmaceutical drug samples and did not involve human participants, animals, human-derived biological samples, or identifiable personal data.

RESULTS

Method development

Chromatographic separation

Accurate detection of the analyte at 269 nm was facilitated by the use of an Inertsil ODS-3V C18 column (4.6 mm × 250 mm, particle size 5 µm), acetonitrile and a 0.1% trifluoroacetic acid solution (50:50 v/v) as the mobile phase, a runtime of 10 minutes, and a flow rate of 1.0 mL/min. A symmetric peak tailing factor of 1.12 and a retention period of 5.06 minutes indicated separation.

Method validation

Linearity

The developed RP-HPLC method exhibited a satisfactory linear relationship within the validated concentration range of 5–75 µg/mL, yielding a correlation coefficient (r) of 0.9994. The corresponding peak area responses at different concentration levels are summarised in Table 1, whereas the calibration profile is illustrated in Figure 2. Regression analysis yielded the equation y = 744.38x + 3061, where y denotes the chromatographic peak area and x represents the analyte concentration (µg/mL). The sensitivity of the method was evaluated by determining the limits of detection and quantification, which were found to be 1.58 µg/mL and 4.8 µg/mL, respectively. Low limits of detection and quantification indicate that the proposed method has adequate sensitivity for the routine estimation of mavacamten in capsule dosage forms.

Table 1. Linearity data of mavacamten.

Concentration (µg/mL)	Peak area 1	Peak area 2	Peak area 3	Average area
5	5819	5818	5817	5820
10	10571	10574	10573	10574
20	18202	18201	18200	18201
30	25877	25876	25878	25878
40	33203	33204	33203	33204
50	40561	43560	40562	40562
60	48215	48216	48217	48216
75	57907	57906	57908	57907

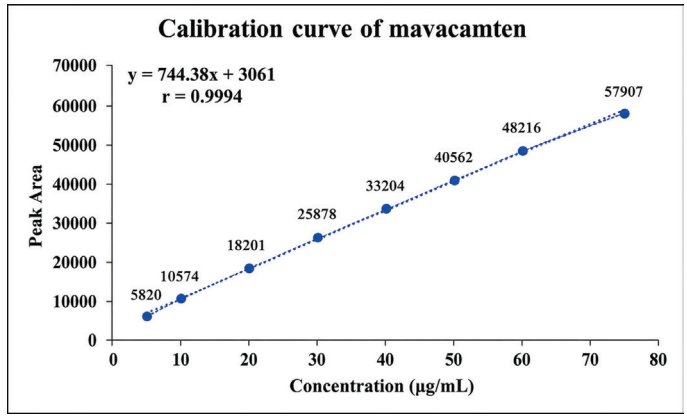

Figure 2. Linear calibration curve depicting the concentration-response relationship of mavacamten.

Table 2. Intraday precision data of mavacamten.

Sr. no	Morning (10:00 AM)	Afternoon (1:00 PM)	Evening (4:00 PM)
	Assay %	Assay %	Assay %
1	100.64	99.81	99.78
2	100.23	100.0	99.41
3	100.16	99.76	100.52
4	100.66	100.53	101.33
5	100.48	99.84	100.59
6	100.09	100.81	100.10
Mean	100.38	100.13	100.29
SD	0.226	0.438	0.678
RSD %	0.225	0.437	0.676
Limit for RSD %	NMT 2%		

SD, standard deviation; RSD %, percent relative standard deviation; NMT, not more than.

Precision

The intraday precision study showed mean assay values of 100.38%, 100.13%, and 100.29% for the morning, afternoon, and evening measurements, respectively, as shown in Table 2. The corresponding % RSD values were 0.225%, 0.437%, and 0.676%, demonstrating good intraday precision of the developed method. Interday precision was assessed by analysing mavacamten samples on two separate days, and the results are summarised in Table 3. The percentage assay values ranged from 99.70 ± 0.171% to 100.43 ± 0.245%, with corresponding RSD % values between 0.120% and 0.712%. All RSD % values were below the acceptance limit of 2.0%, indicating good intermediate precision and reproducibility of the developed RP-HPLC method for routine analysis of mavacamten capsules.

Accuracy

The accuracy of the developed RP-HPLC method was assessed by the standard addition method at four concentration levels (100–130%).[17] Percentage recoveries ranged from 100.40% to 100.90%, with RSDs % between 0.34% and 0.62% (Table 4). All RSD % values were below the acceptance limit of 2.0%, indicating satisfactory accuracy and reproducibility of the method. The results confirm the absence of interference from formulation excipients and demonstrate the suitability of the method for the accurate quantification of mavacamten in capsule dosage forms.

System suitability

During validation, the system's suitability characteristics remained unaltered. The average peak area was 40,745; the average theoretical plate count was 15,224; the mean retention time was 5.06 minutes; and the tailing factor was 1.12. Table 5 presents system suitability results, indicating satisfactory performance.

Content uniformity

The assay results met the predetermined limits (98–102%), indicating consistent active pharmaceutical ingredient concentration in mavacamten capsules. The content uniformity results are shown in Table 6.

Robustness

The technique performed robustly under these conditions, as indicated by RSD % readings consistently below 2%, supporting the conclusion that the procedure was resilient to small operational variations. The findings from robustness evaluations are shown in Table 7.

Validation summary

A summary of the validation results for the evaluated RP-HPLC method is presented in Table 8.

FD studies

The specificity of the developed RP-HPLC method was evaluated by analysing blank, standard, sample, and FD preparations.[18] The blank chromatogram did not exhibit any peak at the retention time corresponding to mavacamten, indicating the

Table 3. Interday precision data of mavacamten.

Assay	Day 1		Day 2	
	*Assay % ± SD	RSD %	*Assay % ± SD	RSD %
1	99.70 ± 0.171	0.712	100.39 ± 0.121	0.120
2	100.43 ± 0.245	0.244	99.72 ± 0.242	0.242
Limit for RSD %	NMT 2%			

*Average of 6 determinations; SD, standard deviation; RSD %, percent relative standard deviation; NMT, not more than.

Table 4. Accuracy data by the standard addition method.

Accuracy % level	Amount spiked (µg/mL)	% Mean* recovery	SD	RSD %
100	0	100.9	0.35	0.34
110	5	100.40	0.37	0.37
120	10	100.7	0.5	0.50
130	15	100.6	0.6	0.62
Limit for RSD %	NMT 2%			

*Average of 3 determinations; SD, standard deviations; RSD %, percent relative standard deviation; NMT, not more than.

Table 5. System suitability data of mavacamten.

Sr. no	Area	Retention time	Theoretical plates	Tailing factor
1	40547.81	5.06	15376	1.13
2	40582.48	5.04	15325	1.12
3	40886.32	5.05	15207	1.11
4	40761.51	5.08	15191	1.12
5	40859.36	5.06	15148	1.13
6	40532.95	5.04	15101	1.12
Average	40745.07	5.06	15224	1.12
SD	145.85	0.02	105.44	0.01
RSD %	0.36	0.30	0.69	0.67
Limit	NMT 2%	NMT 2%	NLT 2000	NMT 2%

SD, standard deviation; % RSD, percent relative standard deviation; NMT, not more than; NLT, not less than.

Table 6. Content uniformity data of mavacamten.

Sr. no	Label claim (mg/capsule)	Estimated amount (mg)	Purity %
1	2 mg	1.97	99.7
2	5 mg	5.01	100.28
3	10 mg	10.11	101.27
Limit for peak purity	98-102%		

Table 7. Robustness data of mavacamten.

Parameter	Deliberate variation	Percent estimation	Mean % estimation	SD	RSD %
Wavelength (nm)	267	99.72	100.42	0.52	0.5
	269	100.58			
	271	100.97			
Flow (ml/min)	0.8	99.80	100.13	0.328	0.327
	1.0	100.58			
	1.2	100.02			
Temperature (°C)	33	100.29	100.5	0.141	0.14
	35	100.60			
	37	100.58			
Mobile phase composition (v/v)	48:52	99.88	100.34	0.375	0.374
	50:50	100.33			
	52:48	100.80			
Limit for RSD %	NMT 2%				

SD, standard deviation; RSD %, percent relative standard deviation; NMT, not more than.

Table 8. Summary of validation results of mavacamten.

Sr. no	Parameter	Result	Acceptance criteria	Remark
1	Linearity-correlation coefficient (r)	0.9994	r ≥ 0.99	Passed
2	Limit of detection (µg/mL)	1.58	S/N = 3:1	Passed
3	Limit of quantification (µg/mL)	4.8	S/N = 3:1	Passed
4	Accuracy (mean % recovery)	100.50	Recovery % = 98–102%	Passed
5	Precision (mean RSD %)	< 2	RSD % ≤ 2	Passed
6	Robustness (mean RSD %)	< 2	RSD % ≤ 2	Passed
7	Content uniformity (%)	100.2	98–102%	Passed
8	System suitability RSD %	< 2	RSD % ≤ 2	Passed
	Theoretical plates	15,224	≥ 2000	Passed
	Tailing factor	1.12	≤ 2	Passed

RSD %, percent relative standard deviation.

absence of interference from diluent components. Similarly, no interfering peaks arising from formulation excipients were observed in the sample chromatograms. Under various stress conditions, including acidic, alkaline, oxidative, thermal, and photolytic, additional degradation peaks were generated; however, these peaks were well resolved from the Mavacamten peak, as shown in Figure 3. The retention time of mavacamten remained consistent, and no interference was observed at the analyte elution position. These findings demonstrate that the developed method is capable of selectively quantifying mavacamten in the presence of its degradation products and formulation-related components. Table 9 displays the computed results.

DISCUSSION

The current project was designed to develop and validate a rapid and reliable RP-HPLC method for quantifying mavacamten in capsule dosage forms. The increasing clinical value of mavacamten as a pioneering cardiac myosin inhibitor necessitates stringent quality control and the availability of a validated analytical method suitable for routine analysis.

Chromatographic conditions were selected to achieve acceptable retention, adequate peak symmetry, and satisfactory column efficiency within a short analysis time. The Inertsil ODS-3V C18 column, combined with an isocratic mobile phase consisting of acetonitrile and a trifluoroacetic acid solution, produced a sharp, symmetrical peak for mavacamten with a retention

time of approximately 5 min. The relatively short retention time reduces solvent consumption and improves analytical throughput, thereby making the method suitable for routine quality control. The system suitability parameters, including tailing factor and theoretical plate count, indicated efficient chromatographic performance and adequate interaction between the drug and the stationary phase.

Method validation, performed according to ICH recommendations, demonstrated excellent linearity over the studied concentration range, indicating a proportional relationship between analyte concentration and detector response, thereby confirming the method's suitability for quantitative applications such as assay and content-uniformity determinations. The calculated limits of detection and quantification further indicate that the method possesses adequate sensitivity for the analysis of finished pharmaceutical products.

The precision studies revealed low intra-day and inter-day variability, underscoring satisfactory repeatability and intermediate precision. The small variation observed among replicate injections and analyses performed on different days confirms the reproducibility of the developed procedure under

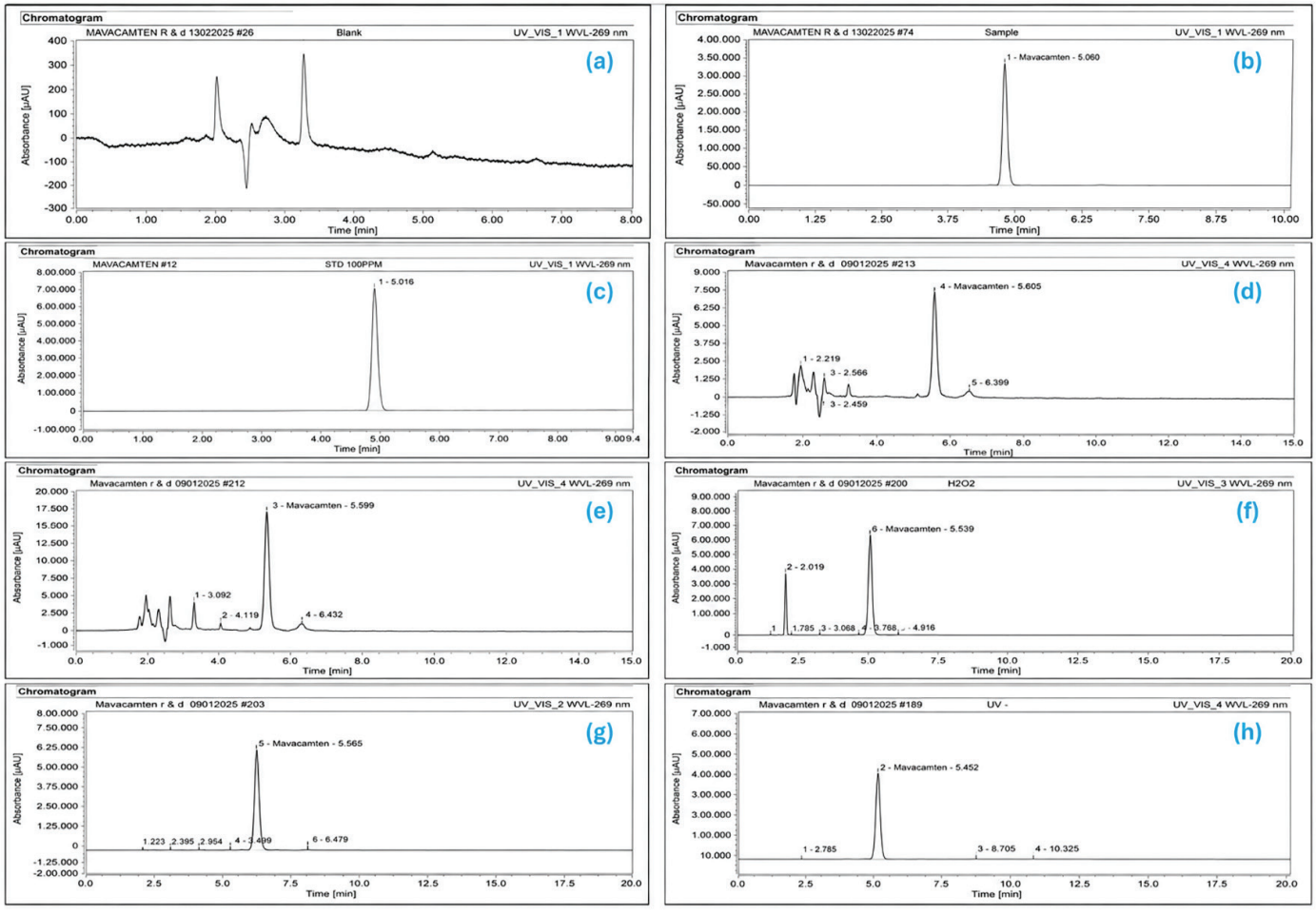

Figure 3. Representative RP-HPLC chromatograms of mavacamten under various conditions: (a) blank; (b) test sample; (c) reference standard; (d) acid-induced degradation; (e) base-induced degradation; (f) oxidative stress condition; (g) thermal degradation; (h) photolytic degradation.

Table 9. Forced degradation data of mavacamten.

Test	Forced degradation conditions	Duration	Percent (%) degradation	Percent (%) residual drug
1	Acidic (0.1 M HCL)	24 hours at room temperature	10.97	89.63
2	Alkali (0.1M NAOH)	24 hours at room temperature	4.19	95.81
3	Oxidative (3% H_2O_2)	24 hours at room temperature	2.56	97.44
4	Thermal (60 °C)	24 hours at 60 °C	1.66	98.34
5	Photolytic (at 254 nm)	24 hours at room temperature	0.93	99.07

normal laboratory operating conditions. Such reproducibility is particularly important for analytical methods intended for routine quality control and stability testing.

Accuracy evaluation using recovery experiments produced values close to 100%, indicating that the excipients in the capsule formulation did not interfere with the quantification of mavacamten. The low variability observed during recovery studies further confirms the reliability of the method for determining the drug in pharmaceutical matrices. These findings demonstrate that the method possesses adequate selectivity toward the analyte in the presence of formulation components.

System suitability results remained within the prescribed acceptance criteria throughout validation, demonstrating the consistency and reliability of the chromatographic system. Stable retention time, acceptable peak symmetry, and satisfactory column efficiency indicate that the analytical system can generate reproducible results during prolonged use; this is particularly important for methods intended for routine stability assessment.

The developed method was successfully applied to the analysis of marketed capsule formulations, yielding assay values within the pharmacopeial acceptance limits. Content uniformity studies demonstrated minimal variability among individual dosage units, indicating homogeneous distribution of mavacamten within the capsule formulations. These results support the practical applicability of the method for routine quality control testing of different capsule strengths.

Robustness evaluation demonstrated that deliberate changes in chromatographic conditions, including flow rate, mobile phase composition, and detection wavelength, did not significantly affect analytical performance. The absence of substantial variation in assay results and system suitability parameters confirms the rugged nature of the method and indicates that minor operational changes are unlikely to compromise analytical performance during routine laboratory use.

FD studies constitute an essential component of method development because they provide information on the intrinsic stability characteristics of drug substances and demonstrate the ability of the analytical method to separate degradation products from the intact drug. In the present investigation, mavacamten exhibited differential susceptibility to various stress conditions. The drug remained relatively stable under thermal, photolytic, and oxidative conditions, whereas acidic conditions produced the greatest extent of degradation.

The pronounced degradation observed under acidic stress may be attributed to proton-mediated chemical transformations within the mavacamten molecule. The presence of amide functionality can facilitate acid-catalysed hydrolysis through protonation of the carbonyl group, thereby increasing the susceptibility of the molecule toward nucleophilic attack. Additionally, protonation of nitrogen-containing heterocyclic moieties may alter the electronic distribution within the molecule and promote subsequent degradation pathways. The greater extent of degradation under acidic conditions, therefore, suggests that acid-catalysed reactions represent the predominant degradation mechanism of mavacamten under the investigated stress conditions.

Importantly, the developed chromatographic method achieved adequate resolution between the parent drug and degradation products without interference at the retention time of mavacamten. The ability to selectively quantify the intact drug in the presence of degradation products makes the method suitable for stability studies, shelf-life evaluation, and quality control applications.

The findings of the present study have practical significance for pharmaceutical industries and quality control laboratories. The method combines short analysis time, satisfactory validation characteristics, and stability-indicating capability, thereby offering an economical and efficient analytical approach for routine analysis of mavacamten capsule formulations. Furthermore, the degradation behaviour observed during stress studies may provide useful information for formulation development, packaging selection, and optimization of storage conditions.

Overall, the developed RP-HPLC method demonstrated satisfactory validation characteristics, adequate specificity, and effective separation of degradation products from the parent drug.

Study limitations

Although the method is suitable for routine quality control, we acknowledge certain limitations. The moderate sensitivity and reliance on isocratic elution may restrict its applicability to highly complex impurity profiling. Additionally, the use of trifluoroacetic acid, while beneficial for improved peak shape and resolution, may have implications for long-term system maintenance. Table 10 summarises the limitations of the proposed method. Nevertheless, within the context of routine assay, content uniformity, and stability evaluation of mavacamten capsules, these limitations do not compromise the method's overall suitability.

CONCLUSION

The present investigation resulted in the successful development of a selective, stability-indicating RP-HPLC method for the determination of mavacamten in capsule dosage forms. The optimised chromatographic conditions enabled rapid analysis with satisfactory peak characteristics and effective separation of the drug from its degradation products, demonstrating the suitability of the method for stability-related applications.

Comprehensive validation, performed in accordance with ICH recommendations, established the reliability of the method with respect to linearity, accuracy, precision, robustness, sensitivity, and specificity. The consistent analytical performance observed during validation and the successful analysis of commercial capsule formulations confirm the applicability of the method for routine pharmaceutical quality assessment.

Table 10. Limitations of the developed RP-HPLC method for mavacamten.

Limitation	Impact
Moderate LOD/LOQ	Not suitable for eluting low-level analytes
Isocratic system	Not as appropriate for complex impurity profiles
Trifluoroacetic acid usage	Causes issues with advanced detectors
Limited characterization of degradants	There can be an oversight in the regulatory filings

RP-HPLC, reverse-phase high-performance liquid chromatography; LOD, limit of detection; LOQ, limit of quantification.

Stress-degradation studies provided important insights into the chemical stability profile of mavacamten. The drug exhibited the highest susceptibility to acidic degradation, whereas limited degradation was observed under thermal, oxidative, and photolytic conditions. The clear resolution of degradation products from the parent drug peak demonstrates the method's ability to accurately quantify mavacamten in the presence of these products.

The developed analytical procedure offers practical advantages, including simple sample preparation, short chromatographic run time, reproducible performance, and suitability for routine laboratory operation. In addition to supporting assay and content- uniformity testing, the method may be effectively employed for stability studies, quality- control investigations, and the evaluation of pharmaceutical products during storage.

The study provides a validated, reliable analytical approach for determining mavacamten in capsule formulations and valuable information on its degradation behaviour. The proposed method may serve as a useful tool for pharmaceutical industries and quality control laboratories involved in the development, evaluation, and stability monitoring of mavacamten-containing products.

Ethics

Ethics Committee Approval: Ethics committee approval was not required for this study, as the research involved only the development and validation of an analytical method for pharmaceutical drug samples and did not involve human participants, animals, human-derived biological samples, or identifiable personal data.

Informed Consent: Informed consent approval was not required for this study, as the research involved only the development and validation of an analytical method for pharmaceutical drug samples and did not involve human participants, animals, human-derived biological samples, or identifiable personal data.

Acknowledgements

The authors express their sincere gratitude to the Central Drug Testing Laboratory (CDTL) for supplying the equipment, supplies, and technical assistance required to conduct the experimental work for this study.

Footnotes

Authorship Contributions

Concept: P.A.D., V.M., Design: P.A.D., V.M., B.S., Data Collection or Processing: P.P., Analysis or Interpretation: P.A.D., V.M., Literature Search: P.A.D., B.S., Writing: P.P., B.S.

Conflict of Interest: The authors declare no conflicts of interest.

Financial Disclosure: The authors declared that this study received no financial support.

REFERENCES

1. Sisakian H. Cardiomyopathies: evolution of pathogenesis concepts and potential for new therapies. World J Cardiol. 2014;6:478-494.
2. Soczynska J, Gawelczyk W, Mozdziak PE. Cardiomyopathies - genetic and molecular issues. Med J Cell Biol. 2024;12:34-41.
3. Tuohy CV, Kaul S, Song HK, Nazer B, Heitner SB. Hypertrophic cardiomyopathy: the future of treatment. Eur J Heart Fail. 2020;22:228-240.
4. Liu RL, Yang YF, Gong K, Wang L, Yao Y, Xie L. Whole exome sequence reveals genetic profiles of primary cardiomyopathy and genotype-phenotype association in Chinese population. BMC Genomics. 2025;26:150.
5. Musigk N, Suwalski P, Golpour A, Fairweather D, Klingel K, Martin P, Frustaci A, Cooper LT, Lüscher TF, Landmesser U, Heidecker B. The inflammatory spectrum of cardiomyopathies. Front Cardiovasc Med. 2024;11:1251780.
6. Lala IR, Pop-Moldovan A. Inflammation-a possible link between myocarditis and arrhythmogenic cardiomyopathy. Diagnostics (Basel). 2024;14:248.
7. Wenzl FA, Ambrosini S, Mohammed SA, Kraler S, Lüscher TF, Costantino S, Paneni F. Inflammation in Metabolic Cardiomyopathy. Front Cardiovasc Med. 2021;8:742178.
8. Krejci J, Mlejnek D, Sochorova D, Nemec P. Inflammatory cardiomyopathy: a current view on the pathophysiology, diagnosis, and treatment. Biomed Res Int. 2016;2016:4087632.
9. Wu X, Chen N, Hsu P, Sun J, Li W, Wang Q, Samira M, Wei Q, Yu J, Cao G, Yang H, Wang L, Wang J, Jin Y, Liu W, Wu J, He J, Lyu C, Zhang J. Pharmacokinetics and safety of mavacamten in healthy Chinese participants with different CYP2C19 phenotypes. Clin Transl Sci. 2024;17:e13877.
10. Maron BJ, Desai MY, Nishimura RA, Spirito P, Rakowski H, Towbin JA, Dearani JA, Rowin EJ, Maron MS, Sherrid MV. Management of hypertrophic cardiomyopathy: JACC state-of-the-art review. J Am Coll Cardiol. 2022;79:390-414.
11. Ma W, Del Rio CL, Qi L, Prodanovic M, Mijailovich S, Zambataro C, Gong H, Shimkunas R, Gollapudi S, Nag S, Irving TC. Myosin in autoinhibited off state(s), stabilized by mavacamten, can be recruited in response to inotropic interventions. Proc Natl Acad Sci U S A. 2024;121:e2314914121.

12. Nag S, Gollapudi SK, Del Rio CL, Spudich JA, McDowell R. Mavacamten, a precision medicine for hypertrophic cardiomyopathy: from a motor protein to patients. Sci Adv. 2023;9:eabo7622.
13. Reyes KRL, Bilgili G, Rader F. Mavacamten: A first-in-class oral modulator of cardiac myosin for the treatment of symptomatic hypertrophic obstructive cardiomyopathy. Heart Int. 2022;16:91-99.
14. Bishev D, Fabara S, Loseke I, Alok A, Al-Ani H, Bazikian Y. Efficacy and safety of mavacamten in the treatment of hypertrophic cardiomyopathy: a systematic review. Heart Lung Circ. 2023;32:1049-1056.
15. Młynarska E, Radzioch E, Dąbek B, Leszto K, Witkowska A, Czarnik W, Jędraszak W, Rysz J, Franczyk B. Hypertrophic cardiomyopathy with special focus on mavacamten and its future in cardiology. Biomedicines. 2024;12:2675.
16. Masri A, Lester SJ, Stendahl JC, Hegde SM, Sehnert AJ, Balaratnam G, Shah A, Fox S, Wang A. Long-term safety and efficacy of mavacamten in symptomatic obstructive hypertrophic cardiomyopathy: interim results of the PIONEER-OLE study. J Am Heart Assoc. 2024;13:e030607.
17. Tarole T, Daroi P, Munipalli VK, Warde S, Singh RS, Nandi A, Vaidhun B. Stability indicating RP-HPLC method development for the estimation of molnupiravir in capsule dosage form. Int J Pharm Sci Drug Res. 2023;15:222-228.
18. Patil P, Daroi P, George S, Bhaskar V. Stability-indicating reverse-phase high-performance liquid chromatographic method for quantitative estimation of remdesivir oral solution dosage form. World J Pharm Res. 2022;11:1670-1684.

Turk J Pharm Sci 2026;23(2):85-104
DOI: 10.4274/tjps.galenos.2026.10001

ORIGINAL ARTICLE

Development of Mucoadhesive Nanofiber as an Alternate Therapeutic Regimen for Subclinical Endometritis in Cattle

Priyanka KUMARI[1], Shivlal YADAV[1], Ashutosh TRIPATHI[2], Manish Kumar SHUKLA[3], Surabhi PARANGI[4], Janmejay PANDEY[4], Rakesh Kumar SAHOO[5], Goutam RATH[5], Debasmita DUBEY[6], Amit Kumar GOYAL[1]*

[1]Central University of Rajasthan, Department of Pharmacy, Ajmer, Rajasthan, India
[2]Sardar Vallabhbhai Patel University of Agriculture and Technology, College of Veterinary and Animal Sciences, Department of Livestock Farm Complex, Meerut, Uttar Pradesh, India
[3]Sardar Vallabhbhai Patel University of Agriculture and Technology, College of Veterinary and Animal Sciences, Department of Veterinary Gynaecology and Obstetrics, Meerut, Uttar Pradesh, India
[4]Central University of Rajasthan, Department of Biotechnology, Ajmer, Rajasthan, India
[5]Siksha 'O' Anusandhan School of Pharmaceutical Sciences, Bhubaneswar, Odisha, India
[6]Siksha 'O' Anusandhan, IMS and Sum Hospital, Department of Medical Research, Bhubaneswar, Odisha, India

ABSTRACT

Objectives: Subclinical endometritis in cattle is still a problem that has a detrimental effect on dairy production and fertility. Traditional intrauterine or systemic antibiotic treatments frequently result in suboptimal uterine drug levels, encourage resistance, and increase the possibility of drug residues in food items. The current study aimed to treat subclinical endometritis in repeat breeders by creating and testing an ofloxacin (Ofx)-loaded mucoadhesive polyvinyl alcohol/chitosan nanofiber using the electrospinning technique.

Materials and Methods: The process constants were optimised using a central composite design to create a uniform nanofiber with maximum mechanical properties. Furthermore, *in vitro* (drug release, antibacterial activity), *ex vivo* (mucoadhesion and retention), and *in vivo* (endometrial cytology and plasma drug concentration) parameters were evaluated.

Results: The scanning electron microscopy image of Ofx nanofiber suggests a diameter of 190–210 nm and tensile strength of 1.33 tensile strength with an entrapment efficiency of 97.54 ± 0.89%. Ofx delivered via nanofiber exhibited sustained release of Ofx up to 216 hours. *Ex vivo* assessments demonstrated stronger adherence and higher retention, while *in vitro* studies showed no cytotoxic effects. *In vivo* studies on the cattle suggested suitability for localized intrauterine administration. These findings indicate that encapsulation of Ofx in nanofibers stabilises the formulation and offers enhanced treatment efficiency compared to a conventional treatment regimen for subclinical endometritis in repeated breeders.

Conclusion: Ofx-loaded nanofibers offer a novel and promising localized and mucoadhesive drug delivery approach for subclinical endometritis in cattle. Future research must prioritise further *in vivo* validation, long-term reproductive effects, and resistance management to translate into practical veterinary uses.

Keywords: Ofloxacin, nanofiber, mucoadhesive, QbD, CCD, subclinical endometritis, chitosan, PVA, pharmacokinetic parameters

***Correspondence:** amitkumargoyal1979@gmail.com, **ORCID-ID:** orcid.org/0000-0002-6045-3525

Received: 06.10.2025 **Accepted:** 18.08.2026 **Publication Date:** 01.09.2026

Cite this article as: Kumari P, Yadav S, Tripathi A, Shukla M, Surabhi S, Pandey J, Sahoo RK, Rath G, Dubey D, Goyal AK. Development of mucoadhesive nanofiber as an alternate therapeutic regimen for subclinical endometritis in cattle. Turk J Pharm Sci. 2026;23(2):85-104

INTRODUCTION

Dairy animals can suffer from subclinical endometritis (SE), a uterine condition that affects reproduction without obvious clinical signs, affecting about 30% globally.[1] Unlike clinical endometritis, SE is characterized by endometrial inflammation that is only detectable through cytological or histological testing. Often overlooked by farmers and veterinarians, SE negatively impacts conception rates, prolongs the interval between calving and conception, and increases culling, leading to significant financial losses in the dairy industry.[2] Its pathophysiology is linked to abnormal postpartum inflammatory responses, persistent bacterial infections, poor uterine involution, and immunological dysregulation.[3]

Numerous investigations argue that *Fusobacterium necrophorum, Escherichia coli, Trueperella pyogenes, Prevotella* spp., and *Staphylococcus* spp. (including coagulase-negative strains and *S. aureus*), are the prominent uterine pathogens that play a significant role in the pathophysiology of SE.[4] These pathogens become problematic at post-parturition due to factors like delayed placenta and messy calving techniques, resulting in infertility, inflammation, and disruptions in the oestrous cycle.[5,6] The diagnosis of SEs remains challenging as it is often asymptomatic; however, methods such as low-volume uterine lavage or cytobrush for measuring polymorphonuclear neutrophils are used for assessment.[7]

Therapy using hormones, antiseptic sanitation, and antibiotics has historically been employed to treat bacterial infections; however, their application in specific environments has resulted in prolonged interventions and the emergence of multidrug-resistant bacterial strains.[8,9] These treatment protocols frequently fail to achieve adequate drug concentrations in uterine tissue, leading to systemic toxicity and antibiotic resistance, alongside potential residues in milk and meat.[10] Intrauterine treatments suffer from reduced drug retention due to contractions and discharge, complicating the evaluation of treatment impacts on reproductive success without clear diagnostic criteria.[11] The public health concern regarding antibiotic resistance and residues in food animals underscores the shortcomings of conventional systemic treatments for uterine infections, which often show ineffectiveness, adverse effects, and insufficient tissue penetration.[12] This highlights the urgent need for localized treatment approaches, such as mucoadhesive drug delivery systems (MDDS), which are designed to adhere to mucosal tissues, facilitating prolonged drug residence at infection sites while minimizing systemic effects.[13,14] MDDSs enhance therapeutic efficacy and lower the risk of antimicrobial resistance, systemic toxicity, and drug overuse, improving treatment compliance and reducing economic burdens through controlled and sustained drug release.[15,16]

Nanofibers (NFs) are emerging as effective frameworks for MDDS, facilitating the targeted delivery of therapeutic agents across mucosal tissues.[17] This approach minimizes drug dosage, reduces wastage, and diminishes the risk of systemic side effects and drug resistance.[18] A key method for producing these polymeric NFs is electrospinning, which involves applying an electric field to a polymeric solution, resulting in the formation of thin fiber membranes on a collector.[19] Various factors, including the strength of the electric field, the distance between the nozzle and the collector, environmental conditions, and the properties of the polymer solution, influence the quality of NF production.[20,21]

Commonly used polymers for developing mucoadhesive NFs include chitosan (CS) and polyvinyl alcohol (PVA).[22] Both are biocompatible and non-toxic, with PVA providing advantageous traits such as water solubility and mechanical stability, while CS offers biodegradability and antibacterial properties.[23] CS's ability to dissolve in acidic conditions makes it suitable for targeting drug release at diseased tissues.[24] The combination of PVA and CS results in hybrid NFs that enhance drug retention and stability on mucosal surfaces while promoting controlled release through pH-responsive mechanisms.[25] Therefore, PVA/CS electrospun NFs are posited as a versatile and cost-effective solution for prolonged, localized drug administration in biomedical contexts.[26]

Ofloxacin (Ofx), a fluoroquinolone antibiotic, is noted for its effectiveness against a wide range of bacterial organisms and is considered a potential treatment for endometritis.[27,28] It acts by inhibiting crucial bacterial enzymes necessary for DNA replication, offering a dual-target approach that enhances efficacy while minimizing the development of resistance.[29] With favourable pharmacokinetic properties, including significant tissue penetrability and prolonged activity, Ofx is an ideal candidate for localized application within the uterine environment.[30,31]

The goal of the currently designed study was to treat SE in repeat breeders by developing and conducting tests on an Ofx-loaded mucoadhesive PVA/CS NF via the electrospinning approach. The process parameters were optimized using a central composite design (CCD) to produce a uniform NF with enhanced loading capacity. Additionally, *ex vivo* (mucoadhesion and retention), *in vitro* (drug release and antibacterial activity), and *in vivo* (endometrial cytology) parameters were evaluated. This study addresses the drawbacks of traditional treatment techniques and proposes a new, efficient, and focused strategy for controlling SE.

MATERIALS AND METHODS

Ofx was snapped up from Sigma Aldrich. CS (Deacetylated ± 75%, Shrimp shell), PVA (M.W. 60-1.25 KDa), Acetic acid acquired from Himedia. Other chemicals used in the experiments were of analytical grade. Acetonitrile and methanol [high-performance liquid chromatography (HPLC) grade] were purchased from Thermo Fisher Scientific (U.K.).

PVA/CS NF formulation development and optimization

PVA solution (10% w/v) was prepared in 10 mL of hot distilled water (< 60 ºC). Then, 2% (w/v) CS was initially soaked by adding 0.2 g in 10 mL of aqueous acetic acid solution (2% v/v) overnight. CS and PVA solutions were stirred separately until a clear solution was obtained. Furthermore, solutions of PVA

and CS were combined in ratios of 9:1, 8:2, and 7:3 and stirred for 6 hours at room temperature (RT) to obtain a clear and homogeneous solution.

The devised blend was electrospun through E-Spin Nanotech (Central University of Rajasthan). The above-prepared PVA/CS solution was loaded and pumped out through a 5 mL syringe, keeping the tip-to-collector distance at 12 cm, and electrospinning was carried out under ambient conditions (temperature: 32 ± 2 °C; relative humidity: 33-50%). The applied high voltages ranged from 18 to 21 kV, with the flow rate (0.5 to 1.5 µL/hr) as the independent variable. This relatively low flow rate was optimized to ensure stable Taylor cone formation, minimize bead formation, and produce uniform NFs by allowing sufficient time for solvent evaporation during jet travel, particularly given the polymeric system's viscosity and intermolecular interactions. All the electrospun NFs were collected on aluminum foil and then placed in a desiccator for 1 day at RT to cross-link in glutaraldehyde vapor (15 mL of 50% v/v). After cross-linking, the fibers were kept in the desiccator for an additional 24 hours to facilitate the removal of excess glutaraldehyde vapor.[32]

The first step in developing a formulation is to optimize the formulation with the variables, which may be accomplished using software or a one-factor-at-a-time experiment. In this experimental design, a CCD was employed to optimize the PVA/CS NFs using Design-Expert (version 13.0.5.0, Stat–Ease, Minneapolis, MN).[33] The ratio of CS used in PVA/CS, the voltage applied to stretch the polymer from tip to collector to form a thread-like structure, and the flow rate of polymer oozing from the needle were taken as independent variables. The impact of these independent factors on fiber diameter and tensile strength (MPa) was optimized by response surface methodology. Seventeen experiments were conducted to run CCD and to analyze optimal responses for NF diameter and MPa, as shown in Table 1. It reduces the duration of experiments and unnecessary expenses. It helps create response surface plots that reveal interaction effects and highlight the optimal conditions for achieving the desired NF characteristics. CCD also generated a non-linear second-order quadratic equation, as illustrated in the equation.

$$Y = \beta_0 + \beta_1 A + \beta_2 B + \beta_3 C + \beta_3 C + \beta_{12} AB + \beta_{13} AC + \beta_{23} BC + \beta_{11} A^2 + \beta_{22} B^2 + \beta_{33} C^2 \quad \text{(i)}$$

A, B, C = independent factor, β_0 = intercept, β_1, β_2, β_3 = regression coefficients, β_{12}, β_{13}, β_{23} = regression coefficients interaction, β_{11}, β_{22}, β_{33} = quadratic terms, respectively.[34]

The statistical significance of the model was assessed using analysis of variance (ANOVA), as indicated by the *p*-value, determination coefficient, correlation coefficients, adjusted R^2, sufficient precision, and coefficient of variance for each response.[35]

Table 1. The experimental design's variables of intervention, the corresponding respondent variables, and desirability.[36]

Independent factors (X)	Unit	Level		
		-1	0	+1
Cs	Ratio	1	2	3
Voltage	kV	18	19.5	21
Feed rate	µl/hr	0.5	1	1.5
Dependent factors (Y)	**Unit**	**Response with desirability**		
Fiber diameter	nm	Minimum		
Tensile strength	MPa	Maximum		

Characterization

Scanning electron microscopy (SEM)

Using SEM, the NF's structural traits were evaluated (Thermo Fisher Scientific, Central University of Rajasthan). A 1 × 1 cm^2 NF was coated with gold, sputtered, and imaged at 20 kV. Fifty arbitrarily chosen fibers were used to calculate the mean diameter of the fiber using ImageJ software, and a frequency size distribution curve was plotted in Origin software.

Swelling index

To calculate the swelling index of the produced NFs, the specimen was weighed initially in a dried condition and then stored at 37 ± 1°C in an agar gel plate with 15 mL of 2% w/v agar. After a different time interval, the NFs were weighed again. The following formula was used to determine the swelling index:

$$\%\ Swelling\ Index = \frac{final\ weigth\ (t) - Initial\ weigth}{Initial\ weight} * 100 \quad \text{(ii)}[37]$$

MPa

The Instron-5967 testing equipment measured the MPa of blank NFs (B-NF) and Ofx-NFs. The NFs were fragmented into a rectangular form (5 × 30 mm^2) and secured in an Instron Jaws Tensile-clamped paper holder. At RT, the 50 N tension was torqued at an expansion rate of 5 mm/min.[38]

Fourier-transform infrared spectroscopy (FTIR)

The chemical structure and alteration were identified by FTIR (PerkinElmer spectrometer, Central University of Rajasthan). The sample was mixed with FTIR-grade KBr in a 1:100 ratio to prepare thin pellets for analysis. Spectra of the drug, excipient, and formulation were taken in the 4000–400 cm^{-1} range and plotted in Origin.

Differential scanning colorimeter (DSC)

DSC (Netzsch Geratebau GmbH, Germany) experiments were performed on pure Ofx, CS, PVA, B-NF, and Ofx-NF. An appropriate quantity of sample was taken, sealed in an aluminum pan, and heated at 10 °C/min under a nitrogen atmosphere. Thermograms of the samples were observed at a range between 0 °C to 300 °C.[39]

Drug loading and encapsulation

An Agilent Cary 60 UV-Vis spectrophotometer was used to measure the drug loading and the quantity of Ofx trapped in the designed nanofibrous mat. 2 x 2 cm^2 of the optimized nanofibrous matrix was weighed and submerged in 10 milliliters of simulated uterine fluid (SUF) (pH~6.8) using a sonicator and mechanical shaking. Before analysis, the solution was centrifuged and filtered through a 0.45 μm filter. The concentration of Ofx was analyzed at 287.5 nm. The calibration curve was produced in SUF (pH~6.8) (composition mentioned in Table 2).[40] The formula for calculating the mass of Ofx retrieved (W_{uv}) was calculated as concentration × total volume. The total drug distribution during fabrication of the NF mat was 20 mg in a 320 cm^2 nanofibrous mat; the theoretical drug content in a 2 × 2 cm^2 sample calculated was approximately 0.25 mg.

Table 2. Composition of simulated uterine fluid (pH 6.8).

Chemical name	Quantity (g/L)
NaCl	4.97
KCl	0.224
$CaCl_2$	0.167
$NaHCO_3$	0.25
Glucose	0.5
$NaH_2PO_4{\cdot}2H_2O$	0.072

NaCl, sodium chloride; KCl, potassium chloride, $CaCl_2$, calcium chloride; $NaHCO_3$, sodium bicarbonate; $NaH_2PO_4{\cdot}2H_2O$, sodium dihydrogen phosphate dihydrate.

$$\%DL = \frac{Wuv}{Wnf} * 100 \quad \text{(iii)}$$

$$\%EE = \frac{Wuv}{Wes} * 100 \quad \text{(iv)}$$

Where W_{nf} is the weight of 2 x 2 cm^2 NF, Wes is the amount of Ofx added before the electrospinning process. The data were presented as mean ± standard deviation (SD), and all assays were made in triplicate (n = 3).

In vitro drug release and kinetics

The drug release profile of Ofx from NFs was evaluated using the dialysis method, which was filled with SUF. A 2 x 2 cm^2 Ofx-NF was added to a 5 cm dialysis membrane-50 (MWCO: 12–14 kDa) and immersed in 50 mL SUF at 37 °C. The medium was continuously stirred at 100 rpm to ensure proper mixing of diffused Ofx from the membrane. At a predetermined time, 5 mL of the sample was collected and returned with fresh medium. The samples were further analyzed using a UV-Vis spectrophotometer at 287.5 nm. A standard calibration curve (R^2 = 0.9988) was prepared to determine the drug concentration. The DD Solver add-in software was used to construct and monitor various kinetic models and to investigate the improved drug release kinetics of Ofx from NFs.[41]

Ex vivo permeation of Ofx

The Franz diffusion cell was used for the permeation study on the uterine mucosa. The goat's uterine mucosa was obtained from a nearby slaughterhouse, cleaned with 0.9% w/v saline solution, and preserved in formalin before the experiment. The mucosa was positioned between the donor and receptor compartments of a 25 mL Franz diffusion cell, which was the recommended model. The two compartments of the Franz cell were then secured together after a strip of the NF film was placed on the mucosa. Throughout the investigation, the shaker was operated at 100 rpm, and the temperature was maintained at 37 ± 1 °C. For up to 8 hours into the trial, samples were collected via lumbar puncture at predetermined intervals. To maintain a consistent volume, 1 mL samples were collected at each interval and replaced with the same volume of new medium. All *ex vivo* permeation studies were performed in triplicate under identical experimental conditions to ensure reproducibility. A UV spectrophotometer was used to determine the amount of Ofx in the filtered samples. A graph of cumulative Ofx penetrated through the mucosa (μg/cm^2) against time (min) was also used to determine the permeability of Ofx from the NF film. The slope of the graph was used to calculate the permeability flow using linear regression. The apparent permeation coefficient was determined.

$$Papp = \frac{dQ}{dt}/(A.Co) \quad \text{(vi)}$$

dQ/dt = rate of drug transport across the membrane (μg/s)

A = surface area of the membrane (1 cm^2)

Co = initial drug concentration in the donor (μg/mL).

Plotting the amount of Ofx penetrated against time yielded a graph, the slope of which indicated the steady-state flow value (J = μ/cm^2/h). However, there is a metric that may be applied to determine flow.

$$J = \frac{dQ}{dt} * A \quad \text{(vii)}[42]$$

Mucoadhesion test

Fresh goat uterine mucosa and a modified manual glass-slide technique, adapted from popular *ex vivo* adhesion tests, were used to assess mucoadhesion.[43] The mucosal side of fresh mucosa was cleansed, clipped, and used within two hours of collection. It was adhered to a stiff glass slide. A second glass slide was brought into contact with a NF patch measuring about 1 × 1 cm^2, which was applied to the mucosa. A 50-g preload weight was applied for 60 seconds to ensure close contact. Following the contact period, tiny calibrated weights were added to the upper slide, one at a time, until detachment occurred; the total mass at detachment was recorded. The formula for detachment force (N) was mass (kg) × 9.81 ($m{\cdot}s^{-2}$). Six sextuplicate tests were conducted for

each formulation. The mucosa sample assembly was placed on a slanted holder, and SUF (0.5 mL·min^{-1}) was flowed down the outermost layer to assess the residence duration under steady PBS flow at 37 °C. The time until complete expulsion of NFs was noted.

Cell viability assay

A colourimetric MTT experiment was used to assess the cell viability of the proposed NF-based formulations, i.e., B-NF and Ofx-NF, compared to pure Ofx, following an approved protocol.[44] This MTT-mediated cell toxicity investigation was conducted on HeLa cells. To provide consistent conditions in each well, adherent cells were concentrated in 96-well plates (TPP96, Hi Media Laboratories) at a density of 10^4 cells per well. The cells sown in the plates were cultured for 24 hours in a CO_2 incubator (Heracell 150i, ThermoFisher). To investigate the effect of Ofx and nanoformulation, various concentrations of each material have been produced using culture media. The maximal drug concentration for HeLa cells was 100 μM. The HeLa cells on the culture plates were incubated for twenty-four hours after receiving the therapy with the indicated concentrations of pure Ofx, B-NF, and Ofx-NF. Throughout the entire experiment, culture media were regarded as the control. After the incubation period, 50 μL of 3-(4,5-dimethylthiazol-2-yl)-2,5-diphenyltetrazolium bromide (MTT) solution (5 mg/mL) was applied to each well of the 96-well plate. Dimethyl sulfoxide (150 μL) was added to MTT-treated plates after incubating them for an additional four hours. This caused the formazan crystals to disintegrate and turn a purplish colour. The absorbance of each specimen at λmax 570 nm was measured using a microplate reader. The IC_{50} value and percentage viability graph were plotted against the concentration of pure Ofx, B-NF, and Ofx-NFs in relation to HeLa cells. All experiments were performed in triplicate, and the results are expressed as mean ± SD. Statistical analysis was performed using two-way ANOVA.

Antimicrobial activity

The antibacterial properties of B-NFs and Ofx-NFs were evaluated using the agar disc diffusion technique against the bacterial strains *S. aureus* and *E. coli* (both gram-negative and gram-positive). The agar plate was prepared by pouring 30 mL of nutrient agar into petri plates, and then 100 μL of bacterial suspension was evenly distributed on the plates. Then, the plate was allowed to add B-NFs and Ofx-NFs and be maintained at 37 °C in an incubator for 24 hr. The experiment was carried out three times to observe the inhibitory zone.[45]

In vivo study

All animal experiments adhered to the CPCSEA guidelines and received approval from the IAEC of Sardar Vallabh Bhai Patel University (approval no: IAEC/SVPUAT/2022/109, dated May 24, 2022).

This study did not involve human participants; hence, patient consent was not required.

A total of 24 indigenous cattle with SE, screened from the repeat breeder group, were enrolled for the study. The cattle were housed at LRC, SVPUAT, Meerut and nearby Gaushalas. The body condition score of the cattle under study was 3.5 or above and was maintained under optimum nutritional and management conditions.

The animals were randomly allocated into three groups (n = 8 per group) using a simple randomization approach to minimize selection bias. SE was diagnosed based on the presence of polymorphonuclear cells (PMNs) in the uterine cytology. The animals were randomly allocated into three groups (n = 8 per group) using a simple randomization approach to minimize selection bias. SE was diagnosed based on the presence of PMNs in the uterine cytology. Group I served as the untreated control. Group II (positive control) received Ofx (3 mg/kg), while Group III was administered Ofx-loaded NFs (Ofx-NF) intrauterinely (1 mg/kg). Treatments were administered for three consecutive days in Group II and as a single dose in Group III.

Due to practical constraints, blinding was not implemented during treatment administration; however, outcome assessment was performed by an independent investigator blinded to group allocation. All experimental procedures were conducted under standardized conditions to minimize bias. The sample size (n = 8 per group) was selected based on commonly reported group sizes in similar veterinary studies for comparative evaluation of treatment efficacy.

Endometrial samples for microbial culture were collected aseptically using a cytobrush following standard cytology protocols. Samples were collected twice from each animal: before treatment initiation (day 0) and 30–45 minutes prior to artificial insemination in the subsequent estrus cycle.

Isolation and identification of bacteria

The sample withdrawn for endometrial cytology was used for staining on brain heart infusion agar and MacConkey lactose agar plates, which were incubated at 37 °C for 24 hours in an aerobic incubator. To identify mould sp. and yeast sp., the Sabouraud dextrose agar plate was incubated at 37 °C and 25 °C, respectively. The bacteria were identified by their evolutionary history, chemical composition, colony morphology, and microscopic characteristics. Before molecular and resistance testing, the identified colonies were stored in glycerol stock at -20 °C. To subculture pure colonies for a further 24 hours, they were cultivated on blood agar at 37 °C.[46]

Vaginal mucus pH

Vaginal pH was measured once on day 0 and on the last day after the treatment.

Endometrial cytology

This method involved aseptically inserting the cytobrush (Marfair Surgical Corporation, Ludhiana) into the uterine canal after screwing it onto the cytobrush gun's piston. The cytobrush was softly brushed across the uterine endometrium and then drawn off in the cytobrush cannon. The brush was then pressed onto an uncontaminated glass microscopic slide, allowed to dry, and fixed with methanol, after which it was stained. The proportion of PMNs was determined by counting cells at 40X magnification (Olympus CX21, Japan). A valid diagnosis of SE required a threshold PMN volume of 5% or higher.[47]

Pharmacokinetic study

The *in vivo* pharmacokinetic study was conducted on the same experimental cattle mentioned. The calves were treated with the tailored pure Ofx, Ofx-NF, and Ofx-hydrogel formulations via the intrauterine route at a prescribed dosage for cattle. Ofx hydrogel was taken as an alternative novel drug delivery system, to be compared with the NF. The Ofx-loaded hydrogel (Ofx-hydrogel) was prepared as described previously,[31] with a composition consisting of PVA (10% w/v) and CS (2% w/v) in a ratio of (7:3). The blood samples (~5 mL) were drawn from the jugular vein into EDTA vials at prearranged intervals (0, 1, 2, 4, 6, 8, 10, 12, 16, 24, and 30 days). All samples were centrifuged at 3000 rpm for 10 minutes, and the plasma was stored at -20 °C until further analysis. The quantification of Ofx in plasma was performed using a validated reverse-phase high-performance liquid chromatographic method.[48] A standard stock solution (500 ppm) was generated by dispersing 0.5 mg of Ofx in 10 mL of a mobile phase containing 10 mM phosphate buffer (pH 3.0, modified with 10% o-phosphoric acid) and methanol (50:50 v/v). Working standards (2-10 μg/mL) were generated by successively diluting the stock solution, and blank bovine plasma was spiked with aliquots of these working standards to create calibration curves in the 0.05–10 μg/mL range. 200 μL plasma from each sample was processed by protein precipitation using three volumes of acetonitrile, vortexed, and centrifuged for 10 minutes at 10,000 rpm. The transparent supernatant was filtered using a 0.22 μm syringe filter before injection.[49] The NovaSil C18 100 Å column (250 × 4.6 mm, 5 μm) was used for chromatographic separation, with isocratic elution at a flow rate of 1.0 mL/min and detection at λ_{max} of 290 nm. The approach demonstrated good linearity with a correlation coefficient (R^2 = 0.998). The limit of detection (LOD) and limit of quantification (LOQ) were calculated using the equations LOD = 3.3σ/S and LOQ = 10σ/S. Non-compartmental analysis (PK Solver) was used to compute the pharmacokinetic parameters [C_{max} (maximum concentration), T_{max} (maximum time), area under the curve $(AUC)_{0-t}$, $AUC_{0-\infty}$, $t_{½}$ (half life), and mean residence time (MRT)].[50] The data were presented as mean ± SD, and two-way ANOVA was used to assess statistical significance ($p < 0.05$).

Pregnancy diagnosis

The pregnancy diagnosis was performed on day 45 following artificial insemination through rectal palpation and ultrasonography (Minitube, 6.5 MHz, rectal probe).[51]

Statistical analysis

Kinetic modeling was performed using the DD Solver add-in for Microsoft Excel, and non-compartmental pharmacokinetic parameters were analyzed using the PK Solver add-in for Microsoft Excel (written in Visual Basic for Applications). Statistical analysis of all experimental data was carried out using GraphPad Prism (version 8.0.1, Boston, USA).

All results are expressed as mean ± SD. Continuous variables, such as CFU count and PMN percentage, were analyzed using one-way ANOVA followed by Dunnett's multiple-comparison test. Categorical data, such as pregnancy rate, were analyzed using the chi-square test. Pharmacokinetic parameters were statistically compared using two-way ANOVA. A value of $p < 0.05$ was considered statistically significant.

RESULTS

Optimization of NF

PVA/CS NFs were prepared via electrospinning. The CS concentration in PVA/CS was a limiting factor in forming a spinnable solution. Changes in the electrospinning machine's flow rate and voltage significantly influence the formation of a continuous stretch jet to the collector, resulting in uniform NFs. Thus, optimized CS ratios were required to prepare PVA/CS NFs. The optimization of the formulation was carried out by the CCD using three independent variables: X1 = CS ratio in PVA/CS solution, X2 = applied voltage to form a jet of polymeric solution from the tip of the needle, and X3 = flow rate of the pump, which pushes the polymeric needle plunger to ooze out polymer. Seventeen runs were processed, and the design generated the levels (-1, 0, +1) and α (1.681). ANOVA was used to validate the effects of the independent variables (X1, X2, and X3) on the response variables [Y1 = NF diameter (nm) and Y2 = MPa], as listed in Table 3. These response variables were analyzed and fitted to various models, including linear, 2-factor interaction, quadratic, and cubic models. A suitable model was selected by determining the highest correlation coefficient value. Based on a significant *p*-value and sum of squares from a sequential model, the best fit model for each response was a quadratic model. Therefore, the quadratic model was used to elucidate the effects of the independent variables (CS ratio, voltage, and feed rate) on fiber diameter and MPa.[52]

Effect of input variables on NF diameter

The diameter of the B-NF was recorded in the range of 100–400 nm, based on the variation in the values of independent and dependent variables. The smallest diameter (173.14 nm) was observed for run 2, whereas the largest diameter (375.51 nm) was observed for run 17. The effect of variables on NF diameter suggests a quadratic model, which was effectively used to determine the correlation coefficient. Table 4 presents a summary of the statistical analysis of three independent variables on diameter, with R^2, adjusted R^2, and predicted R^2 of 0.9911, 0.9797, and 0.9389, respectively. Figure 1a represents the 3D response surface and contour plots illustrating the interactive influence of CS ratio (A), applied voltage (B), and feed rate (C) on the fiber diameter of electrospun NFs. The contour plots clearly show that increasing the CS ratio and feed rate led to a progressive increase in fiber diameter. Li and Xia[53] (2004 reported that an increase in polymer concentration or viscosity results in thicker NFs due to reduced elongation of the electrospinning jet. At higher polymer concentrations, the solution viscosity increases due to enhanced chain entanglement and intermolecular interactions. This increased viscosity resists the stretching forces induced by the applied electric field, thereby reducing jet elongation during electrospinning. As a result, the fibers formed are thicker.[53,54] In contrast, higher voltage exerted the opposite effect, reducing

Table 3. Experimental design matrix with independent variable and dependent responses.

Std	RUN	Space type	Factor 1	Factor 2	Factor 3	Response 1	Response 2
			A: Chitosan ratio	B: Voltage	C: Feed rate	Fiber diameter	Tensile strength (MPa)
				kV	µl/hr	nm	MPa
1	1	Factorial	1	18	0.5	262.105	2.2
3	2	Factorial	1	21	0.5	173.142	2.33
11	3	Axial	2	16.9773	1	267.224	1.56
2	4	Factorial	3	18	0.5	265.105	1.27
7	5	Factorial	1	21	1.5	244.575	1.84
12	6	Axial	2	22.0227	1	238.21	1.74
14	7	Axial	2	19.5	1.8409	355.645	1.092
15	8	Center	2	19.5	1	262.105	1.75
13	9	Axial	2	19.5	0.159104	254.128	1.99
6	10	Factorial	3	18	1.5	322.644	0.986
9	11	Axial	0.318207	19.5	1	181.567	2.56
16	12	Center	2	19.5	1	254.117	1.901
5	13	Factorial	1	18	1.5	284.684	1.74
17	14	Center	2	19.5	1	263.384	1.8
10	15	Axial	3.68179	19.5	1	298.11	0.967
4	16	Factorial	3	21	0.5	279.635	1.54
8	17	Factorial	3	21	1.5	375.516	1.11

the diameter and thereby improving the stretching forces of the electrospinning jet. Additionally, higher viscosity limits jet instability and whipping, further contributing to the formation of uniform, but larger, fibers.[55]

Specifically, the A-B interaction revealed that fiber diameter decreased with increasing voltage but increased with higher CS concentration. The B-C interaction further confirmed that higher feed rates favored the formation of thicker fibers, whereas voltage continued to reduce the diameter. Similar findings were observed: higher feed rates supply more solution to the jet, leading to insufficient stretching and, consequently, larger fiber diameters. Similarly, the A-C interaction highlighted a positive correlation among the two parameters and fiber thickness. These findings were further validated by the corresponding 3D surface plots, which depicted smooth response surfaces confirming the trends. Collectively, the analysis indicates that thinner fibers can be obtained at lower CS ratios, higher applied voltage, and reduced feed rates. In contrast, thicker fibers are produced under opposite conditions, as finalized by SEM images of the highest and lowest values of the dependent and independent variables (Figure 1c). In terms of mathematics, it is expressed as:

$$Y1\ (\text{NF diameter}) = 259.24 + 34.74A - 8.09B + 30.62C + 24.5AB + 7.43AC + 10.90BC - 4.92A^2 - 0.3637B^2 + 18.08C^2 \quad \text{(viii)}$$

Effect of input variables on MPa

The MPa of the B-NF was recorded in the range of 0.8 to 2.7 MPa, depending on the values of the independent and dependent variables. The lowest strength (0.967 MPa) was observed for run 16, whereas the strongest bond (2.56 MPa) was observed for run 11. A quadratic model was used to depict the effect on MPa, which effectively determined the correlation coefficient. Figure 1b presents contour plots and a response surface illustrating the combined effects of CS ratio (A), applied voltage (B), and feed rate (C) on MPa. The results indicate that higher CS ratios and feed rates negatively affected MPa, whereas the applied voltage exerted a relatively mild synergistic effect. The decrease in MPa at higher CS ratios can be attributed to increased rigidity and reduced flexibility of the polymeric network, leading to structural inhomogeneity and weaker fiber integrity. Similarly, higher feed rates can result in insufficient solvent evaporation and poor fiber consolidation, thereby reducing mechanical strength. In contrast, increasing the applied voltage improves fiber alignment and stretching, thereby enhancing molecular orientation within the fibers and increasing MPa. However, excessively high voltage may induce jet instability, limiting further improvement.[56]

The contour lines' curved and elliptical shapes demonstrate that curvature, rather than a linear trend, controls the response, confirming the presence of significant quadratic interactions.

A perfect balance of feed rate, CS ratio, and voltage maximizes MPa, and this is the projected optimum, symbolized by a stationary point in the red-marked area. In terms of mathematics, it is expressed as:

$$Y2\ (MPa) = 1.82 - 0.4308A + 0.0678B - 0.2324C + 0.0205AB + 0.0295AC - 0.0220BC - 0.0221A^2 - 0.0623B^2 - 0.1008C^2 \quad \text{(ix)}$$

Final process optimization

The Design-Expert software optimization module was used to minimize Y1 and maximize Y2. Each variable was kept within a specified limit for this purpose. Based on numerical optimization using the CCD model, the optimized formulation parameters were predicted as follows: CS ratio (A) = 2% w/v, applied voltage (B) = 20 kV, and feed rate (C) = 1 µL/hr. Under these conditions, the predicted NF diameter and MPa were 256.504 ± 7.29 nm and 1.833±0.08 MPa, respectively. Table 5 presents the MPa experimental and anticipated findings for NFs under optimal conditions, which align with the observed values. Once the optimized formulation was obtained, 10 mg of the drug was loaded into the final formulation for further characterization.

Table 4. Computed coefficients, model, *p*-values, and fitting statistics of two responses using ANOVA according to CCD used for blank nanofiber optimization.

Response	Y1 (nanofiber diameter)	Y2 (tensile strength)
Intercept	+259.24	+1.82
A	+34.74	-0.4308
B	-8.09	+0.0679
C	+30.62	-0.2324
AB	+24.56	+0.02025
AC	+7.43	+0.0295
BC	+10.90	-0.0220
A^2	-4.92	-0.0221
B^2	-0.3637	-0.0623
C^2	+18.08	-0.1008
R^2	0.9911	0.9871
R^2 predicted	0.9389	0.9193
R^2 adjusted	0.9797	0.9703
SD	7.29	0.0805
CV %	2.70	4.82
Model F value	86.81	59.61
Model *p*-value	< 0.0001	< 0.0001
Model suggested	Quadratic	Quadratic

ANOVA, analysis of variance; CCD, central composite design; SD, standard deviation.

SEM

Figure 2 (a and b) visually represents the comparative SEM micrographs of B-NFs (optimised by CCD) and Ofx-NFs with their mean diameters and frequency distribution histograms. The FESEM characterization data showed that the Ofx-loaded NFs had a consistent, smooth, and nonwoven shape. Furthermore, the surface morphology of the Ofx-loaded NFs was cylindrical, like the NFs, and somewhat entangled in some areas. No drug crystals were visible on the surface of the NFs, indicating that Ofx was evenly distributed within the polymeric NFs. Additionally, compared to B-NFs without Ofx, the average fiber diameter of Ofx-NFs was 187.1±12.87 nm, a decrease in fiber diameter in a range of 120 nm to 50 nm. The decrease in fiber mean diameter upon the addition of Ofx may be ascribed to the enhanced conductivity of the polymer solution following the inclusion of Ofx.[57]

Swelling index

An agar plate technique was used to assess the stability of PVA/CS NF patches over 24 hours. Over the first 8 hours, the swelling behavior of B-NFs increased rapidly, peaking at about 120%. The swelling leveled off at about 100% after a day. The hydrophilic properties of PVA/CS and CS's exceptionally high-water retention, which promote fluid absorption, are responsible for this rise. The polymer network's slight degradation and structural relaxation are probably the causes of the subsequent decline.[58] The swelling trend of drug-loaded NFs was slower, stabilizing at around 105% after 20 to 24 hours and reaching approximately 95% at 8 hours (Figure 2c). This reduced initial swelling suggests that Ofx was incorporated into the polymer chains, forming hydrogen-bonded interactions that provide long-term structural stability while temporarily preventing water penetration. Because it facilitates controlled release by keeping the polymer matrix wet while gradually releasing the drug, its stability is highly beneficial for localised drug delivery.

MPa

Tensile testing was used to assess the mechanical characteristics of both unloaded and drug-laden NF mats (crosshead speed: 5 mm/min, 18 °C). The blank mat's yield strength was 1.99 ± 0.14 MPa, its elongation rate was 17%, its Young's modulus was 16.921 MPa, and its maximum load was 11.15 N. The Ofx-NF mat MPa (1.32 ± 0.08 MPa), elongation rate (13%), and Young's modulus (7.7 MPa) were found to be decreased after drug loading, keeping the maximum load (11.09 N) constant (Figure 2d). This suggests that the integration of the active moiety within the fiber compromises and reduces toughness,[59] possibly owing to enhanced porosity, microstructural imperfections or specific plasticization.[60] As drug loading resulted in a ~56% decrease

Table 5. Illustrates the predicted and observed values of the PVA/CS nanofiber.

Responses (blank nanofiber)	Actual	Predicted
Nanofiber diameter (nm)	244.60 ± 14.21	256.504 ± 7.29
Tensile strength	1.99 ± 0.14	1.833 ± 0.08

PVA, polyvinyl alcohol; CS, chitosan.

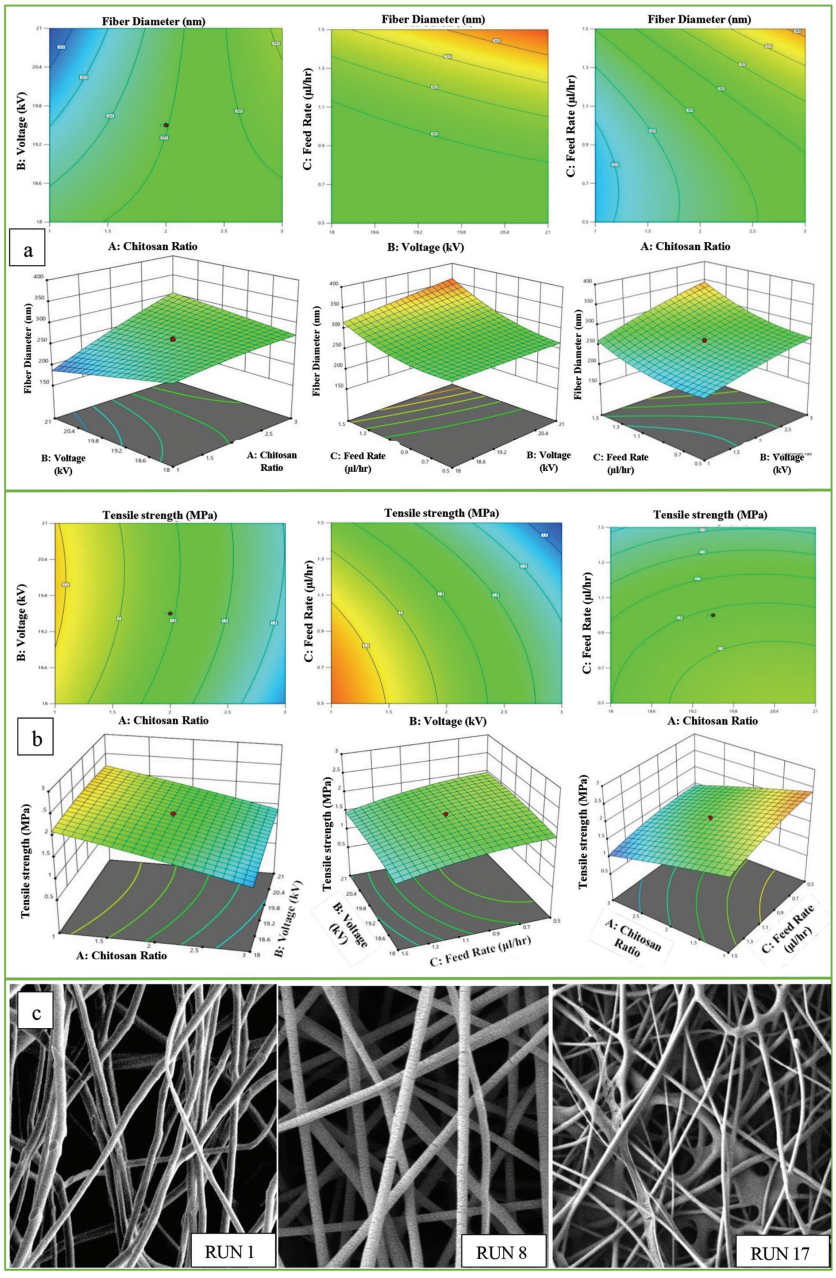

Figure 1. a, b) Contour and 3D response graph effect of the independent variable nanofiber diameter (nm), tensile strength (MPa), respectively. c) SEM images of 1,8 and 17 run numbers used in the design experiment show the nanofiber's quality and density with a 200–400 nm diameter.

SEM, scanning electron microscopy.

in stiffness, a ~41% decrease in MPa, and a ~34% decrease in elongation when compared with blank mats.

FTIR

To observe chemical changes or interactions between the drug and excipients, a FTIR study was performed. The FTIR spectra of the active moiety Ofx, PVA, CS, B-NF, and Ofx-NFs are depicted in Figure 3a. The existence of distinctive peaks of Ofx at 3426 cm^{-1} is due to N-H stretching of the secondary amine group, C = O stretching of carboxylic acid at 1720 cm^{-1}, 1620 cm^{-1} (C = O stretching of the quinolone group), 1287 cm^{-1} (CN stretching), and 1057 cm^{-1} (C-F stretching). PVA showed distinctive absorption bands highlighting a broad peak at 3426 cm^{-1}, indicating OH stretching brought by intermolecular hydrogen bonding, 2428 cm^{-1} (CH stretching), and 1080–1140 cm^{-1} (CO, acetyl groups). At approximately 3469 cm^{-1} (OH and NH stretching), 1650 cm^{-1} (amide I, CO stretching), and 1560 cm^{-1} (amide II, NH bending), CS exhibited distinct peaks. The strong peaks of both polymers were observed in the B-NFs spectra, with minor shifts and decreased intensities, indicating interactions and hydrogen bonding between PVA and CS. The main Ofx characteristic

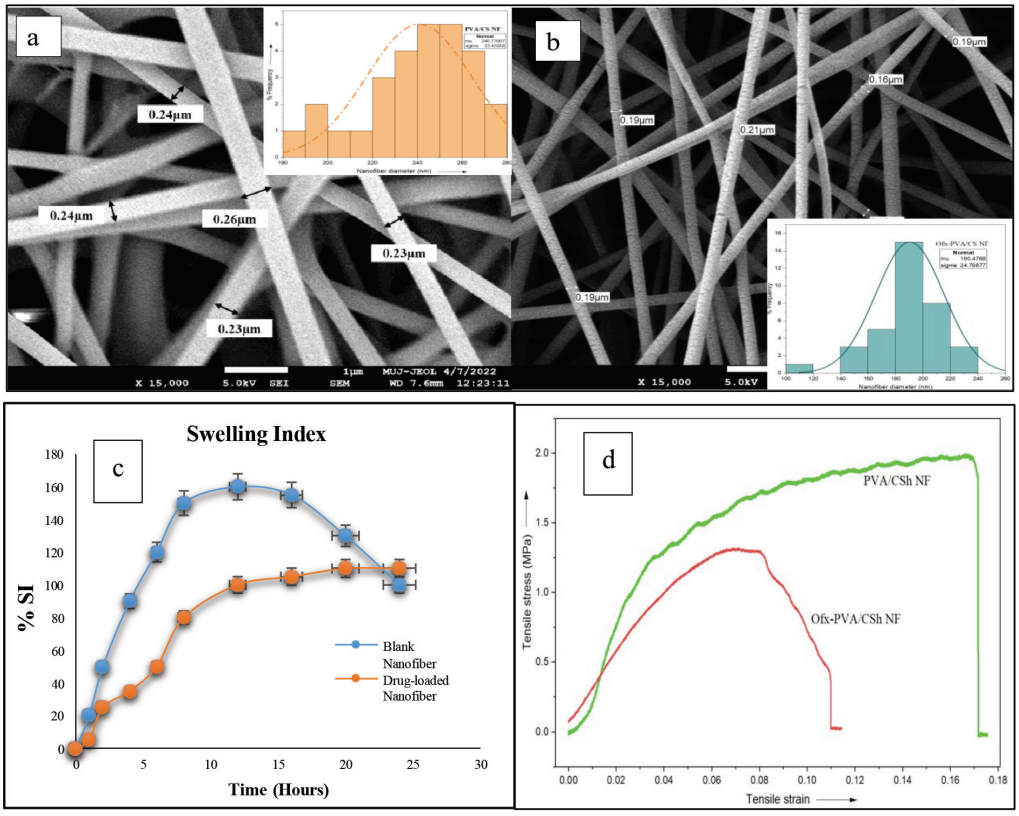

Figure 2. SEM image and frequency distribution curve of a) B-NF (optimised via CCD), b) Ofx-loaded NF; comparative graph of, c) Swelling index, and d) Tensile strength of both the formulations.

Ofx, ofloxacin; PVA, polyvinyl alcohol; CS, chitosan; NF, nanofiber; SEM, scanning electron microscopy; CCD, central composite design.

peaks were visible in the Ofx-NFs spectra, albeit slightly shifted or with diminished strength. This shows that the active moiety was successfully incorporated within the polymeric NF matrix without experiencing any notable disintegration or chemical reactivity. The lack of additional peaks suggested that the drug was loaded primarily through physical trapping and hydrogen bonding, rather than covalent chemical bonding.

DSC

Differential scanning calorimetry was used to determine the thermal properties of Ofx-NF and its constituent parts. Figure 3b shows the DSC temperature maps of Ofx, PVA, CS, B-NFs, and Ofx-NFs. As shown, OFX exhibits a distinct endothermic peak at 276.36 °C, attributed to the melting of the drug and indicating the substance's crystallinity. At approximately 72.81 °C, PVA exhibited an extended endothermic peak, indicating moisture loss. This was promptly followed by a thermal transition indicative of its semi-crystalline structure at 223.05 °C. At 87.35 °C, CS showed an endothermic peak ascribed to structural relaxation and dehydration. Endothermic transitions were observed in the B-NFs at 72.81 °C and 223.05 °C, indicating partial disruption of crystallinity and polymer mixing. Pure Ofx did not exhibit a prominent melting peak, indicating that the drug was successfully entrapped in the polymeric matrix in an amorphous or molecularly dispersed condition. In contrast, the Ofx–PVA/CS NF had peaks at 72.81 °C and 232.75 °C. These results show that Ofx and the PVA/CS network exhibit significant intermolecular interactions, thereby enhancing the formulation's heat stability.[61]

Drug loading and % EE

The theoretical content of the drug in a 2 × 2 cm^2 sample of NFs was calculated to be about 0.25 mg. The drug content obtained was about 0.244 mg, corresponding to an encapsulation efficiency of 97.54 ± 0.89% (n = 3). The drug load in the NFs was 4–7%, depending on the weight of the NF sample. This indicates that nearly all of the active moiety incorporated during electrospinning was effectively retained within the NF matrix, resulting in efficient drug delivery. Appropriate drug loading and higher entrapment of Ofx within the NFs appear capable of providing prolonged and efficient release of it, making them suited for a localized drug delivery system.

In vitro drug release and kinetics

According to the findings, NFs can regulate drug release for up to 216 hours (Figure 4a). The crosslinked Ofx-NFs showed 95.61% drug release over 216 hours, and Ofx alone showed nearly 97% release within 12 hours in SUF at pH 6.8.

An initial burst release of approximately 29% was observed within the first 2 hours, likely due to rapid drug release from the

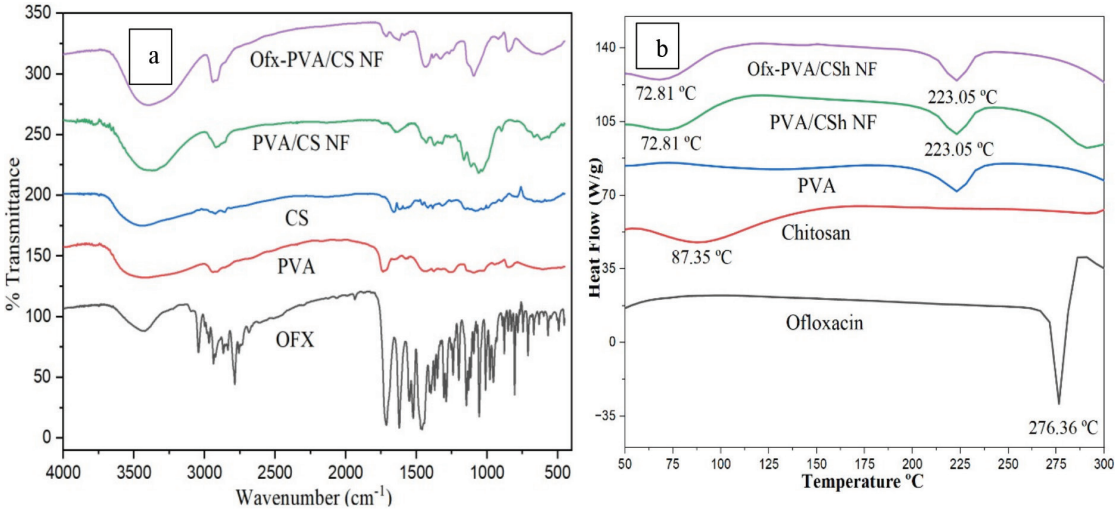

Figure 3. a) FTIR spectra and b) DSC curve of ofloxacin, polymers alone, blank nanofibers, and drug-loaded nanofibers.

Ofx, ofloxacin; PVA, polyvinyl alcohol; CS, chitosan; NF, nanofiber; FTIR, Fourier-transform infrared spectroscopy; DSC, differential scanning colorimeter.

NF surface. This was followed by a sustained-release phase, indicating controlled drug diffusion from the polymeric matrix.

The key factor influencing how long the Ofx remained on the NF was crosslinking the fiber with glutaraldehyde for 24 hours. When PVA/CS NFs are immersed in uterine fluid, they dissolve instantly into a substance comparable to a gelatinous compound.[59] This may limit the application of a PVA/CS coating in uterine tissues. The mechanical properties were improved due to the link created between the reactive side groups of CS (NH) and PVA (OH), achieved by chemical crosslinking with GA vapour.[62] The GA caused the reaction to move from the exterior layer to the interior layer of NF. Therefore, the resulting intermolecular pressures cause both the swelling pace and the pharmaceutical delivery rate to decrease.[37]

Four different mathematical models, along with their corresponding regression values, were employed to describe the release kinetics of Ofx and its release from NFs, as listed in Table 6.

Table 6. Regression coefficient values of the different drug release models.

Model	Ofloxacin	Ofx-NF
Zero order	0.1138	0.113
First order	0.8308	0.2717
Higuchi model	0.9062	0.9062
Korsmeyer–Peppas	0.9492 (n=0.383)	0.9647 (n = 0.236)

Ofx, ofloxacin; NF, nanofiber.

Four distinct mathematical models were employed to explain the release kinetics of Ofx and its release from NFs. However, the Korsmeyer–Peppas model fitted the curves of Ofx (R^2 = 0.9492, n = 0.383) and Ofx Nf (R^2 = 0.9647, n = 0.236) very well, indicating a release mechanism regulated by Fickian diffusion. The dissolution mechanism in both instances was primarily controlled by diffusion through the hydrated polymeric medium, as further demonstrated by the strong correlation with the Higuchi model (R^2 = 0.9062). The first-order (R^2 = 0.8308 and 0.2717) and zero-order (R^2 = 0.1138 and 0.113) models did not fit the data well, suggesting that the release was neither concentration-dependent nor occurring at a steady rate over time. Instead, drug-polymer interactions, hydration, and swelling affected the release. Crucially, Ofx's diffusion rate was decreased when it was incorporated into the PVA/CS NF matrix as opposed to when it was pure, indicating a sustained release behaviour of the drug delivery system.[63,64]

Ex vivo permeation

A sustained release of the active moiety was found to be released across the uterine mucosa of a goat in the *ex vivo* permeation testing. The cumulative permeation profile (Figure 4b) reveals an initial lag phase, followed by a linear rise, and ultimately forms a plateau. Normalization versus membrane surface area was compared by the cumulative amount penetrated per unit area. The computed steady state flux (J) and apparent permeability coefficient (Papp) were 1.027 µg/cm^2/h and 0.01027 cm/h, respectively. These results correlate well with the sustained release profile, indicating that prolonged drug availability from the NFs supports continuous permeation across the mucosal barrier.[65]

It is worth noting that preserved mucosal samples in formalin were used in this experiment; therefore, the natural permeability might be affected by protein cross-linking and decreased fluidity of cell membranes. Thus, the presented outcomes can only be considered relative rather than actual data, since the

permeability of living tissues may differ. Identical results were achieved during multiple tests under the same conditions.

Mucoadhesion study

Using the manual modified glass-slide method, the mucoadhesive strength of the composed fiber was assessed on goat uterine mucosa. The detachment force and residence duration of B-NF were 0.72 ± 0.13 N and 65 ± 0.8 min, respectively, while drug-loaded had somewhat lower values (0.45 ± 0.14 N; 40 ± 0.15 min). This decrease in the range is explained by Ofx molecules interfering with the hydrogen bonding between polymers and mucin, which weakens adherence.[66] NF formulations maintained strong adherence due to their large surface area, porous structure, and close penetration into the mucosal folds, which improve physical entanglement and adhesive interactions.[67]

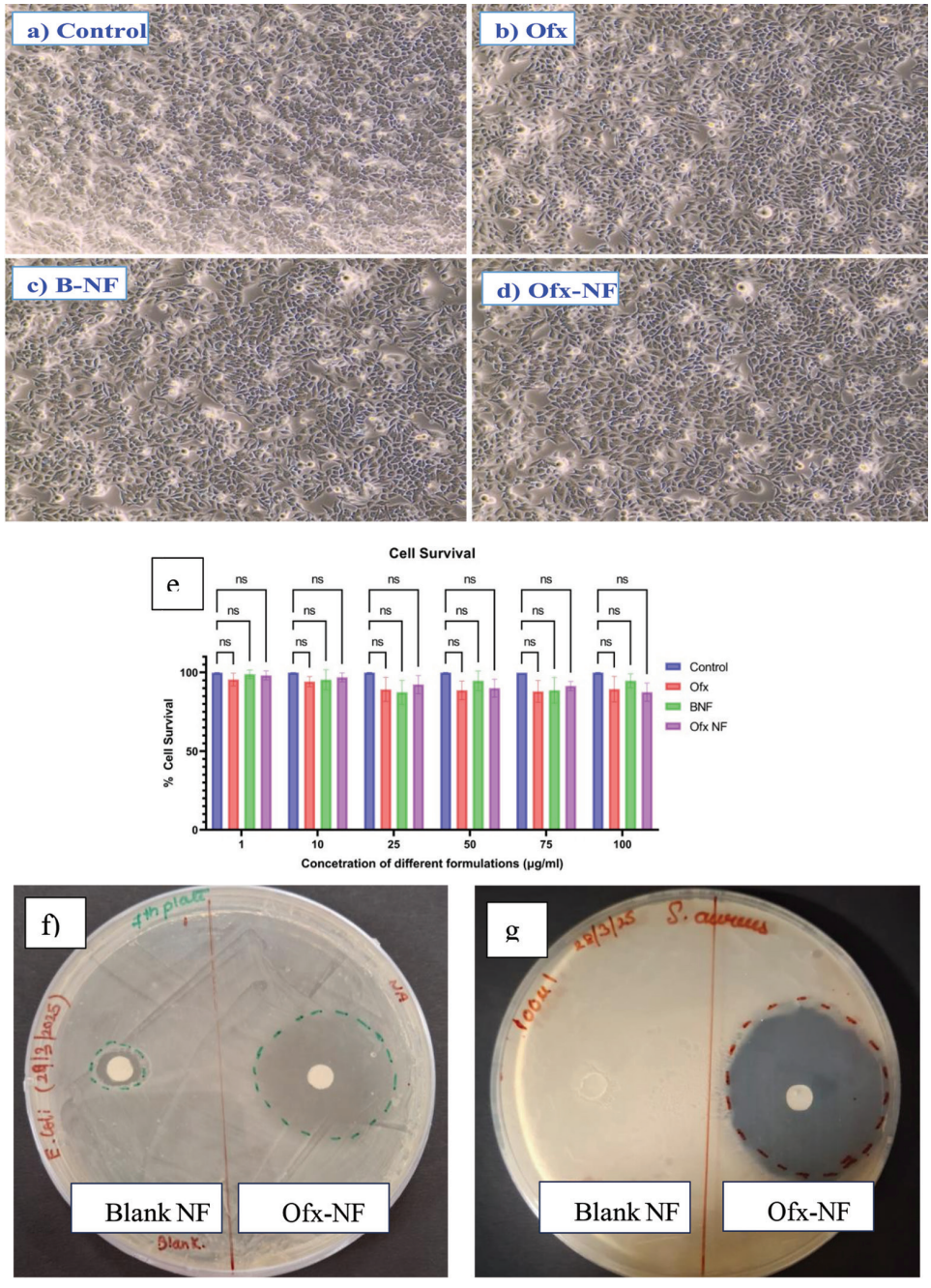

Figure 4. *In vitro,* (a-e) cell viability performed on HeLa cells after being treated for 24 h under a 40× inverted microscope: (a) control (DMSO), (b) Ofx, (c) B-NF, (d) Ofx-NF (100 µg/mL Conc.), and (e) graphical representation of % cell viability v/s drug and formulation at different concentrations (ns = statistically non-significant, $p > 0.05$) (f, g) antimicrobial study showing zone of inhibition on f) *E. coli* g) *S. aureus.*

Ofx, ofloxacin; NF, nanofiber; B-NF, black NF.

Cell viability study

The cytotoxicity test was used to determine cell viability of Ofx, B-NF, and Ofx-NF at doses ranging from 1 to 100 µg/mL against HeLa cells, and was evaluated by microscopic observation. All examined groups remained viable (> 90%), and there was no discernible difference between the Ofx, B-NF, and Ofx NF groups. Adding Ofx did not result in cytotoxic effects, and the NF matrix was non-toxic. Using DMSO as a control, microscopic pictures of the treated cells were taken at a concentration of 100 µg/ml (Figure 5a). Neither the B-NF nor Ofx-NF exhibited any cytotoxic effects on HeLa cells when observed under a microscope. Cell viability was somewhat lower in pure Ofx at a 100 µg/ml dose. Figure 5e also shows the cytotoxic effects of several samples as a percentage plot of cell viability against concentration. Since there was no discernible 50% decrease in cell viability, the IC_{50} values for Ofx, B-NF, and Ofx NF were more than 100 µg/mL, respectively. Although cell viability reveals a negative impact on increasing the concentration for all treatment groups (Ofx, B-NF, and Ofx NF), statistical analysis using two-way ANOVA followed by Dunnett's multiple comparison test revealed that the changes were not statistically significant (NS) ($p > 0.05$). These findings indicate that the developed nanoformulations exhibit good cytocompatibility and do not significantly affect mammalian cell viability under the studied conditions.

Antimicrobial study

Using the disc diffusion agar method, the effectiveness of Ofx, NF, and Ofx-NF was evaluated against Gram-positive and Gram-negative bacteria (i.e., *S. aureus* and *E. coli*). Figure 5f and Figure 5g displays the antibacterial performance of each sample. The presence of innate antibacterial activity was confirmed by the B-NFs and Ofx-NFs exhibiting a 5 ± 1.68 mm and 25 ± 0.65 mm zone of inhibition (ZOI) in *E. coli*, respectively, in Figure 5f. The *S. aureus* culture plate in Figure 5g showed no ZOI by B-NFs, but the ZOI for OFX-NFs was 35 ± 0.08 mm. Due to the drug's rapid accessibility in the medium, the drug-loaded NFs exhibited the largest ZOI, indicating strong antibacterial capabilities. Detecting an inhibitory zone in the NF blank in *E. coli* demonstrates that OFX-NFs function as a synergistic system. The presence of CS with antibacterial qualities, which results from the regulated release of the active moiety from the confined extracellular matrix of the NF, may be the source of this.[68]

In vivo study

Isolation and identification of bacteria

To identify and isolate bacteria from the uterus of cattle with SE, a sample must be aseptically collected using cytobrush technology. MLA, BHI, SDA, and other selective and nonselective media are inoculated with the sample and incubated under the appropriate conditions. A critical step in identifying bacteria is the Gram stain technique, which distinguishes bacteria based on the arrangement of their cell wall's membrane.

Under a microscope, Gram-negative bacteria, such *as E. coli*, absorb the contrast dye (safranin), making them appear pink (Figure 6a), whereas Gram-positive bacteria, such as *Staphylococcus* species, retain the crystal violet pigment and appear purple (Figure 6b).[69] *E. coli* was the most frequently isolated bacterium, followed by *Staphylococcus* spp., a hybrid infection (gram-positive and gram-negative rods), and *Candida* spp. The outcomes were analysed using statistics, and it was found that *E. coli* was a ubiquitous bacterium isolated from the uteri of the cattle under research.[70] Meanwhile, the incidence of *Staphylococcus* sp. and a combined infection was also documented. Only *Candida* spp. was detected in uterine samples (Figure 6c).

Effect of treatment on bacterial load of uterine lavage samples

The impact of therapy on the number of microorganisms present in uterine lavage samples was analyzed during oestrus. In Group 1 (control), normal saline was administered, and a slight reduction in CFU/mL was observed; however, this was not statistically significant, as it was similar to the pretreatment levels in Groups 2 and 3. In groups 2 and 3, the CFU count

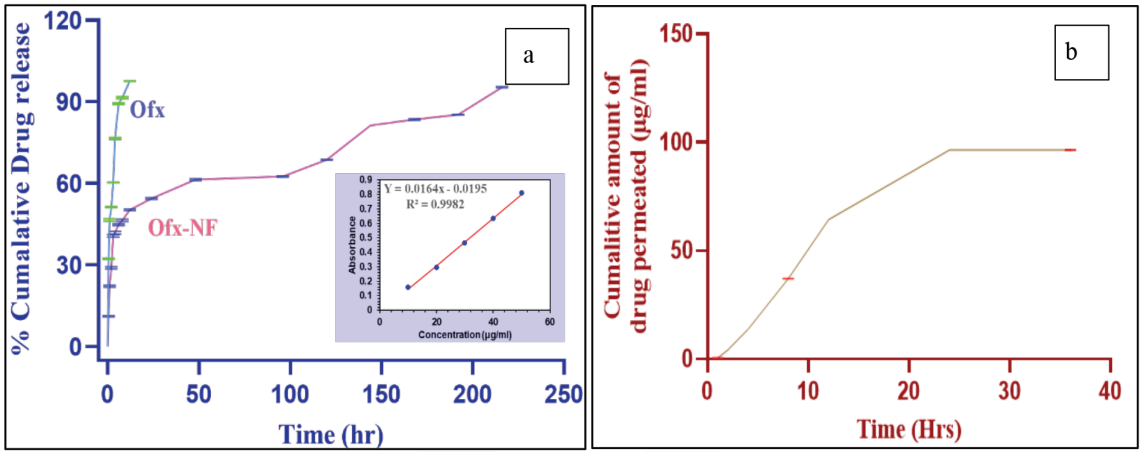

Figure 5. Graphical representation of a) *in vitro* release and b) *ex vivo* permeation studies of Ofx from Ofx NFs.
Ofx, ofloxacin; NF, nanofiber.

decreased significantly ($p \leq 0.05$) post-treatment, even though the values were numerically lower in group 3 than in group 2; however, this difference was not significant ($p \leq 0.05$), as depicted in Table 7.

pH of vaginal mucus

The pH of cervicovaginal mucus in the control and treatment group (Ofx, Ofx-NFs) was recorded during oestrous. No significant difference ($p < 0.05$) was recorded between the mean pH value of cervicovaginal mucus of the control group and the positive control group, both at the pre-treatment and post-treatment stages. A significantly ($p < 0.05$) higher mean pH value of cervicovaginal mucus was observed in the Ofx-NF-treated group as compared to the positive control group after post-treatment (Table 7).

Endometrial cytology for the diagnosis of SE

The proportion of PMN cells, a marker of infection or inflammation, was assessed in three groups: the positive control group (group 2; Ofx-treated group), the control group (normal saline), and the Ofx-NFs group (Table 7) before and after treatment. In groups 2 and 3, significant reductions in PMNs ($p \leq 0.05$, one-way ANOVA) were observed both before and after treatment. The PMN count was lower in group 3 than in group 1, but the difference was not significant. Post-treatment, PMN cells decreased significantly in both groups 2 and 3; however, the incorporation of Ofx in NF showed greater effectiveness (Figures 7a and 7b). The Ofx-NF treatment was found equally efficient as that of Ofx even at 1/3rd doses (total 400 mg intrauterine) and single administration, compared to that of Ofx, given at comparatively high doses, i.e., total 1200 mg, which was administered for 3 days in divided doses (conventional treatment, i.e., 400 mg daily intrauterine), suggesting sustained release potential of the Ofx-NF.

Pregnancy diagnosis

Pregnancy rates in Groups I, II, and III were evaluated following artificial insemination during the subsequent estrus. The highest pregnancy rate was observed in Group III (Ofx-NF), followed by Group II, while the lowest was recorded in Group I (control) (Figure 7c). The differences among groups were statistically significant ($p < 0.05$, chi-square test). However, none of the animals in group 1 conceived, as previously reported, indicating

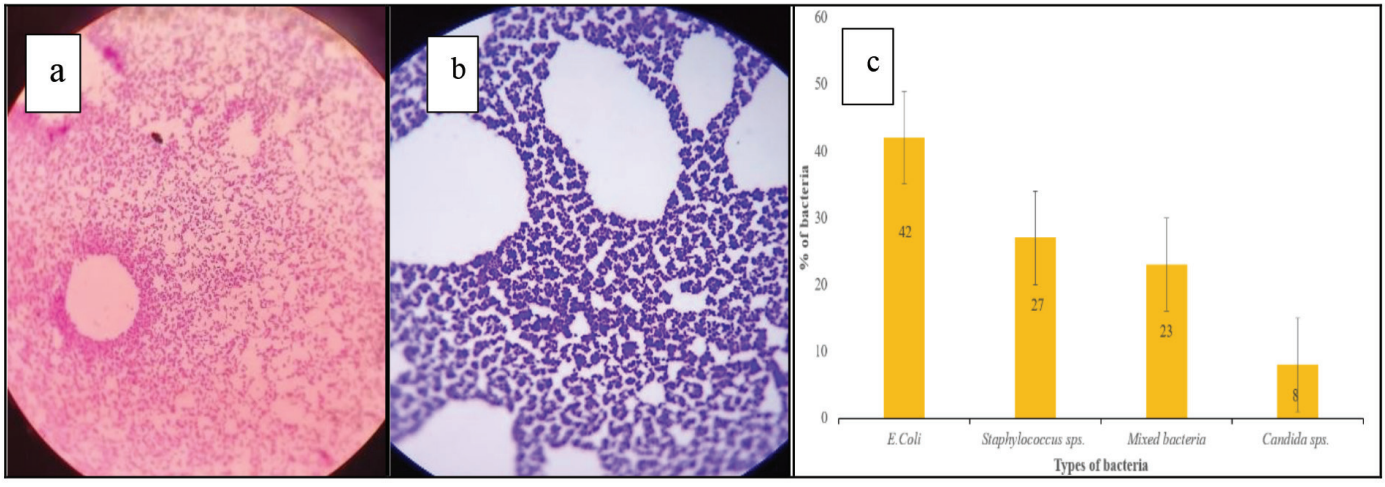

Figure 6. Microscopic image of a) *E. coli*, b) *Staphylococcus* spp. and c) graphical representation of identified types of bacteria in uterine samples.

Table 7. Effect of bacterial load in uterine samples, pH of cervicovaginal mucus in cattle, PMN cells, and pregnancy status of experimental animals (n = 8).

Type of treatment	Pre/post treatment	Group 1 (Control)	Group 2 (positive control)	Group 3 (nanofiber)
Effect of bacterial load	Pre	$2.33\times10^5 \pm 47.06^A$	$2.32X10^5 \pm 89.57^A$	$2.33X10^5 \pm 70.21^A$
	Post	$2.31X10^5 \pm 71.23^A$	$2.32X10^3 \pm 12.09^B$	$1.23X10^3 \pm 20.86^B$
pH of cervicovaginal mucus	Pre	7.13 ± 0.09^A	7.52 ± 0.7^A	7.2 ± 0.7^A
	Post	7.28 ± 0.06^A	7.92 ± 0.1^A	8.2 ± 0.9^B
PMN cells	Pre	7.57 ± 0.35^A	7.52 ± 0.29^A	7.66 ± 0.61^A
	Post	7.73 ± 0.36^A	2.50 ± 0.32^B	1.83 ± 0.30^B
Pregnancy outcome	Post	8 not conceived	4 pregnant	4 pregnant

Data in an identical row containing various superscripts vary considerably ($p \leq 0.05$).
PMN, polymorphonuclear cell.

that SE severely impacts reproductive performance.[71] The NF was equally effective in treating SE, even at one-third the dose of the conventional treatment regimen. Thus, the NF-treated group achieved the highest pregnancy rates after insemination (Table 7). It was found that vaginal pH also affects the rate of conception.[72] Thus, pH estimation can be an alternative, non-invasive method for tracking cattle fertility and uterine health. While values around pH ≥ 8.0 are substantially associated with better conception and pregnancy outcomes, a threshold of pH ≥ 7.0 is a reliable predictor of SE.[73] Similar results support the use of vaginal pH monitoring as a reliable measure for both early disease identification and reproductive performance prediction, despite slight discrepancies across studies due to methodological variables.[74]

Pharmacokinetic study

Ofx concentrations in plasma samples were quantified using an RP-HPLC method. A calibration curve was constructed over the concentration range of 2-10 µg/mL, showing good linearity (R^2 = 0.998). The LOD and LOQ were 0.54 µg/mL and 1.65 µg/mL, respectively.

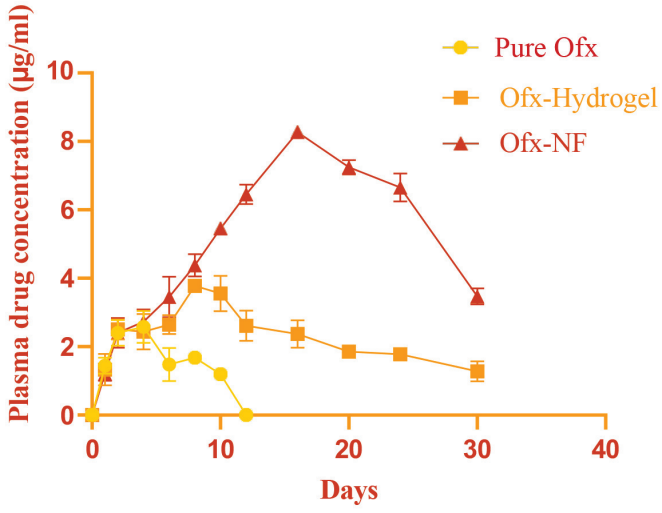

Figure 7. Plasma concentration time graph of drug and formulations.
Ofx, ofloxacin; NF, nanofiber.

Ofx, Ofx-hydrogel (taken for a comparative study), and Ofx-NF were assessed for additional *in vivo* pharmacokinetic research. Figure 8 displays the graph against drug plasma concentration with time. Ofx, Ofx-hydrogel (used for comparative purposes), and Ofx-NF were assessed for additional *in vivo* pharmacokinetic studies. The animals treated with Ofx-NF (Group III) and Ofx-hydrogel (Group IV) exhibited significantly higher plasma drug concentrations at various time points than those treated with pure Ofx (Group I) ($p < 0.0001$; two-way ANOVA).

Pharmacokinetic parameters were calculated using PK Solver software, and the results are summarized in Table 8. Ofx-NF and Ofx-hydrogel exhibited significantly higher mean residence times and C_{max} values than pure Ofx. The clearance rate of the free drug was 10-15 times higher than that of the nanoformulation. This may be due to the high entrapment of Ofx into the nanoformulation, resulting in a low volume of distribution for Ofx-NF/Ofx-HG. The significance of the pharmacokinetic factors makes it clear that the production of Ofx (400 mg: dose at once) in the form of NF resulted in a sustained effect with a higher T_{max} value and MRT, with a lower volume of drug distribution in comparison to pure Ofx (cumulative dose of 1200 mg : 400 mg for 3 consecutive days), which resulted in lower MRT, T_{max} with higher clearance rate. These outcomes reinforce Ofx-NF as a potential drug delivery system, extending the drug's biological half-life and increasing its bioavailability.[37] These favorable data may suggest greater efficacy and the potential for dose reduction in veterinary treatment.

DISCUSSION

The goal of the current study was to develop and statistically optimize Ofx-loaded PVA/CS NF via a CCD approach to deliver intrauterine in bovines during SE. This model enabled the systematic evaluation of formulation variables, such as the effect of the polymer (CS), applied voltage, and flow rate, on critical quality attributes, including fiber diameter and MPa. The statistical analysis indicated a quadratic fit model for both responses, with regression coefficient values (R^2) of 0.979 and 0.970 for NF diameter and MPa, respectively.

Table 8. Various pharmacokinetic parameters.

Parameter	Unit	Ofx	Ofx-hydrogel	Ofx-nanofiber
$t_{1/2}$	D	4.54 ± 2.57	12.03 ± 1.93	9.39 ± 3.25
T_{max}	D	2 ± 1.07	10 ± 0.57	16 ± 1.12
C_{max}	µg/mL	2.68 ± 1.27	3.92 ± 2.97	8.14 ± 1.98
$AUC_{0-\infty}$	µg/mL*d	21.82 ± 2.46	86.60 ± 1.62	215.28 ± 1.63
MRT	D	7.55 ± 1.03	20.35 ± 1.82	22.83 ± 2.51
Vz/F	(mg)/(µg/mL)	180.68 ± 0.52	40.11 ± 2.29	12.59 ± 1.05
Cl/F	(mg)/(µg/mL)/d	27.49 ± 1.87	2.30 ± 3.99	0.92 ± 0.89

AUC, area under the curve; Ofx, ofloxacin.

The predicted formulation, as per the CCD model, yielded bead-free, smooth, and uniformly sized NFs with an average diameter of 256.504 ± 7.29 nm, as analysed by SEM, and a MPa of 1.833 ± 0.08 MPa, as analysed by the texture analyzer. The minimum discrepancy between the experimental and anticipated values supports the validity of the optimization procedure used in this investigation. The inclusion of the active moiety (Ofx) within the predicted NF structure (CCD) resulted in an overall decrease in MPa and a reduction of NF diameter from 120 nm to 50 nm, due to adequate encapsulation of the drug within the polymeric matrix system. The physicochemical properties of the drug, excipients, and formulation were verified using FTIR and DSC. FTIR reveals no incompatibility between the drug and excipients used in the formulation. In contrast, a slight shift or diminished strength of a sharp peak shows that the active moiety was successfully incorporated within the polymeric NF matrix without experiencing any notable disintegration or chemical reactivity. The absence of a prominent melting point peak of Ofx-NF in the DSC thermogram suggests that the drug is successfully entrapped in the polymeric matrix, either in an amorphous or molecularly dispersed condition. The higher encapsulation efficiency and lower swelling index of Ofx-NF result in efficient drug release. The *in vitro* release studies unveiled burst release of Ofx solution within a few hours, and in the case of Ofx-NF, a sustained release of Ofx from the polymeric matrix for more than 7 days. A polymeric matrix of PVA/CS encapsulated with Ofx acts as a diffusion barrier, enabling a slow release of the molecule. Thus, crosslinking of these PVA/CS NFs with glutaraldehyde may lower the release rate. At the same time, strong electrostatic interactions and hydrogen bonds between both the polymers further contribute to a compact structure that restricts rapid drug diffusion.[75] Furthermore, the Korsmeyer–Peppas kinetic model was well-fitted, suggesting the diffusion of Ofx from the NF through the hydrated polymeric medium. The antimicrobial study revealed that the Ofx-loaded NF effectively inhibited the growth of *E. coli* and *S. aureus*, the predominant pathogens associated with bovine metritis. The observed antibacterial effect can be correlated with the sustained availability of Ofx at the target site, which ensures prolonged exposure of bacteria to the therapeutic concentration of the drug. The mucoadhesive properties of the NF were significantly enhanced by incorporating CS into the PVA matrix. Mucoadhesion testing confirmed strong adherence of the NF to goat uterine mucosa, which is likely due to the cationic nature of CS and its interaction with negatively charged mucin. This property is particularly beneficial for intrauterine application, as it enhances retention time and prevents premature expulsion of the formulation. Similar findings have been reported for PVA/CS-based systems used in vaginal and wound applications.[76] Experiments on the survival of HeLa cells have demonstrated that NFs are non-toxic and biocompatible, maintaining viability of over 80–90% after 24 hours of exposure. The lack of

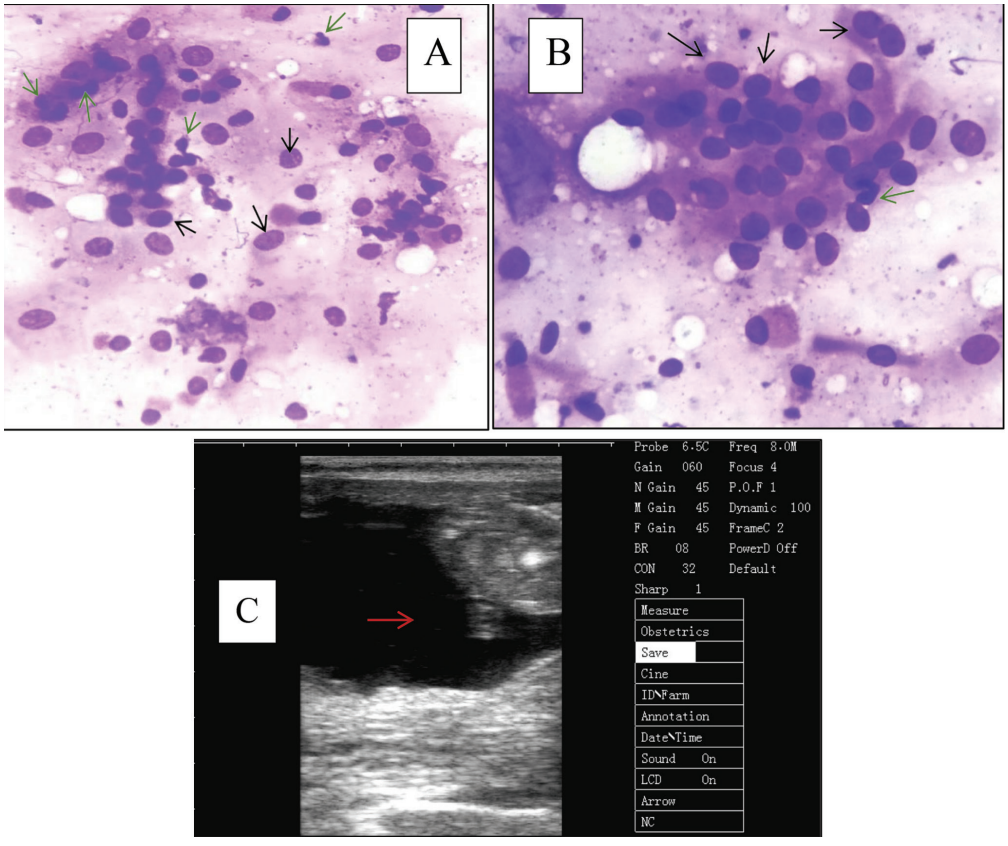

Figure 8. Microscopic picture (40X) of endometrial cytology showing PMNs (green arrows) in between endometrial cells (black arrows) A) pre-treatment b) post-treatment c) ultrasonography image of bovine pregnancy (red arrow showing embryo).

cytotoxicity indicates that both the polymers (PVA and CS) and the incorporation Ofx are suitable for mucosal application. The *ex vivo* permeation investigation with excised goat mucosa revealed a progressive and regulated elimination of Ofx from the NF scaffold. The potential of the NF to maintain drug transport across the uterine epithelium was confirmed by its permeation flux and cumulative drug permeation. The intimate contact of mucoadhesive NFs with the mucosal surface and CS's bioadhesive properties momentarily open epithelial tight junctions, promoting drug diffusion, which may be the cause of the enhanced permeation. However, the present study is not limited to *in vitro* and *ex vivo* evaluations.

Future studies should include *in vivo* pharmacokinetic and pharmacodynamic investigations in bovine models to assess the real-time drug release, local absorption, and therapeutic efficacy. Isolation of bacteria from cattle uterus was identified using staining technique, which indicated the presence of *E. coli* > *Staphylococcus* spp. > mixed bacteria > *Candida* spp. in SE animals. The CFU count revealed a significant difference in Ofx and Ofx NF between treated cattle and controls. A similar result was observed in the case of cervico vaginal pH, which was brought up, i.e., shifting of neutral pH to slightly alkaline. The most crucial pharmacodynamic study to assess SE treatment efficacy is the endometrial cytology study for SE diagnosis. Since PMS cells are recognized as markers of inflammation, a significant reduction in PMN cells was observed after post-treatment with Ofx NF compared to Ofx alone. The conventional treatment involved a cumulative dose of 1200 mg of Ofx (400 mg administered over three consecutive days), whereas the Ofx-NF formulation was administered as a single intrauterine dose of 400 mg. Despite the lower total dose, the Ofx-NF formulation demonstrated comparable therapeutic efficacy, likely due to its sustained-release properties and enhanced local retention at the site of action. This study was designed to evaluate the sustained-release and localized delivery efficiency of the NF system rather than direct dose equivalence. Therefore, the findings should be interpreted in terms of improved drug retention, prolonged release, and localized bioavailability rather than in terms of cumulative dose comparisons. Furthermore, the therapeutic effectiveness was supported by pregnancy outcomes, with the NF-treated group exhibiting a higher conception rate than the conventional Ofx-treated group, indicating improved clinical efficacy of the developed formulation. This suggests that the NF was equally effective in treating SE, even at one-third the dose of the conventional treatment regimen. It was also found that animals with vaginal pH levels of 8 or higher have a higher chance of pregnancy or better conception than those with acidic or neutral pH levels. Thus, vaginal pH evaluation can also serve as an alternative diagnostic tool for identifying SE. A pharmacokinetic study further supported the controlled release and retention behavior of the optimized formulation. Drug concentration-time profiles were compared with those of pure Ofx, Ofx-NF, and Ofx-Hydrogel, which showed notably greater mean residence times and maximum concentrations. The clearance rate of Ofx alone was 10–15 times higher than that of the nanoformulation. This might be due to a lower volume of distribution of the formulation compared to a larger trapping of Ofx within it. Ofx-NF produced prolonged effects, with enhanced T_{max} and MRT, following a single 400 mg dose; however, pure Ofx administered over 3 days resulted in reduced T_{max} and MRT, accompanied by higher clearance.

These results demonstrate that Ofx-NF is a viable drug delivery method that improves the bioavailability and retention of medications in veterinary therapy, leading to enhanced efficacy and potential dose reduction. It sustains therapeutic levels at the target site for an extended period, benefitting clinical outcomes and presenting a cost-effective solution for intrauterine infections. While the development of Ofx-loaded PVA/CS NFs shows promise for localized treatment in bovine uterine infections, further research is required to assess long-term safety and effectiveness.

Study limitations

The present study has some limitations that should be considered when interpreting the findings. The study was conducted using a relatively limited number of animals and under controlled experimental conditions; therefore, the findings may not fully represent the variability encountered in field conditions. Although the developed mucoadhesive nanofiber demonstrated promising therapeutic potential for managing subclinical endometritis, the observation period was limited and did not allow assessment of long-term reproductive outcomes or infection recurrence. Furthermore, comprehensive long-term safety and local tissue tolerance studies are required to establish the safety profile of repeated or prolonged administration. A larger-scale, multicentric field study with extended follow-up and direct comparison with established therapeutic regimens would be valuable to further confirm the efficacy, safety, and practical applicability of the developed nanofiber formulation. Future studies should also investigate its effects on subsequent reproductive performance, calving-to-conception interval, and pregnancy rates under commercial farm conditions.

CONCLUSION

Intrauterine delivery of Ofx-loaded PVA/CS NF was hypothesized to improve the efficacy of Ofx in the treatment of SE in cattle. The encapsulation of Ofx in NFs provides a larger surface when applied at the site of action. The design of localized treatment of bovine endometritis presents a promising advancement in veterinary drug delivery. The incorporation of mucoadhesive polymers such as CS and PVA, along with process parameter optimization through CCD, results in NFs exhibiting desirable mechanical strength, mucoadhesive properties, and controlled drug release profiles. The current data, including both *in vitro* and *in vivo* research, demonstrate an innovative strategy for delivering Ofx via intrauterine NF encapsulation, facilitated by the development of Ofx-NFs. The creation of Ofx-NFs improved Ofx's residence time, increased its t1/2, and enhanced treatment efficiency, even at 1/3rd the doses of the conventional treatment regimen, with optimum pregnancy rates. This could result in a single administration of the formulation during the

entire course of treatment for SEs. The overall performance and cytotoxicity of Ofx against HeLa cells were improved upon encapsulation in the NF, as shown in cell viability studies. This can be investigated further in preclinical studies to confirm and explore.

Advantages over conventional treatments and research gaps

Cattle with SE are frequently treated with systemic or intrauterine antibiotics, including fluoroquinolones, tetracyclines, and cephalosporins. The aforementioned remedies can lower the microbial load. Still, they are often ineffective due to systemic adverse reactions, limited bioavailability at the site of infection, minimal drug retention in the uterine lumen, and the potential for the development of antimicrobial resistance after recurrent administration. Additionally, only a portion of the drug is delivered to the tissue of the uterus in therapeutically beneficial doses via oral or intravenous delivery. Localized delivery methods based on NFs are a viable substitute. With their high drug-loading capacity, regulated release, robust adherence to mucosal surfaces, and enhanced penetration, electrospun NFs, particularly those made with mucoadhesive polymers like CS and PVA, ensure sustained medication availability at the target site. Thus, Ofx-loaded NFs may be able to address several issues with traditional intrauterine antibiotic infusions, such as rapid clearance, medication waste, and suboptimal therapeutic response. Large-scale livestock operations may find localized NF systems appealing for their potential economic benefits, including reduced treatment frequency and easier administration, as well as their improved antibacterial efficacy. Research on veterinary applications is still lacking; nevertheless, significant gaps exist in long-term safety assessments, standardized testing procedures, *in vivo* efficacy studies, and regulatory approval processes for animals used in food production. For Ofx-loaded NFs to be used in veterinary medicine, several issues must be resolved. Ultimately, in bovine SE, localized mucoadhesive NF systems offer a significant opportunity to enhance treatment outcomes, aid in fertility restoration, and mitigate antibiotic resistance.

Ethics

Ethics Committee Approval: All animal experiments adhered to the CPCSEA guidelines and received approval from the IAEC of Sardar Vallabh Bhai Patel University (approval no: IAEC/SVPUAT/2022/109, dated May 24, 2022).

Informed Consent: This study did not involve human participants; hence, patient consent was not required.

Footnotes

Authorship Contributions

Surgical and Medical Practices: P.K., Concept: P.K., A.K.G., Design: P.K., A.K.G., Data Collection or Processing: P.K., A.T., M.K.S., S.P., J.P., R.K.S., G.R., D.D., A.K.G., Analysis or Interpretation: P.K., S.Y., A.T., J.P., R.K.S., G.R., A.K.G., Literature Search: P.K., A.K.G., Writing: P.K.

Conflict of Interest: The authors declare no conflicts of interest.

Financial Disclosure: The author thanks to Department of Biotechnology (BT/PR46598/AAQ/1/938/2022) and the Indian Council of Medical Research (RBMH/FW/2021/9).

REFERENCES

1. Sheldon IM, Cronin J, Goetze L, Donofrio G, Schuberth HJ. Defining postpartum uterine disease and the mechanisms of infection and immunity in the female reproductive tract in cattle. Biol Reprod. 2009;81:1025-1032.
2. Adnane M, Kaidi R, Hanzen C, England GCW. Risk factors of clinical and subclinical endometritis in cattle: a review. Turk J Vet Anim Sci. 2017;41:1-11.
3. Angel QAL, Vigo FM, José BGJ, Barrio LM, José GH, Ana IPMP. Subclinical endometritis in dairy cattle. In: Payan-Carreira R, ed. New Insights into Theriogenology. London; UK; 2018:79-97.
4. Cai XS, Jiang H, Xiao J, Yan X, Xie P, Yu W, Lv WF, Wang J, Meng X, Chen CZ, Zhang M, Zhang Y, Yuan B, Zhang JB. Changes in bacterial community composition in the uterus of Holstein cow with endometritis before and after treatment with oxytetracycline. Sci Rep. 2024;14:9511.
5. Karstrup CC, Pedersen HG, Jensen TK, Agerholm JS. Bacterial invasion of the uterus and oviducts in bovine pyometra. Theriogenology. 2017;93:93-98.
6. Sundrum A. Metabolic disorders in the transition period indicate that the dairy cows' ability to adapt is overstressed. Animals (Basel). 2015;5:978-1020.
7. Wagener K, Gabler C, Drillich M. A review of the ongoing discussion about definition, diagnosis and pathomechanism of subclinical endometritis in dairy cows. Theriogenology. 2017;94:21-30.
8. Di Gennaro F, Guido G, Frallonardo L, Pennazzi L, Bevilacqua M, Locantore P, Vitagliano A, Saracino A, Cicinelli E. Chronic endometritis and antimicrobial resistance: towards a multidrug-resistant endometritis? an expert opinion. Microorganisms. 2025;13:197.
9. Hurtgen JP. Pathogenesis and treatment of endometritis in the mare: a review. Theriogenology. 2006;66:560-566.
10. Hussain AM, Daniel RC. Bovine endometritis: current and future alternative therapy. Zentralbl Veterinarmed A. 1991;38:641-651.
11. Ghimpețeanu OM, Pogurschi EN, Popa DC, Dragomir N, Drăgotoiu T, Mihai OD, Petcu CD. Antibiotic use in livestock and residues in food-a public health threat: a review. Foods. 2022;11:1430.
12. Kasimanickam R, Duffield TF, Foster RA, Gartley CJ, Leslie KE, Walton JS, Johnson WH. The effect of a single administration of cephapirin or cloprostenol on the reproductive performance of dairy cows with subclinical endometritis. Theriogenology. 2005;63:818-830.
13. Alaoui Mdarhri H, Benmessaoud R, Yacoubi H, Seffar L, Guennouni Assimi H, Hamam M, Boussettine R, Filali-Ansari N, Lahlou FA, Diawara I, Ennaji MM, Kettani-Halabi M. Alternatives therapeutic approaches to conventional antibiotics: advantages, limitations and potential application in medicine. Antibiotics (Basel). 2022;11:1826.
14. Hariharan A, Tran SD. Localized drug delivery systems: an update on treatment options for head and neck squamous cell carcinomas. Pharmaceutics. 2023;15:1844.
15. Bassi da Silva J, Ferreira SBS, de Freitas O, Bruschi ML. A critical review about methodologies for the analysis of mucoadhesive properties of drug delivery systems. Drug Dev Ind Pharm. 2017;43:1053-1070.

16. Yao J, Zou P, Cui Y, Quan L, Gao C, Li Z, Gong W, Yang M. Recent advances in strategies to combat bacterial drug resistance: antimicrobial materials and drug delivery systems. Pharmaceutics. 2023;15:1188.

17. Yang Y, Han M, Kong J, Jin Y, Huang Y, Wang J, Li R, Pan Y, Fan J, Li Z. Application of electrostatic spinning technology for oral mucosal drug delivery. AIP Advances. 2025;15:1-12.

18. Hiwrale A, Bharati S, Pingale P, Rajput A. Nanofibers: A current era in drug delivery system. Heliyon. 2023;9:e18917.

19. Maliszewska I, Czapka T. Electrospun polymer nanofibers with antimicrobial activity. Polymers (Basel). 2022;14:1661.

20. Henriques C, Vidinha R, Botequim D, Borges JP, Silva JA. A systematic study of solution and processing parameters on nanofiber morphology using a new electrospinning apparatus. J Nanosci Nanotechnol. 2009;9:3535-3545.

21. Al-Abduljabbar A, Farooq I. Electrospun polymer nanofibers: processing, properties, and applications. Polymers (Basel). 2022;1:65.

22. Shakeri H, Shokrollahi M, Tolabi H, Haghbin Nazarpak M, Solouk A. Design and manufacture of propolis loaded multilayer nanofibrous mucoadhesive patch for the treatment of oral mucosal lesions. J Drug Deliv Sci Technol. 2025;105:106630.

23. Elgharbawy AS, El Demerdash AM, Sadik WA, Kasaby MA, Lotfy AH, Osman AI. Enhancing the biodegradability, water solubility, and thermal properties of polyvinyl alcohol through natural polymer blending: an approach toward sustainable polymer applications. Polymers (Basel). 2024;16:2141.

24. Yan D, Li Y, Liu Y, Li N, Zhang X, Yan C. Antimicrobial properties of chitosan and chitosan derivatives in the treatment of enteric infections. Molecules. 2021;26:7136.

25. Pramanik S, Aggarwal A, Kadi A, Alhomrani M, Alamri AS, Alsanie WF, Koul K, Deepak A, Bellucci S. Chitosan alchemy: transforming tissue engineering and wound healing. RSC Adv. 2024;14:19219-19256.

26. Türkoğlu GC, Khomarloo N, Mohsenzadeh E, Gospodinova DN, Neznakomova M, Salaün F. PVA-based electrospun materials-a promising route to designing nanofiber mats with desired morphological shape-a review. Int J Mol Sci. 2024;25:1668.

27. Monk JP, Campoli-Richards DM. Ofloxacin. A review of its antibacterial activity, pharmacokinetic properties and therapeutic use. Drugs. 1987;33:346-391.

28. Nash DM, Giles JL. Uterine inflammation and lessons from large animal models of endometritis. Nat Rev Immunol. 2025;25:934-946.

29. Ihrke PJ, Papich MG, DeManuelle TC. The use of fluoroquinolones in veterinary dermatology. Vet Dermatol. 1999;10:193-204.

30. Aramă V. Topical antibiotic therapy in eye infections - myths and certainties in the era of bacterial resistance to antibiotics. Rom J Ophthalmol. 2020;64:245-260.

31. Kumari P, Shukla MK, Tripathi A, Pandey J, Goyal AK. Development of ofloxacin-loaded CS/PVA hydrogel for the treatment of metritis in bovine. Drugs Drug Candidates. 2025;4:17.

32. Yazdanpanah M, Khanmohammadi M, Mehdinavaz Aghdam R, Shabani K, Rajabi M. Optimization of electrospinning process of poly(vinyl alcohol) via response surface methodology (RSM) based on the central composite design. Curr Chem Lett. 2014;3:175-182.

33. Batheja S, Sahoo RK, Rani S, Gupta S, Tejavath KK, Sinha S, Ajazuddin, Yadav AK, Goyal AK, Gupta U. Central composite design based optimization of carbohydrate coated albumin nanoparticles for HCC: synthesis, extensive characterization and in vivo pharmacokinetic evaluation. Biopolymers. 2025;116:e70028.

34. Yang Y, Khan H, Gao S, Khalil AK, Ali N, Khan A, Show PL, Bilal M, Khan H. Fabrication, characterization, and photocatalytic degradation potential of chitosan-conjugated manganese magnetic nano-biocomposite for emerging dye pollutants. Chemosphere. 2022;306:135647.

35. Chaurawal N, Quadir SS, Joshi G, Barkat MA, Alanezi AA, Raza K. Development of fucoidan/polyethyleneimine based sorafenib-loaded self-assembled nanoparticles with machine learning and DoE-ANN implementation: optimization, characterization, and in-vitro assessment for the anticancer drug delivery. Int J Biol Macromol. 2024;279:135123.

36. Hadipour-Goudarzi E, Hemmatinejad N, Shokrgozar MA. Fabrication and DOE optimization of electrospun chitosan/gelatin/PVA nanofibers for skin tissue engineering. Macromol Mater Eng. 2023;308:2200562.

37. Mirzaeei S, Taghe S, Asare-Addo K, Nokhodchi A. Polyvinyl alcohol/chitosan single-layered and polyvinyl alcohol/chitosan/eudragit RL100 multi-layered electrospun nanofibers as an ocular matrix for the controlled release of ofloxacin: an in vitro and in vivo evaluation. AAPS PharmSciTech. 2021;22:170.

38. Daelemans L, Van Paepegem W, D'hooge DR, De Clerck K. Excellent nanofiber adhesion for hybrid polymer materials with high toughness based on matrix interdiffusion during chemical conversion. Adv Funct Mater. 2019;29:1807434

39. Vogt FG, Dell'Orco PC, Diederich AM, Su Q, Wood JL, Zuber GE, Katrincic LM, Mueller RL, Busby DJ, Debrosse CW. A study of variable hydration states in topotecan hydrochloride. J Pharm Biomed Anal. 2006;40:1080-1088.

40. Jinying L, Ying L, Xuan G, Yanli G, Jianping L. Investigation of the release behavior of cupric ion for three types of Cu-IUDs and indomethacin for medicated Cu-IUD in simulated uterine fluid. Contraception. 2008;77:299-302.

41. Uhljar LÉ, Kan SY, Radacsi N, Koutsos V, Szabó-Révész P, Ambrus R. In vitro drug release, permeability, and structural test of ciprofloxacin-loaded nanofibers. Pharmaceutics. 2021;13:556.

42. Ajmal G, Bonde GV, Thokala S, Mittal P, Khan G, Singh J, Pandey VK, Mishra B. Ciprofloxacin HCl and quercetin functionalized electrospun nanofiber membrane: fabrication and its evaluation in full thickness wound healing. Artif Cells Nanomed Biotechnol. 2019;47:228-240.

43. Nair AB, Shah J, Jacob S, Al-Dhubiab BE, Patel V, Sreeharsha N, Shinu P. Development of mucoadhesive buccal film for rizatriptan: in vitro and in vivo evaluation. Pharmaceutics. 2021;13:728.

44. Cruz E, Diniz BV, Ochikubo LM, Kawasaki TE, Veiga FF, Lazarin-Bidóia D, Cesar GB, Radovanovic E, Caetano W, Svidzinski TI, Negri M. Polycaprolactone nanofibers colonized by HeLa cells: an alternative for in vitro investigation of fungal infection. Future Microbiol. 2023;18:199-213.

45. Brighenti MS, Montanheri LRDS, Duque MD, Andreo-Filho N, Lopes PS, Garcia MTJ, Mackenzie L, Leite-Silva VR. In vitro drug release and ex vivo dermal drug permeation studies of selected commercial benzoyl peroxide topical formulations: correlation between human and porcine skin models. Mol Pharm. 2025;22:1365-1372.

46. Dolezel R, Palenik T, Cech S, Kohoutova L, Vyskocil M. Bacterial contamination of the uterus in cows with various clinical types of metritis and endometritis and use of hydrogen peroxide for intrauterine treatment. Vet Med. 2010;55:504-511.

47. Shivhare M, Singh S, Tayeng K, Chakravarti S. Endometrial cytology to diagnose subclinical endometritis in cows. Int J Agric Environ Biotechnol. 2018;11:623-631.

48. Attimarad MV, Nagaraja SH, Setty RS. Simultaneous determination of ofloxacin and flavoxate hydrochloride in human plasma by RP HPLC. J Liq Chromatogr Relat Technol. 2012;35:768-777.

49. Bhoir SI, Gaikwad P, Parab LS, Shringarpure RN, Savant S, Verma PJ. RP-HPLC method development and validation for the simultaneous estimation of satranidazole and ofloxacin in pharmaceutical dosage form. J Chromatogr Sci. 2011;49:84-87.

50. Hughes JH, Upton RN, Reuter SE, Phelps MA, Foster DJR. Optimising time samples for determining area under the curve of pharmacokinetic data using non-compartmental analysis. J Pharm Pharmacol. 2019;71:1635-1644.

51. Romano JE, Thompson JA, Forrest DW, Westhusin ME, Tomaszweski MA, Kraemer DC. Early pregnancy diagnosis by transrectal ultrasonography in dairy cattle. Theriogenology. 2006;66:1034-1041.

52. Rooholghodos SH, Pourmadadi M, Yazdian F, Rashedi H. Optimization of electrospun CQDs-Fe_3O_4-RE loaded PVA-cellulose nanofibrils via central composite design for wound dressing applications: Kinetics and in vitro release study. Int J Biol Macromol. 2023;237:124067.

53. Li D, Xia Y. Electrospinning of nanofibers: reinventing the wheel. Adv Mater. 2004;16:1151-1170.

54. Geng X, Kwon OH, Jang J. Electrospinning of chitosan dissolved in concentrated acetic acid solution. Biomaterials. 2005;26:5427-5432.

55. Huang ZM, Zhang YZ, Kotaki M, Ramakrishna S. A review on polymer nanofibers by electrospinning and their applications in nanocomposites. Compos Sci Technol. 2003;63:2223-2253.

56. Deitzel JM, Kleinmeyer J, Harris D, Beck Tan NC. The effect of processing variables on the morphology of electrospun nanofibers and textiles. Polymer. 2001;42:261-272.

57. Chavanpatil MD, Jain P, Chaudhari S, Shear R, Vavia PR. Novel sustained release, swellable and bioadhesive gastroretentive drug delivery system for ofloxacin. Int J Pharm. 2006;316:86-92.

58. Salama AH, AbouSamra MM, Awad GEA, Mansy SS. Promising bioadhesive ofloxacin-loaded polymeric nanoparticles for the treatment of ocular inflammation: formulation and in vivo evaluation. Drug Deliv Transl Res. 2021;11:1943-1957.

59. Mohite P, Puri A, Munde S, Dave R, Khan S, Patil R, Singh AK, Tipduangta P, Singh S, Chittasupho C. Potential of chitosan/gelatin-based nanofibers in delivering drugs for the management of varied complications: a review. Polymers (Basel). 2025;17:435.

60. Chinnappan BA, Krishnaswamy M, Xu H, Hoque ME. Electrospinning of biomedical nanofibers/nanomembranes: effects of process parameters. Polymers (Basel). 2022;14:3719.

61. Liang X, Zhong HJ, Ding H, Yu B, Ma X, Liu X, Chong CM, He J. Polyvinyl alcohol (PVA)-based hydrogels: recent progress in fabrication, properties, and multifunctional applications. Polymers (Basel). 2024;16:2755.

62. Garnica-Palafox IM, Sánchez-Arévalo FM. Influence of natural and synthetic crosslinking reagents on the structural and mechanical properties of chitosan-based hybrid hydrogels. Carbohydr Polym. 2016;151:1073-1081.

63. Ahmad Wsoo M, Izwan Abd Razak S, Shahir S, Ahmed Abdullah Al-Moalemi H, Rafiq Abdul Kadir M, Hasraf Mat Nayan N. Development of prolonged drug delivery system using electrospun cellulose acetate/polycaprolactone nanofibers: future subcutaneous implantation. Polym Adv Technol. 2021;32:3664-3678.

64. Vashisth P, Raghuwanshi N, Srivastava AK, Singh H, Nagar H, Pruthi V. Ofloxacin loaded gellan/PVA nanofibers - synthesis, characterization and evaluation of their gastroretentive/mucoadhesive drug delivery potential. Mater Sci Eng C Mater Biol Appl. 2017;71:611-619.

65. Mosallanezhad P, Rajabifar N, Rostami A, Ahmadi Z, Taghdimi R, Nazockdast H. Preparation and structural analyses of antimicrobial core-shell chitosan-polycaprolactone nanofibers for controlled curcumin release. Colloids Surfaces A Physicochem Eng Asp. 2025;716:136736.

66. Brako F, Thorogate R, Mahalingam S, Raimi-Abraham B, Craig DQM, Edirisinghe M. Mucoadhesion of progesterone-loaded drug delivery nanofiber constructs. ACS Appl Mater Interfaces. 2018;10:13381-13389.

67. Gavali P, Desai J, Shah P, Sawarkar S. Transmucosal delivery of peptides and proteins through nanofibers: current status and emerging developments. AAPS PharmSciTech. 2024;25:74.

68. Sola P, Garikapati KK, Krishnamurthy PT, Kumari M. Polysorbate 80 surface modified SLNs of formoterol suppress SNCA gene and mitochondrial oxidative stress in mice model of Parkinson's disease. Sci Rep. 2023;13:19942.

69. Becerra SC, Roy DC, Sanchez CJ, Christy RJ, Burmeister DM. An optimized staining technique for the detection of Gram positive and gram negative bacteria within tissue. BMC Res Notes. 2016;9:216.

70. Gonzalez Moreno C, Torres Luque A, Oliszewski R, Rosa RJ, Otero MC. Characterization of native *Escherichia coli* populations from bovine vagina of healthy heifers and cows with postpartum uterine disease. PLoS One. 2020;15:e0228294.

71. Plöntzke J, Madoz LV, De la Sota RL, Drillich M, Heuwieser W. Subclinical endometritis and its impact on reproductive performance in grazing dairy cattle in Argentina. Anim Reprod Sci. 2010;122:52-57.

72. Damarany AI. Physical traits of vaginal mucus discharge and their relations to conception rate of Egyptain Baladi cows. Egypt J Anim Prod. 2020;57:63-70.

73. Hässig M, Steinmann B, Wittenbrink MM. Nutzen von klinischen und labordiagnostischen Parametern zur Diagnostik der Endometritis beim Rind [Benefit of clinical and laboratory parameters for the diagnosis of endometritis in dairy cows]. Schweiz Arch Tierheilkd. 2010;152:411-416.

74. Bartolome ND, Jongsuwanwattana R, Asawakarn S, Suadsong S, Sangpradit K, Swangchan-Uthai T. Assessment of the physical and chemical properties of vaginal discharge for the diagnosis of endometritis in dairy cattle. 2025;18:1322-1332.

75. Cui Z, Zheng Z, Lin L, Si J, Wang Q, Peng X, Chen W. Electrospinning and crosslinking of polyvinyl alcohol/chitosan composite nanofiber for transdermal drug delivery. Adv Polym Technol. 2018;37:1917-1928.

76. Qureshi D, Pattanaik S, Mohanty B, Anis A, Kulikouskaya V, Hileuskaya K, Agabekov V, Sarkar P, Maji S, Pal K. Preparation of novel poly (vinyl alcohol)/chitosan lactate-based phase-separated composite films for UV-shielding and drug delivery applications. Polym Bull. 2022;79:3253-3290.

Turk J Pharm Sci 2026;23(2):105-112
DOI: 10.4274/tjps.galenos.2026.43334

ORIGINAL ARTICLE

Exploring the Role of Metabolites in Torsadogenic Risk Assessment: A Text-Mining Approach

Egemen BİLGİN, Gülçin TUĞCU, Ahmet AYDIN*

Yeditepe University Faculty of Pharmacy, Department of Toxicology, İstanbul, Türkiye

ABSTRACT

Objectives: Torsades de pointes (TdP) is a life-threatening ventricular arrhythmia often caused by the inadvertent inhibition of the human ether-à-go-go-related gene (hERG). Conventional pre-market evaluations, which emphasize parent molecules, often yield inaccurate predictions due to the multifaceted nature of TdP. This study aimed to investigate the role of metabolites and their interplay with parent molecules in the manifestation of TdP.

Materials and Methods: A literature-based text-mining approach was employed, using the adverse outcome pathway-helpFinder tool. The analysis scrutinized 64 selected active ingredients, categorized by their torsadogenic risks, to evaluate the distinct proarrhythmic contributions of their metabolites.

Results: This text-mining exploration revealed qualitative evidence that metabolites variably modulate TdP vulnerability. Specifically, certain metabolites can independently exacerbate proarrhythmic profiles, whereas others do not inhibit hERG and therefore represent safer therapeutic alternatives than their parent molecules.

Conclusion: Metabolites play a paramount role in altering the torsadogenic risk profile of pharmaceutical products. Incorporating comprehensive metabolite data into cardiac safety evaluations is essential for a more accurate risk assessment and should be considered in future pharmaceutical development.

Keywords: Adverse outcome pathway (AOP), cardiotoxicity, human ether-à-go-go-related gene (hERG), metabolites, torsades de pointes (TdP)

INTRODUCTION

Various medications, encompassing anti-histamines, anti-microbials, anti-psychotics, and gastrointestinal stimulants, have been withdrawn from the market in the past decades due to their association with the life-threatening ventricular arrhythmia, torsades de pointes (TdP).[1,2] Compounds that induce TdP tend to prolong the QT interval on the electrocardiogram (ECG).[1]

Regulatory directives, including non-clinical [International Council for Harmonization (ICH) S7A and S7B http://www.ich.org] and clinical evaluations (ICH E14), have been implemented to delineate the requisite studies for assessing whether a new drug has the potential to prolong the QT interval, despite the QT interval prolongation being an insufficient predictor of TdP.[1] Sanguinetti et al.[3] underscored the significance of the association between QT prolongation and the blockade of voltage-dependent K+ channels, predominantly the rapid delayed rectifier current (I_{Kr}) pivotal in ventricular repolarization. Moreover, the molecular interaction involving this channel is correlated with the human ether-à-go-go-related gene (hERG), which encodes the channel's primary subunit.[3] Figure 1 schematically illustrates the mechanism of TdP initiation, beginning with the blockade of hERG.[4]

Recent advancements indicate that the cardiac safety assessments of drugs largely rely on *in vitro* hERG blockade,

***Correspondence:** ahmet.aydin@yeditepe.edu.tr, **ORCID-ID:** orcid.org/0000-0003-3499-6435

Received: 01.09.2025 **Accepted:** 18.08.2026 **Publication Date:** 01.09.2026

Cite this article as: Bilgin E, Tuğcu G, Aydın A. Exploring the role of metabolites in torsadogenic risk assessment: a text-mining approach. Turk J Pharm Sci. 2026;23(2):105-112

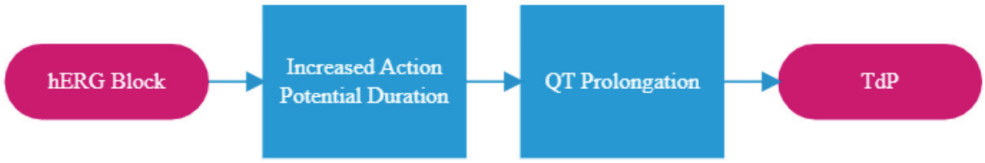

Figure 1. Mechanism of TdP caused by hERG block.
hERG, human ether-à-go-go-related gene; TdP, torsades de pointes.

the I_{Kr} current induced by the compounds, as well as *in vivo* QT interval prolongation.[5] In the case of *in vitro* hERG blockade, the hERG IC50 value is usually the initial metric employed to assess the torsadogenic risk during the drug development process; the 50% inhibitory concentration value, or the amount of drug needed to lower an ion channel's current (hERG I_{Kr} current) by 50%, is used to measure a compound's affinity for a particular channel.[6] Indeed, various studies have revealed that the obstruction of I_{Kr} amplifies the probability of proarrhythmic occurrences by fostering drug-induced long QT syndrome. Clinically, the emergence of TdP has historically been correlated with the extension of the QT interval. Nonetheless, certain hERG blockers, such as verapamil, do not induce TdP.[5]

Current methodologies for evaluating *in vitro* hERG potassium channel activity, *in vivo* pre-clinical assessments, and clinical evaluations of effects on the corrected QT (QTc) interval of the ECG are recognized as sensitive approaches for identifying torsadogenic risk. The QT interval on an ECG represents the total duration of ventricular depolarization and repolarization.[7] Since this interval is influenced by heart rate, it is adjusted using established correction formulas to calculate the QTc interval. Consequently, QTc prolongation signifies an abnormal delay in ventricular repolarization, serving as a primary biomarker for increased susceptibility to TdP and other potentially fatal arrhythmias.[8] However, these techniques may require greater precision. Moreover, the efficacy of these screening methods has been criticized because *in silico* methods predominantly focus on predicting the drug binding affinities for the hERG potassium channel, thereby providing limited information regarding the drug's impact on ventricular repolarization.[9] Furthermore, current guidelines have inherent limitations that can inadvertently halt the development of otherwise valuable therapeutics.[10]

Age, gender, electrolyte imbalances, variations in heart rate (especially bradycardia), and structural heart disease are well-recognized concurrent risk factors that significantly influence the incidence of TdP. However, the occurrence of TdP is also attributed to multi-channel interactions, hERG-independent proarrhythmic mechanisms, and the influence of drug metabolites or of the drug's anti-arrhythmic effects. These factors highlight the limitations of relying solely on surrogate markers for estimating actual TdP risks. Consequently, safety assessments should include a comprehensive evaluation that considers the combined effects of all active substances (such as parent drugs and their metabolites), rather than assessing only the parent molecule. The route-dependent pharmacokinetics of pharmaceuticals should be meticulously considered during drug safety studies.[11]

In our analysis, we used core components of the adverse outcome pathway (AOP) approach. This involves a sequence of events commencing with the interaction of a stressor with an organism that causes a disruption at the molecular level, referred to as the molecular initiating event (MIE). This sequence can then evolve through a series of interconnected "key events (KEs)", culminating in an adverse outcome (AO). The AO is considered pertinent to evaluating risk and informing decision-making.[12]

The ultimate goal of our analysis was to shed light on the role of metabolites that may affect TdP risk indicators, such as hERG inhibition and QT prolongation. The information obtained from data mining can benefit future drug design, since relying solely on the parent molecule and its hERG inhibition and/or QT prolongation may lead to false-positive risk assessments.

MATERIALS AND METHODS

We used AOP-helpFinder (https://aop-helpfinder.u-paris-sciences.fr/index.php), a web-based tool, to retrieve relevant literature from the PubMed database.[13] The operation of this system requires two primary inputs: the stressors of interest and biological events, encompassing MIE, KEs, and/or AO. Prior to execution, the tool offers two optional parameters to customize the output: a "reduced search" option and a "refinement filter". In addition, users may choose the output format.[14] Applying a 20% "reduced search" threshold is recommended because the initial portion of an abstract typically outlines a hypothesis and can therefore lead to false-positive associations.[13,15] The refinement filter provides a lemmatization procedure and reduces words to their basic, meaningful forms.[13,14]

Llopis-Lorente et al.[16] previously developed an *in silico* tool for the pre-clinical assessment of TdP risk. For their study, they compiled a comprehensive dataset of active ingredients from the CredibleMeds database and supplemented it with relevant literature for compounds not listed therein.[16] We specifically selected this robust dataset as our foundation because it is highly validated for predictive toxicology applications. Using a well-established, curated list of structurally diverse compounds allowed our text-mining study to move beyond anecdotal case reports and to systematically explore the original hypothesis that metabolites consistently modulate the TdP risk profile across a broad, representative pharmacological spectrum. This reference dataset divided the compounds into four categories: known risk, possible risk, conditional risk, and lack of evidence

for TdP risk. In our AOP-helpFinder analysis, the strict inclusion criterion was to include active ingredients with a documented risk of TdP. Therefore, from the initial list of 109 compounds, we excluded the 45 drugs categorized as having no evident TdP risk. This filtering process resulted in our final dataset of 64 active ingredients, which were then used as the stressors of interest in our study. The list of active ingredients and their respective torsadogenic risk levels is shown in Table 1.

For the biological events input required by AOP-helpFinder, we selected three specific keywords: "metabolism", "metabolite", and "torsades de pointes". To specifically investigate the contribution of metabolites to TdP risk, we restricted our search to abstracts containing at least one of these keywords, thereby refining the output. We applied the "reduced search" recommendation to our results to avoid hypothesis sections of abstracts that might produce false-positive results. The refinement filter (lemmatization) was not used because our selected keywords were already in their base forms.

The literature search encompassed all available publications in the PubMed database up to November 2022. The AOP-helpFinder tool was executed on 19 Nov 2022, capturing a comprehensive snapshot of the literature up to that point. Following execution of the search, the retrieved abstracts were exported to an Excel spreadsheet and subsequently manually reviewed and categorized. Articles deemed pertinent were then subjected to a comprehensive full-text review for in-depth analysis. Ethics committe approval and informed consent were not required for our study.

RESULTS

The AOP-helpFinder tool yielded results consistent with our pre-defined search parameters. The generated output included the publication dates, titles, PubMed IDs, and abstracts of articles co-mentioning at least one of the three keywords. Table 2 shows the number of abstracts, grouped by keywords, for each TdP risk classification.

A total of 23,042 abstracts containing the keywords were retrieved. To prevent selection bias, strict criteria were established for the manual categorization of these abstracts. Abstracts were included for full-text review only if they met the following criteria: (1) explicit discussion of the pharmacokinetic profile of the parent drug, highlighting at least one specific active metabolite; and (2) presentation of comparative empirical data (*in vitro, in vivo*, or clinical) regarding cardiotoxic parameters (such as hERG blockade, QT prolongation, or TdP incidence) between the parent molecule and its metabolite. Studies focusing solely on non-cardiac adverse events, generic pharmacokinetic studies without cardiotoxicity data,

Table 1. Torsadogenic risk levels of 64 active ingredients used in our analysis.

Known TdP risk (n = 37)		Possible TdP risk (n = 14)	Conditional TdP risk (n = 13)
Ajmaline	Halofantrine	Clozapine	Amitriptyline
Amiodarone	Haloperidol	Desipramine	Diphenhydramine
Astemizole	Ibutilide	Dolasetron	Famatidine
Azalimide	Levofloxacin	Lapatinib	Fluvoxamine
Azithromycin	Methadone	Lopinavir	Metronidazole
Bepridil	Moxifloxacin	Nilotinib	Nelfinavir
Chloroquine	Ondansetron	Paliperidone	Paroxetine
Chlorpromazine	Pimozide Procainamide	Risperidone	Propafenone
Cilostazol	Quinidine	Ritonavir	Quetiapine
Cisapride	Sotalol	Saquinavir	Quinine
Clarithromycin	Sparfloxacin	Sertindole	Ranolazine
Disopyramide	Tedisamil	Sunitinib	Solifenacin
Dofetilide	Terfenadine	Tolterodine	Voriconazole
Domperidone	Terodiline	Tamoxifen	
Donepezil	Thioridazine		
Dronedarone	Vandetanib		
Droperidol			
Erythromycin			
Flecainide			
Gatifloxacin			

TdP, torsades de pointes.

Table 2. The number of abstracts reviewed divided by the keywords according to torsadogenic risk levels.

Known TdP risk (n = 37)	Possible TdP risk (n = 14)	Conditional TdP risk (n = 13)
Metabolism = 6,305	Metabolism = 4,867	Metabolism = 2,627
Metabolite = 3,964	Metabolite = 2,397	Metabolite = 1,354
TdP = 1,346	TdP = 82	TdP = 100
Total number = 11,615	**Total number** = 7,346	**Total number** = 4,081

TdP, torsades de pointes.

or reviews lacking primary comparative data were strictly excluded. Following this rigorous manual review, 21 highly relevant articles were selected for the core qualitative analysis. Specifically, this included 12 articles from the known risk group, 4 from the possible risk group, and 5 from the conditional risk group. Among these comprehensively analyzed texts, the most illustrative examples of distinct parent-metabolite dynamics were detailed in the subsequent sections.

Active ingredients with known TdP risk

Regarding the active ingredients in the known TdP risk category, we identified relevant comparative data for thioridazine, halofantrine, methadone, procainamide, quinidine, terfenadine, and astemizole.

Salih et al.[17] discovered that both thioridazine and its metabolite, mesoridazine, similarly affect the QTc interval. Their research thus demonstrates that identical QTc prolongation is associated with both thioridazine and mesoridazine following oral administration.

It has been established that the anti-malarial drug halofantrine is linked not only to QT prolongation but also to fatal and non-fatal arrhythmias in individuals without pre-existing cardiac issues. Mbai et al.[18] concluded that both the primary drug halofantrine and its metabolite N-desbutylhalofantrine result in significant blockade of the hERG (K+) channel. Despite previous assertions that N-desbutylhalofantrine is safer than halofantrine as an antimalarial, their study suggests only a slight increase in the safety margin with respect to cardiotoxicity associated with QT interval prolongation.[18]

A pilot study found a substantial association among oral dosage, enhanced methadone metabolism (evidenced by an elevated plasma concentration of the primary methadone metabolite), and significant changes in the QTc interval. The study suggested that the oral dose and plasma concentration of 1,5-dimethyl-3,3-diphenylpyrrolidene, a methadone metabolite, could serve as valuable indicators for identifying patients susceptible to methadone-related arrhythmias.[19]

Another study reported a case of QT interval prolongation in a hemodialysis patient caused by a procainamide metabolite. The patient had been prescribed procainamide for a specific clinical indication, and one-month following procainamide administration, an ECG revealed QT interval prolongation, and procainamide dosage was reduced. However, the patient was transported to the hospital the next day following cardiopulmonary arrest. In a blood analysis, levels of N-acetyl procainamide (NAPA), a metabolite of procainamide, were significantly elevated above the recommended threshold. The administration of procainamide was stopped when NAPA was identified as the cause of the QTc prolongation. By the seventh day, the NAPA levels fell below the recommended threshold, and the QT intervals normalized. This case report documents the first reported case of long QT syndrome induced by NAPA in a hemodialysis patient. It was proposed that concentrations of both procainamide and NAPA should be monitored.[20] Procainamide, along with its metabolite NAPA, is strongly associated with the induction of TdP.[21]

Past studies have proposed that TdP induced by quinidine could be attributed to external factors such as hypokalemia or unidentified active metabolites. It was discovered that, similar to quinidine at prolonged cycle durations, its metabolites—dihydroquinidine and 3-hydroxyquinidine—prolonged the action potential and led to early afterdepolarizations.[22]

The second-generation antihistamine, terfenadine, has an active metabolite, fexofenadine, which does not cause QT prolongation. Medicinal chemists have suggested using fexofenadine/terfenadine as examples for designing zwitterionic compounds to prevent cardiotoxicity.[23] However, fexofenadine, the active metabolite of terfenadine, does not inhibit either hERG or Kv1.5, even though terfenadine efficiently blocks hERG K+ channels.[24] Due to the characteristics of terfenadine's active metabolite, fexofenadine received approval in July 1996. Because a safer version of an identical medication had been developed, the Food and Drug Administration (FDA) requested removal of terfenadine in 1997.[25]

Recent findings have indicated that the desmethyl metabolite of astemizole, which has similar potency at hERG but is present at significantly higher levels than its parent compound, likely plays a substantial role in cardiac repolarization.[26] Corroborating this, another study has posited that the proarrhythmic activity of desmethylastemizole, a metabolite of astemizole, might primarily account for the clinically observed QT prolongation and TdP associated with astemizole use.[27] Zhou et al.[28] suggested that desmethylastemizole is the principal contributor to the long QT syndrome observed in patients following astemizole administration because it becomes the predominant component in the bloodstream.

Active ingredients with possible TdP risk

Among active ingredients classified in the possible TdP risk category, the literature most prominently addresses risperidone and paliperidone.

Leishman articulated that compounds with an intermediate risk of TdP are typically susceptible to metabolic inhibition, or tend to have therapeutically active primary metabolites, or both. Some of these metabolites are recognized for their ability to block the hERG channel. Risperidone is one of the best-known of these molecules. Calculating the therapeutic window of risperidone based solely on the parent molecule and thereby revealing the relationship between hERG inhibition potential and clinical exposure actually led to risperidone being characterized as having an almost low or no TdP risk. However, hERG blockers include risperidone and its primary metabolite, paliperidone.[26] Reports suggest that the metabolite paliperidone is primarily responsible for the QTc prolongation observed after risperidone administration.[29] This circumstance illustrates why, in past years, some authors characterized risperidone as not associated with TdP. However, risperidone has recently been categorized as having an intermediate or possible risk of inducing TdP.[26] Ito et al.[30] reported on two patients experiencing severe arrhythmia due to risperidone. In these two instances, serum concentrations were examined, revealing that only the levels of the parent-molecule metabolite, paliperidone

[9-hydroxyrisperidone (9-OH-RIS)], were elevated. These findings led them to suggest that 9-OH-RIS is an essential indicator of risperidone toxicity and may cause life-threatening arrhythmia.[30]

According to clinical information, paliperidone is thought to be more strongly associated with QT prolongation than risperidone.[29] Additionally, paliperidone, an active metabolite of risperidone, has been reported to modestly prolong the QT interval, possibly by inhibiting hERG K+ channels. Since drug-induced QT interval prolongation often precedes the emergence of TdP—a ventricular arrhythmia that can be lethal—further research is recommended to explore this potential effect of paliperidone.[31]

Active ingredients with conditional TdP risk

Regarding the conditional TdP risk category, the most illustrative literature focuses on ranolazine, propafenone, and quetiapine. Moreno et al.[32] revealed that the interaction of ranolazine's active metabolites with late INa (I_{NaL}) and I_{Kr} significantly influence the therapeutic efficacy of the parent molecule and the likelihood of side effects. Although ranolazine mainly targets and inhibits the I_{NaL}, a component of the Na+ current that causes depolarization, it also interacts with and restrains the repolarizing hERG current I_{Kr} at therapeutic dosages. Overall, the result is a mild, concentration-dependent QTc prolongation. Ranolazine, like other medications, is extensively metabolized, predominantly by cytochrome P450 enzymes. Similar to the parent compound, Ranolazine, all 11 active metabolites potently inhibit I_{NaL} by 12% to 57% at 10 µmol/L. However, the inhibition of I_{Kr} produced by the four primary metabolites, which make up 30% to 40% of the original drug, is significantly less (40–50% inhibition at 50 µmol/L). According to the findings of the study, ranolazine's therapeutic potential is mainly derived from its active metabolites, which exhibit strong selectivity between repolarizing current blockade, I_{Kr}, and pathological current blockade, I_{NaL}. In order to limit the length of the ventricular action potential, I_{Kr} and I_{NaL} must be in equilibrium under the ventricular action potential. For ranolazine and its metabolites, the balance is in the direction of I_{NaL}, which causes the torsadogenic potential of ranolazine to be less.[32]

Arias et al.[33] demonstrated that propafenone and its primary active metabolite, 5-hydroxy-propafenone, block the hERG channel comparably by mainly attaching to the channel's open state. Compared with an intravenous dose yielding equivalent propafenone concentrations, the elevated 5-hydroxy-propafenone levels following oral treatment were associated with considerably greater prolongations of PQ (atrioventricular conduction time) and QRS (ventricular depolarization duration).[34] On a standard ECG, the PQ interval represents the time required for an electrical impulse to propagate from the atria to the ventricles. The QRS duration represents the time taken for the depolarization (and subsequent contraction) of the ventricles. Therefore, QRS prolongation indicates a dangerous delay in ventricular electrical activation and can independently exacerbate a drug's proarrhythmic risk profile.[35] Finally, a study was conducted to investigate the effects of propafenone and its primary metabolite, 5-hydroxy-propafenone, on ECG intervals in eight healthy individuals. A statistically significant additional effect on the QRS duration was observed in seven out of eight participants when both propafenone and 5-hydroxy-propafenone were present.[36]

Prior research has shown that quetiapine and its major metabolite, norquetiapine, have contrasting effects on cardiac currents. While quetiapine blocks the hERG potassium current, norquetiapine blocks the current through the human voltage-gated sodium channel Nav1.5 (hNav1.5). This suggests that norquetiapine's ability to block the sodium current could reduce the duration of cardiac action potentials, thereby mitigating the risks of QT prolongation that arise due to the inhibition of hERG potassium currents.[37]

The results, based on the three sections above, show that metabolites can increase or decrease the TdP risk of parent molecules due to various factors.

- While the parent molecule carries a known risk of TdP, its primary metabolite may not show QT prolongation and may therefore be used instead (e.g. terfenadine - fexofenadine).

- The metabolite formed may be even more arrhythmogenic than the parent molecule in terms of TdP risk (e.g., astemizole-desmethylastemizole).

- Metabolites may cause prolongation of the QT interval to the same extent as the parent molecule and increase the risk of TdP (e.g., thioridazine-mesoridazine).

- Even if the parent molecule inhibits the hERG channel, the metabolite formed can inhibit different currents and reverse the associated risk, so that it is not directed toward TdP (e.g., quetiapine–norquetiapine).

DISCUSSION

Mirams et al.[6] emphasized that, while accounting for the hERG blockade is essential when assessing the risk of torsadogenesis, it is insufficient on its own for accurate prediction. This is due to exceptions to the initial approach, indicating that a more comprehensive evaluation is necessary to accurately predict torsadogenic risk.[6] Apart from hERG inhibition, many factors may affect a patient's TdP risk, including multi-channel interactions, active metabolites, and anti-arrhythmic effects of a drug. Furthermore, patient-specific factors such as age, gender, electrolyte imbalances, and underlying cardiac conditions play crucial roles in TdP risk.[11] Consequently, relying on a single parameter for TdP risk evaluation can lead to erroneous conclusions and hinder the development of otherwise safe therapeutics.

In this study, we demonstrate that incorporating comprehensive metabolite data—rather than relying solely on the parent molecule's properties—yields a significantly more accurate risk assessment.

In this context, the AOP framework utilized in our study presents a distinct advantage over traditional observational reviews. Rather than evaluating risk factors in isolation, researchers using the AOP approach provide a structured, mechanistic

linkage from a MIE (such as parent- or metabolite-driven hERG blockade) to the final AO (TdP). This systematic synthesis of fragmented literature into a cohesive weight-of-evidence model allows for a more dynamic, predictive, and multi-layered risk assessment than conventional single-endpoint methodologies.

Leishman proposed a method that considers not only the parent compound but also its metabolic products when assessing torsadogenic risk. It was noted that evaluating the therapeutic window based solely on the exposure to the parent compound could create a substantial margin between clinical exposure and hERG potency. This factor may explain why, in previous years, some authors did not associate risperidone with TdP. However, when intrinsic and extrinsic factors are considered, risperidone is now classified as a possible TdP risk, and one of the most significant contributors to this reclassification is its metabolite paliperidone.[26]

A notable instance of this is Dolasetron. Thirteen years after its introduction to the market, the FDA withdrew the injectable form of Dolasetron in 2010 due to its associated risk of TdP. The core issue that surfaced was Dolasetron's function as a prodrug: its active metabolites contributed significantly to the risk of TdP.[11]

A previous *in silico* study demonstrated that the false-negative risk assessment of dronedarone likely occurred because its active metabolite was excluded from the model. This finding is critical because the metabolite accounts for one-third of the pharmacological activity and exhibits channel-blocking properties similar to those of the parent molecule. Therefore, when the metabolite was not taken into account, the *in silico* study showed that the molecule had a low TdP risk.[5]

As illustrated by the terfenadine-fexofenadine example, an active metabolite can replace the parent molecule, thereby providing a safer therapeutic alternative.[25]

Our text-mining results, alongside well-documented historical examples such as astemizole and terfenadine, illustrate how metabolites can fundamentally alter the torsadogenic risk profile relative to that of the parent molecule. To provide a more reliable and systematic framework for the TdP risk assessment of novel therapeutics, we propose the evaluation flowchart presented in Figure 2.

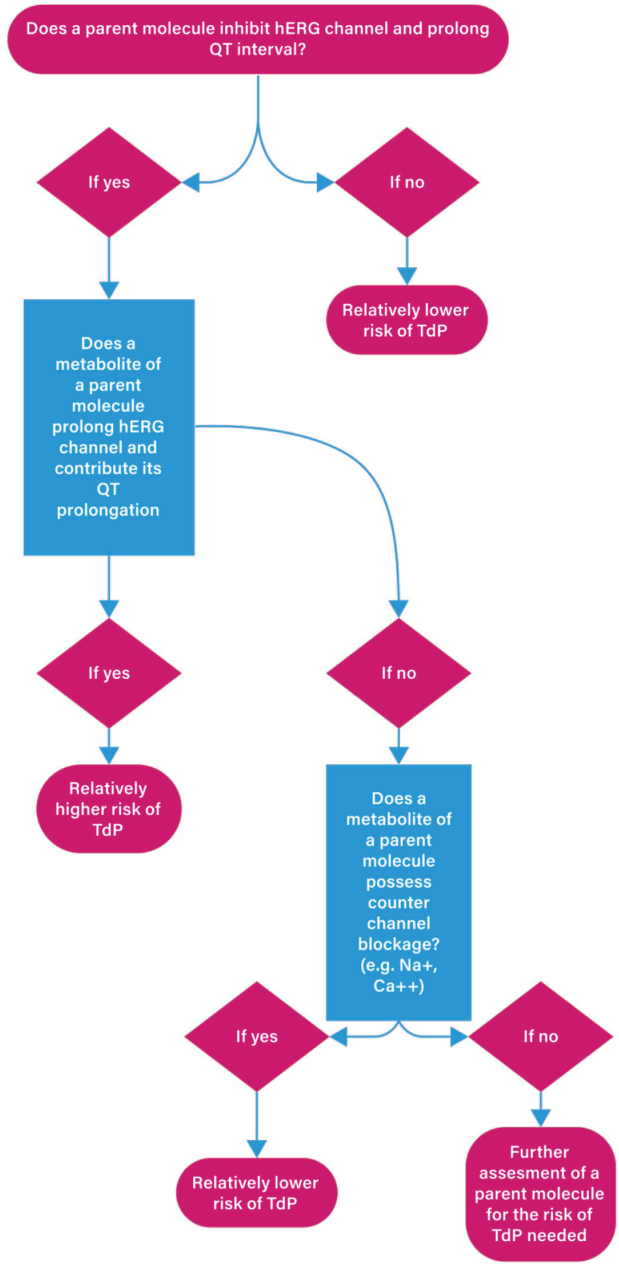

Figure 2. Proposed flowchart for better decision-making of novel products' torsadogenic risk assessment.

hERG, human ether-à-go-go-related gene; TdP, torsades de pointes.

Study limitations

As presented in our results, we observed a significant quantitative disparity in the number of retrieved abstracts concerning TdP across the risk categories (1,346 abstracts for the known risk group versus 82 and 100 for the Possible and Conditional groups, respectively). This discrepancy is not indicative of a lack of sensitivity in our search strategy, which was uniformly applied across all groups. Rather, it reflects the well-documented publication bias in the toxicological literature: drugs classified as "known risk" have historically been the focus of far more extensive and targeted research on cardiotoxicity. Conversely, "possible" and "conditional" risk drugs generally have fewer publications explicitly linking them to TdP, either because they are newer compounds or because their proarrhythmic events manifest only under highly specific, less frequently documented clinical scenarios.

Although assessing the 2D structural similarity of the evaluated compounds using chemoinformatic metrics like the Tanimoto coefficient provides valuable insights, it is well recognized that drug-induced hERG blockade and subsequent TdP can be triggered by structurally diverse chemical scaffolds. Given that the primary methodology of this study is rooted in literature-based text-mining for constructing an AOP framework rather than in ligand-based structure-activity relationship

modeling, detailed computational structural-alert analysis was considered to be beyond the scope of the current study. Nonetheless, integrating such molecular structural parameters with metabolite data remains a promising multimodal approach for future predictive toxicology models.

CONCLUSION

The inhibition of the hERG channel by a drug plays a pivotal role in QT prolongation and the consequential risk of TdP. Our analysis underscores that, for a more nuanced and accurate prediction of TdP risk in new pharmaceutical products, substantial emphasis should be placed on both the parent molecules and their metabolites. These metabolites, through their effects on the hERG channel and broader multi-channel interactions, play a paramount role in modulating QT prolongation. By comprehensively assessing both the parent molecules and their metabolites, the predictability and precision of TdP risk evaluation for novel products are significantly improved, fostering a more robust understanding of and facilitating mitigation of unforeseen TdP risks.

Ethics

Ethics Committee Approval: As the study did not involve human participants or animals, ethical approval from the relevant ethics committees was not required.

Informed Consent: As the study did not involve human participants or animals, patient informed consent was not required.

Footnotes

Authorship Contributions

Concept: E.B., G.T., A.A., Design: E.B., G.T., A.A., Data Collection or Processing: E.B., G.T., A.A., Analysis or Interpretation: E.B., G.T., Literature Search: E.B., Writing: E.B.

Conflict of Interest: The authors declare no conflicts of interest.

Financial Disclosure: The authors declared that this study received no financial support.

REFERENCES

1. Wallis RM. Integrated risk assessment and predictive value to humans of non-clinical repolarization assays. Br J Pharmacol. 2010;159:115-121.
2. De Ponti F, Poluzzi E, Cavalli A, Recanatini M, Montanaro N. Safety of non-antiarrhythmic drugs that prolong the QT interval or induce torsade de pointes: an overview. Drug Saf. 2002;25:263-286.
3. Sanguinetti MC, Jiang C, Curran ME, Keating MT. A mechanistic link between an inherited and an acquired cardiac arrhythmia: HERG encodes the I_{Kr} potassium channel. Cell. 1995;81:299-307.
4. Roden DM, Viswanathan PC. Genetics of acquired long QT syndrome. J Clin Invest. 2005;115:2025-2032.
5. Romero L, Cano J, Gomis-Tena J, Trenor B, Sanz F, Pastor M, Saiz J. In silico QT and APD prolongation assay for early screening of drug-ınduced proarrhythmic risk. J Chem Inf Model. 2018;58:867-878.
6. Mirams GR, Cui Y, Sher A, Fink M, Cooper J, Heath BM, McMahon NC, Gavaghan DJ, Noble D. Simulation of multiple ion channel block provides improved early prediction of compounds' clinical torsadogenic risk. Cardiovasc Res. 2011;91:53-61.
7. Rautaharju PM, Surawicz B, Gettes LS, Bailey JJ, Childers R, Deal BJ, Gorgels A, Hancock EW, Josephson M, Kligfield P, Kors JA, Macfarlane P, Mason JW, Mirvis DM, Okin P, Pahlm O, van Herpen G, Wagner GS, Wellens H; American Heart Association Electrocardiography and Arrhythmias Committee, Council on Clinical Cardiology; American College of Cardiology Foundation; Heart Rhythm Society. AHA/ACCF/HRS recommendations for the standardization and interpretation of the electrocardiogram: part IV: the ST segment, T and U waves, and the QT interval: a scientific statement from the American Heart Association Electrocardiography and Arrhythmias Committee, Council on Clinical Cardiology; the American College of Cardiology Foundation; and the Heart Rhythm Society. Endorsed by the International Society for Computerized Electrocardiology. J Am Coll Cardiol. 2009;53:982-991.
8. Postema PG, Wilde AA. The measurement of the QT interval. Curr Cardiol Rev. 2014;10:287-294.
9. Obiol-Pardo C, Gomis-Tena J, Sanz F, Saiz J, Pastor M. A multiscale simulation system for the prediction of drug-induced cardiotoxicity. J Chem Inf Model. 2011;51:483-492.
10. Pollard CE, Abi Gerges N, Bridgland-Taylor MH, Easter A, Hammond TG, Valentin JP. An introduction to QT interval prolongation and non-clinical approaches to assessing and reducing risk. Br J Pharmacol. 2010;159:12-21.
11. Polak S, Pugsley MK, Stockbridge N, Garnett C, Wiśniowska B. Early drug discovery prediction of proarrhythmia potential and its covariates. AAPS J. 2015;17:1025-1032.
12. Vinken M, Knapen D, Vergauwen L, Hengstler JG, Angrish M, Whelan M. Adverse outcome pathways: a concise introduction for toxicologists. Arch Toxicol. 2017;91:3697-3707.
13. Carvaillo JC, Barouki R, Coumoul X, Audouze K. Linking bisphenol s to adverse outcome pathways using a combined text mining and systems biology approach. Environ Health Perspect. 2019;127:47005.
14. Jornod F, Jaylet T, Blaha L, Sarigiannis D, Tamisier L, Audouze K. AOP-helpFinder webserver: a tool for comprehensive analysis of the literature to support adverse outcome pathways development. Bioinformatics. 2022;38:1173-1175.
15. Benoit L, Jornod F, Zgheib E, Tomkiewicz C, Koual M, Coustillet T, Barouki R, Audouze K, Vinken M, Coumoul X. Adverse outcome pathway from activation of the AhR to breast cancer-related death. Environ Int. 2022;165:107323.
16. Llopis-Lorente J, Gomis-Tena J, Cano J, Romero L, Saiz J, Trenor B. In silico classifiers for the assessment of drug proarrhythmicity. J Chem Inf Model. 2020;60:5172-5187.
17. Salih IS, Thanacoody RH, McKay GA, Thomas SH. Comparison of the effects of thioridazine and mesoridazine on the QT interval in healthy adults after single oral doses. Clin Pharmacol Ther. 2007;82:548-554.
18. Mbai M, Rajamani S, January CT. The anti-malarial drug halofantrine and its metabolite N-desbutylhalofantrine block HERG potassium channels. Cardiovasc Res. 2002;55:799-805.
19. Carlquist JF, Moody DE, Knight S, Johnson EG, Fang WB, Huntinghouse JA, Rollo JS, Webster LR, Anderson JL. A possible mechanistic link between the CYP2C19 genotype, the methadone metabolite ethylidene-1,5-dimethyl-3,3-diphenylpyrrolidene (EDDP), and methadone-induced corrected QT interval prolongation in a pilot study. Mol Diagn Ther. 2015;19:131-138.

20. Ashida K, Mine T, Kodani T, Kishima H, Masuyama T. Long QT syndrome caused by N-acetyl procainamide in a patient on hemodialysis. J Cardiol Cases. 2015;11:147-149.

21. Lazzara R. Antiarrhythmic drugs and torsade de pointes. Eur Heart J. 1993;14:88-92.

22. Roden DM, Thompson KA, Hoffman BF, Woosley RL. Clinical features and basic mechanisms of quinidine-induced arrhythmias. J Am Coll Cardiol. 1986;8(1 Suppl A):73A-78A.

23. Chen C. Some pharmacokinetic aspects of the lipophilic terfenadine and zwitterionic fexofenadine in humans. Drugs R D. 2007;8:301-314.

24. Grzelewska-Rzymowska I, Pietrzkowicz M, Górska M. Wpływ leków przeciwhistaminowych drugiej generacji na serce [The effect of second generation histamine antagonists on the heart]. Pneumonol Alergol Pol. 2001;69:217-226. Polish.

25. Handley DA, Magnetti A, Higgins AJ. Therapeutic advantages of third generation anti-histamines. Expert Opin Investig Drugs. 1998;7:1045-1054.

26. Leishman DJ. Improving prediction of torsadogenic risk in the CiPA in silico model by appropriately accounting for clinical exposure. J Pharmacol Toxicol Methods. 2020;101:106654.

27. Vorperian VR, Zhou Z, Mohammad S, Hoon TJ, Studenik C, January CT. Torsade de pointes with an antihistamine metabolite: potassium channel blockade with desmethylastemizole. J Am Coll Cardiol. 1996;28:1556-1561.

28. Zhou Z, Vorperian VR, Gong Q, Zhang S, January CT. Block of HERG potassium channels by the antihistamine astemizole and its metabolites desmethylastemizole and norastemizole. J Cardiovasc Electrophysiol. 1999;10:836-843.

29. Suzuki Y, Fukui N, Watanabe J, Ono S, Sugai T, Tsuneyama N, Saito M, Inoue Y, Someya T. QT prolongation of the antipsychotic risperidone is predominantly related to its 9-hydroxy metabolite paliperidone. Hum Psychopharmacol. 2012;27:39-42.

30. Ito A, Enokiya T, Kawamoto E, Iwashita Y, Takeda T, Ikemura K, Okuda M, Imai H. Two cases of life-threatening arrhythmia induced by risperidone: evaluation of risperidone and 9-hydroxy-risperidone concentrations. Acute Med Surg. 2017;4:341-343.

31. Hagiwara M, Kambayashi R, Aimoto M, Nagasawa Y, Takahara A. In vivo analysis of torsadogenic potential of an antipsychotic drug paliperidone using the acute atrioventricular block rabbit as a proarrhythmia model. J Pharmacol Sci. 2016;132:48-54.

32. Moreno JD, Yang PC, Bankston JR, Grandi E, Bers DM, Kass RS, Clancy CE. Ranolazine for congenital and acquired late INa-linked arrhythmias: in silico pharmacological screening. Circ Res. 2013;113:e50-e61.

33. Arias C, González T, Moreno I, Caballero R, Delpón E, Tamargo J, Valenzuela C. Effects of propafenone and its main metabolite, 5-hydroxypropafenone, on HERG channels. Cardiovasc Res. 2003;57:660-669.

34. Follath F. Clinical pharmacology of antiarrhythmic drugs: variability of metabolism and dose requirements. J Cardiovasc Pharmacol. 1991;17(Suppl 6):74-76.

35. Surawicz B, Childers R, Deal BJ, Gettes LS, Bailey JJ, Gorgels A, Hancock EW, Josephson M, Kligfield P, Kors JA, Macfarlane P, Mason JW, Mirvis DM, Okin P, Pahlm O, Rautaharju PM, van Herpen G, Wagner GS, Wellens H; American Heart Association Electrocardiography and Arrhythmias Committee, Council on Clinical Cardiology; American College of Cardiology Foundation; Heart Rhythm Society. AHA/ACCF/HRS recommendations for the standardization and interpretation of the electrocardiogram: part III: intraventricular conduction disturbances: a scientific statement from the American Heart Association Electrocardiography and Arrhythmias Committee, Council on Clinical Cardiology; the American College of Cardiology Foundation; and the Heart Rhythm Society. Endorsed by the International Society for Computerized Electrocardiology. J Am Coll Cardiol. 2009;53:976-981.

36. Haefeli EW, Vozeh S, Ha HR, Follath F. Comparison of the pharmacodynamic effects of intravenous and oral propafenone. Clin Pharmacol Ther. 1990;48:245-254.

37. Kim DH, Park KS, Park SH, Hahn SJ, Choi JS. Norquetiapine blocks the human cardiac sodium channel $Na_v1.5$ in a state-dependent manner. Eur J Pharmacol. 2020;885:173532.

Turk J Pharm Sci 2026;23(2):113-121
DOI: 10.4274/tjps.galenos.2026.88998

ORIGINAL ARTICLE

Integrated Botanical and Phytochemical Characterization of *Santolina chamaecyparissus* L. and Evaluation of its Antimicrobial Activity

Şüheda Rumeysa OSMANLIOĞLU DAĞ[1]*, Abdulrahman DAHER[2], Hasan SAĞLAM[2], Turan ARABACI[1]

[1]İnönü University Faculty of Pharmacy, Department of Pharmaceutical Botany, Malatya, Türkiye
[2]İnönü University Faculty of Pharmacy, Malatya, Türkiye

ABSTRACT

Objectives: *Santolina chamaecyparissus* L. is an aromatic medicinal plant with reported phytochemical and biological potential. This study aimed to characterize the botanical and phytochemical features of *S. chamaecyparissus* and to perform a preliminary screening of the antimicrobial activity of its methanolic extract against selected bacterial and fungal microorganisms.

Materials and Methods: In this experimental laboratory study, the morphological and anatomical characteristics of the aerial parts were examined using standard pharmacognostic, histological, and scanning electron microscopic methods. The essential oil was obtained by hydrodistillation, and the methanolic extract was prepared by maceration with 90% methanol. Volatile constituents were analyzed by gas chromatography–tandem mass spectrometry, while phenolic compounds were identified and quantified by liquid chromatography-tandem mass spectrometry. Preliminary antimicrobial activity was screened against five bacterial and two fungal strains using the agar well diffusion method.

Results: The plant exhibited characteristic xeromorphic features, including amphistomatic and isobilateral leaves, multilayered palisade parenchyma, anomocytic stomata, and dense non-glandular trichomes. The essential oil yield was 0.46%, and 33 volatile constituents were identified. Artemisia ketone (55.96%) and camphor (20.84%) were the major components. The methanolic extract yield was 14.40%, with chlorogenic acid (6733.85 µg/g dry extract) and quinic acid (6521.37 µg/g dry extract) identified as the predominant quantified compounds. The extract showed its strongest antimicrobial activity against *Staphylococcus aureus*, with inhibition zones of 8.00, 11.00, and 11.66 mm at concentrations of 5, 10, and 20 mg/mL, respectively. More limited activity was observed against *Enterobacter hormaechei* and *Candida albicans*, while the effects against the remaining microorganisms were weak or close to baseline.

Conclusion: *S. chamaecyparissus* possesses distinctive botanical features and a chemically rich profile characterized by an artemisia ketone- and camphor-dominant essential oil and a chlorogenic acid- and quinic acid-rich methanolic extract. The preferential activity against *S. aureus* suggests selective anti-gram-positive potential. However, the limited spectrum of activity and the absence of minimum inhibitory and bactericidal concentration analyses restrict the direct interpretation of its antimicrobial efficacy. Further studies using quantitative antimicrobial methods and bioactivity-guided fractionation are warranted.

Keywords: Volatile constituents, phytochemicals, plant extracts, antimicrobial agents, plant anatomy

INTRODUCTION

Medicinal and aromatic plants continue to be a major source of structurally diverse natural products with well-recognized pharmaceutical potential. In particular, plant secondary metabolites such as terpenoids, phenolics, and alkaloids have attracted considerable attention because of their broad-

***Correspondence:** rumeysa.osmanlioglu@inonu.edu.tr, **ORCID-ID:** orcid.org/0000-0002-0243-3454

Received: 16.07.2026 **Accepted:** 25.08.2026 **Publication Date:** 01.09.2026

Cite this article as: Osmanlıoğlu Dağ ŞR, Daher A, Sağlam H, Arabacı T. Integrated botanical and phytochemical characterization of *Santolina chamaecyparissus* L. and evaluation of its antimicrobial activity. Turk J Pharm Sci. 2026;23(2):113-121

spectrum antimicrobial properties and their potential use as alternatives or adjuncts to conventional antibiotics in the era of antimicrobial resistance.[1,2] *Santolina chamaecyparissus* L. (Asteraceae), commonly known as cotton lavender, is a small evergreen aromatic shrub native to the Mediterranean region and widely cultivated throughout Europe and other areas.[3] Ethnobotanical reports indicate that *S. chamaecyparissus* and closely related *Santolina* taxa have long been used in Mediterranean folk medicine, particularly as vermifuge and emmenagogue preparations and for digestive, dermatological, and respiratory complaints.[4,5] Previous studies have mostly addressed its essential-oil composition, selected biological activities, or micromorphological features separately. Essential-oil studies have reported variable profiles containing compounds such as camphor, 1,8-cineole, borneol, β-pinene, and artemisia ketone, while biological studies have mainly focused on antioxidant, anti-inflammatory, antibacterial, antifungal, and cytotoxic activities. In particular, the essential oil of this species has demonstrated antibacterial and antifungal effects against selected clinically relevant microorganisms.[3,4,6,7] However, integrated pharmacognostic and phytochemical assessments combining morphological, anatomical, chemical, and antimicrobial evaluations remain limited. Additionally, significant variation in essential oil profiles among different plant populations and organs suggests that phytochemical expression may be influenced by structural and developmental factors.[4,6] Recent evidence has shown that *S. chamaecyparissus* possesses distinct secretory structures, including biseriate glandular trichomes and secretory ducts, which may play a direct role in the production and accumulation of bioactive metabolites.[8] Therefore, this study aimed to provide an integrated pharmacognostic and phytochemical evaluation of *S. chamaecyparissus* by characterizing its morphological and anatomical features, analyzing the volatile profile of its essential oil and the phenolic composition of its methanolic extract, and performing a preliminary screening of antimicrobial activity of the methanolic extract against selected bacterial and fungal strains.

MATERIALS AND METHODS

Plant material

Aerial parts of *S. chamaecyparissus* were collected during the flowering period on 11th June of 2025 from the Medical and Aromatic Plants Garden of the Faculty of Pharmacy, Inonu University, Malatya, Türkiye (Figure 1A). The taxonomic identity of the species was confirmed by Botanist Prof. Dr. Turan Arabacı, and a voucher specimen was deposited in the herbarium of Inonu University Faculty of Pharmacy under voucher number RO2501 (Figure 1B). The plant material was cleaned, shade-dried at room temperature, and powdered before further analyses.

Morphological and anatomical investigations

For morphological evaluation, dried aerial parts of *S. chamaecyparissus* were examined macroscopically using standard pharmacognostic criteria. Diagnostic characters were documented photographically and compared with previously published descriptions and the book of Flora of Turkey and the East Aegean Islands (Grierson).[9] For anatomical analysis, representative samples from stems and leaves were fixed in 70% ethanol and manually dissected. This workflow is consistent with routine plant histological approaches widely used in anatomical characterization and with previous anatomical work on *S. chamaecyparissus* and related taxa.[8] Photographs were taken using a Leica DM1000 light microscope equipped with a Leica DFC290 digital camera. For SEM examination, dried leaf pieces were mounted on stubs using double-sided adhesive tape and coated with gold using a BALTEC SCD-050 sputter coater. SEM observations of the leaf surface were then performed using a Leo Evo 40 scanning electron microscope at the Inonu University Scientific and Technological Research Center, Malatya, Türkiye.

Essential oil isolation

The powdered dried aerial parts (100 g) of *S. chamaecyparissus* were subjected to hydrodistillation for 3 h using a Clevenger-type apparatus. After completion of distillation, the obtained essential oil was collected and stored in sealed amber vials at 4 °C until analysis.

GC–MS/MS analysis of the essential oil

The volatile profile of the essential oil was analyzed at the Research Laboratory Application and Research Center of Iğdır University (Iğdır, Türkiye) using an Agilent Technologies 7000 GC–MS Triple Quad system coupled to a 7890 GC and 7693 autosamplers. Chromatographic separation was achieved on an HP-5ms capillary column [(5%-phenyl)-methylpolysiloxane, 30 m × 0.25 mm × 0.25 µm]. Helium was used as the carrier gas at a constant flow rate of 1 mL/min. The injection volume was 1 µL in split mode (50:1), using hexane as the solvent. The septum purge flow was set at 3 mL/min. The GC transfer line temperature was maintained at 250 °C, and the quadrupole temperature was set at 150 °C. The oven temperature program was as follows: initial temperature 60 °C, held for 4 min; increased at 4 °C/min to 220 °C; and held for 10 min, giving a total run time of

Figure 1. (A) General view of *Santolina chamaecyparissus*, (B) the herbarium specimen.

54 min. Mass spectrometric detection was performed with an inlet temperature of 250 °C and a scan range of 35–550 amu. Compound annotation was based on comparison of EI mass spectra with the NIST MS library and, where applicable, supported by comparison with literature retention index data commonly used in essential-oil GC–MS analysis.[10] No authentic standards were analyzed; therefore, compound identities should be regarded as putative/tentative annotations based primarily on EI-MS library matching supported, where available, by literature RI agreement.

Preparation of the extract

The powdered dried aerial parts of *S. chamaecyparissus* (30 g) were extracted with 90% methanol at a 1:10 (w/v) plant material-to-solvent ratio. Extraction was performed at room temperature under continuous magnetic stirring for 24 h and repeated three times. The combined filtrates were concentrated, and the solvent was completely removed under reduced pressure using a rotary evaporator. The resulting dry extract was stored at 4 °C until further use.

LC–MS/MS analysis of phenolic compounds

The LC–MS/MS analysis for phenolic antioxidant profiling of *S. chamaecyparissus* methanol extract (SME) was performed at the Atatürk University Eastern Anatolia High Technology Application and Research Center.[11] For analysis, the dried methanolic extract was dissolved at a concentration of 1 mg/mL in the extraction solvent. Accordingly, quantitative results were normalized to dry extract weight and expressed as µg/g of dry extract. Chromatographic analyses were carried out using an Agilent Technologies 1290 Infinity UPLC system (Palo Alto, CA, USA) equipped with an autosampler (Agilent 1260 Infinity G1329B ALS), a high-pressure binary pump (Agilent 1260 Infinity G1312B, 600 bar), a degasser (Agilent 1260 Infinity G4225A HIP), and a thermostatted column compartment (Agilent 1290 Infinity TCC G1316C). Separation of phenolic constituents was achieved on a Zorbax SB-C18 column (3.5 µm, 100 mm × 4.6 mm), maintained at 30 °C. The mobile phase consisted of water containing 0.1% formic acid and acetonitrile containing 0.1% formic acid, and elution was performed using a gradient program. Phenolic compounds were identified and quantified according to retention behavior and mass spectral data in comparison with reference standards and previously validated chromatographic conditions.

Antimicrobial activity

The methanolic extract of *S. chamaecyparissus (*SME) was subjected to preliminary antimicrobial screening against seven test microorganisms, including five bacteria—*Escherichia coli* ATCC 25922, *Pseudomonas aeruginosa* ATCC 27853, *S. aureus* ATCC 976, *Enterobacter hormaechei* ATCC 700323, and vancomycin-resistant *Enterococcus* (VRE) and two fungi, *Aspergillus* sp. and *Candida albicans* ATCC 14053. The concentrations of 5, 10, and 20 mg/mL were selected to provide a graded concentration range for preliminary screening and to allow assessment of concentration-related changes in inhibition-zone diameters. Mueller–Hinton agar (MHA) was used for bacterial assays, whereas potato dextrose agar was used for fungal assays. Use of MHA for bacterial susceptibility testing and agar-based screening methods for plant-derived substances is consistent with standard antimicrobial testing practice.[12,13] Before testing, stock cultures were reactivated, and microbial suspensions were adjusted to 0.5 McFarland turbidity. Then, 100 µL of each suspension was spread evenly onto the corresponding agar surface. Wells of 4 mm diameter were made aseptically in the inoculated agar using a sterile cork borer, and the test samples were introduced into the wells. Plates were subsequently incubated under appropriate conditions for each microorganism, and antimicrobial activity was evaluated by measuring the diameter of inhibition zones around the wells. The agar well diffusion assay, 0.5 McFarland inoculum standardization, and approximately 4 mm agar depth/well-based screening are all widely used in antimicrobial evaluation of plant extracts and essential oils.[12,13]

Statistical analysis

Antimicrobial assays were performed in triplicate, and inhibition zone diameters were expressed as mean ± standard deviation. For microorganisms showing measurable inhibition above baseline, differences among the three extract concentrations (5, 10, and 20 mg/mL) were analyzed using one-way analysis of variance (ANOVA), followed by Tukey's honestly significant difference post-hoc test for multiple comparisons. A p-value < 0.05 was considered statistically significant. Statistical analyses were performed using IBM SPSS Statistics for Windows, Version 26.0 (IBM Corp., Armonk, NY, USA).

Ethics committee approval

This study was conducted exclusively using plant material and did not involve humans, human data, human biological materials, or experimental animals. Therefore, ethics committee approval was not required.

Informed consent

Informed consent was not required because the study did not involve human participants or identifiable personal data.

RESULTS

Yields of essential oil and methanol extract

The hydrodistillation of the aerial parts of *S. chamaecyparissus* yielded a pale-yellow essential oil with a percentage yield of 0.46% (w/w). The methanolic extraction process, performed via maceration, resulted in a dry extract (SME) with a yield of 14.40% (w/w).

Morphological and anatomical characterization

The morphological evaluation of *S. chamaecyparissus* confirmed its characteristic appearance as a perennial, silvery-gray subshrub. The capitula was terminal, solitary, and discoid, with bright yellow tubular florets and no ray florets. The stem surface was densely tomentose, contributing to the silvery-gray appearance of the aerial parts (Figure 2A and B). Leaves collected from different stem nodes showed the characteristic segmented morphology of the species (Figure 3). Examination

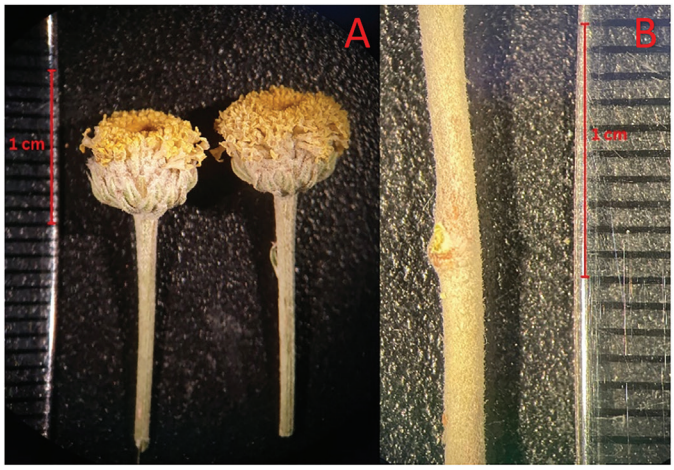

Figure 2. Morphological characteristics of *Santolina chamaecyparissus*: (A) discoid capitula and tubular flowers, (B) stem surface.

Figure 3. Morphological appearance of the leaves of *Santolina chamaecyparissus* from different nodes.

of the reproductive structures demonstrated tubular florets originating from both the peripheral and central regions of the capitulum. Longitudinal dissection of the florets revealed the ovary and corolla organization, while the mature cypselae lacked a pappus (Figure 4A–C). Scanning electron microscopy of the adaxial leaf surface revealed a densely pubescent surface (Figure 5). Higher-magnification observations demonstrated anomocytic stomata surrounded by densely interlaced non-glandular trichomes (Figure 6A and B). Detailed examination of the mature cypselae showed an oblong-obovoid shape, distinct longitudinal ribs, and the absence of a pappus (Figure 7A and B).

Anatomical examination of the stem revealed a typical eustelic organization. A well-developed collenchyma layer was located beneath the epidermis, and the vascular bundles contained clearly distinguishable primary and secondary xylem elements (Figure 8A–C). The leaf exhibited an isobilateral structure with multilayered palisade parenchyma on both surfaces. The midrib region contained a well-defined vascular system, and anomocytic stomata were observed in the epidermis. The leaves were amphistomatic and covered by a dense indumentum composed predominantly of non-glandular trichomes (Figure 9A–C).

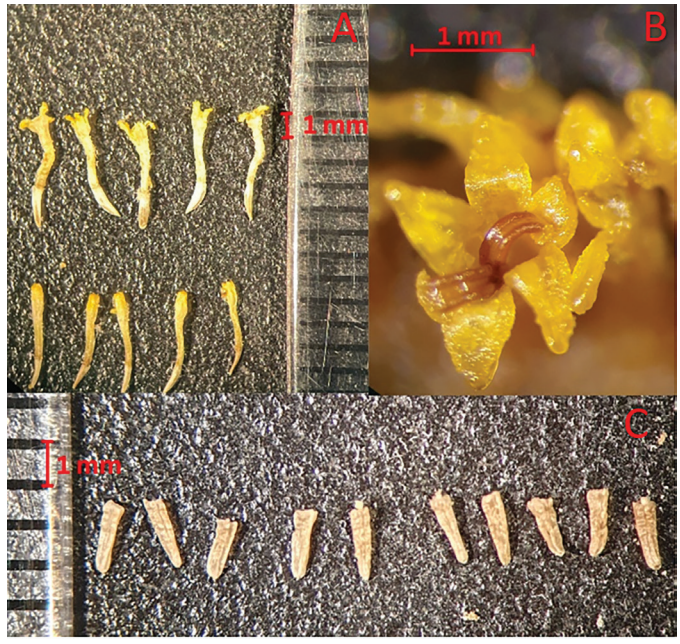

Figure 4. Reproductive morphology of *Santolina chamaecyparissus*: (A) tubular florets from the peripheral and central regions of the capitulum, (B) longitudinal dissection of a floret showing the ovary and corolla structure, (C) mature cypselae demonstrating the characteristic oblong shape and the absence of a pappus.

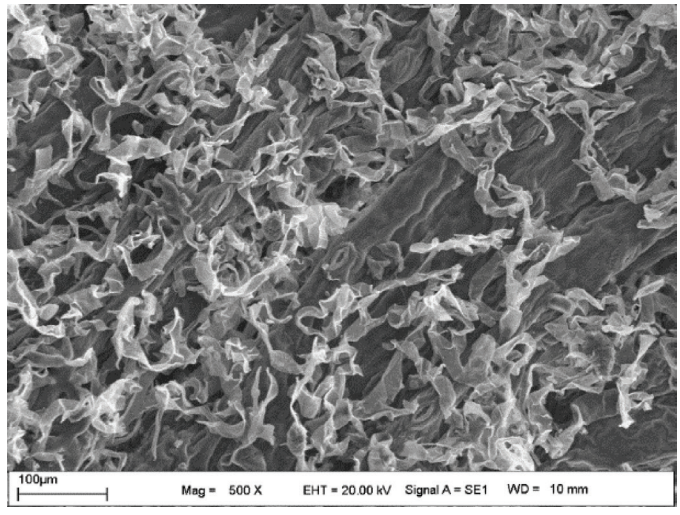

Figure 5. Scanning electron micrographs of the adaxial leaf surface of *Santolina chamaecyparissus*.

Phytochemical composition of the essential oil

The volatile profile of *S. chamaecyparissus* essential oil, analyzed by GC–MS/MS, led to the identification of 33 compounds, representing the majority of the total oil composition (Table 1). The essential oil was characterized by a high content of ketones and monoterpenoids. The major constituent was found to be artemisia ketone (55.96%), followed by camphor (20.84%). Other notable components included camphene (4.79%), benzylacetone (2.36%), and santolina triene (2.03%). The presence of these oxygenated monoterpenes defines the characteristic aromatic profile of the species.

LC–MS/MS analysis of phenolic compounds

The phenolic profile of the methanol extract (SME) was characterized using LC–MS/MS, focusing on antioxidant compounds (Table 2). A total of 35 phenolic compounds were screened. The analysis revealed that chlorogenic acid (6733.85 µg/g dry extract) and quinic acid (6521.37 µg/g dry extract) were the most abundant quantified compounds.

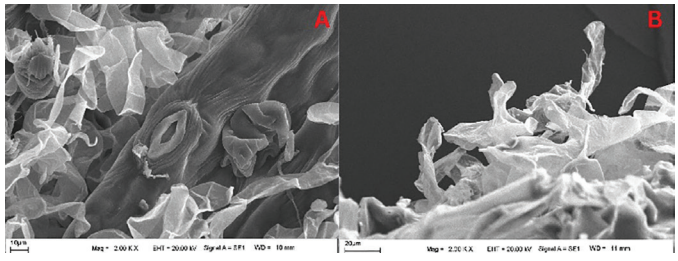

Figure 6. Scanning electron micrographs of the adaxial leaf surface of *Santolina chamaecyparissus*: (A) high-magnification view showing an anomocytic stoma, (B) dense indumentum consisting of interlaced non-glandular trichomes.

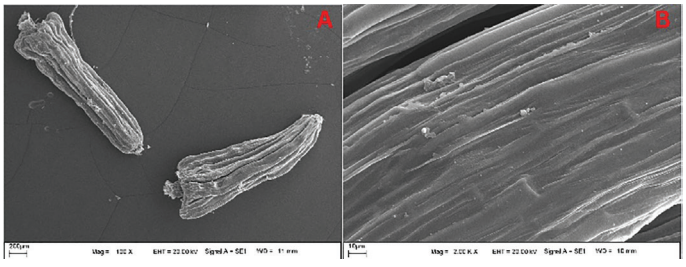

Figure 7. Detailed seed morphology of *Santolina chamaecyparissus*: (A) general view of mature cypselae, (B) close-up showing the oblong-obovoid shape, longitudinal ribs, and the distinct absence of a pappus.

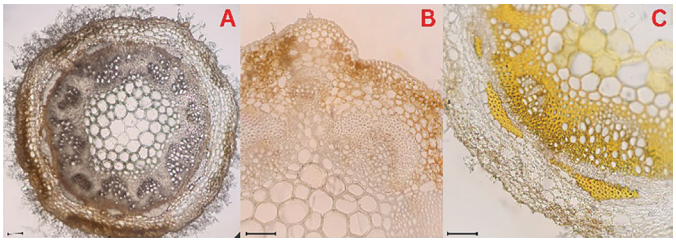

Figure 8. Anatomical structure of the *Santolina chamaecyparissus* stem (transverse section): (A) general view of the eustelic arrangement, (B) detailed view of the cortex and the supportive collenchyma layer beneath the epidermis, (C) vascular bundles showing primary and secondary xylem elements (scale bar 50 µm).

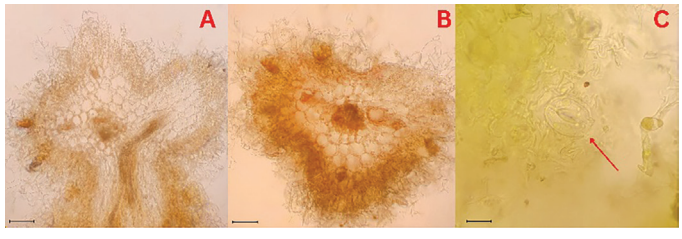

Figure 9. Leaf anatomy and micromorphology of *Santolina chamaecyparissus*: (A) transverse section illustrating the isobilateral mesophyll and multilayered palisade parenchyma, (B) magnified view of the midrib region with vascular tissues, (C) the anomocytic stomata (scale bar 50 µm for A,B; 25 µm for C).

Table 1. Chemical composition of the essential oil of *Santolina chamaecyparissus* L. analyzed by GC–MS/MS.

No	RT	RI (NIST Lib.)	Compound	%
1	7.92	908	Santolina triene	2.03
2	8.46	925	Tricyclene	0.25
3	8.56	926	2,5,5-trimethyl-1,3,6-heptatriene	0.27
4	8.85	929	1R-α-pinene	0.81
5	9.37	952	Camphene	4.79
6	9.77	962	Benzaldehyde	0.10
7	10.22	974	Sabinene	0.23
8	10.35	979	β-pinene	0.91
9	10.81	991	β-myrcene	0.47
10	10.84	994	2-methyl-2-bornene	0.30
11	11.10	998	Yomogi alcohol	1.99
12	12.06	1025	p-cymene	0.27
13	12.24	1031	β-phellandrene	1.75
14	12.64	1043	Lavender lactone	0.25
15	13.49	1062	Artemisia ketone	55.96
16	13.74	-	Not identified	0.22
17	14.21	1084	Artemisia alcohol	1.02
18	14.49	1095	α-pinene oxide	0.75
19	14.97	1107	Hotrienol	0.29
20	16.54	1145	Camphor	20.84
21	17.27	1167	Endo-borneol	0.75
22	17.92	1213	Myrtenol	0.50
23	18.40	1218	Benzylacetone	2.36
24	18.99	1228	Not identified	0.24
25	19.78	1236	2-butenoic acid, 3-methyl-, 3-methyl-2-butenyl ester	0.09
26	22.78	1331	Silphiperfol-5-ene	0.13
27	24.71	1396	Benzyanyl	0.16
28	27.70	1483	α-curcumene	0.19
29	28.36	1500	Pentadecane	0.26
30	30.03	1564	Not identified	0.17
31	30.75	1581	Caryophyllene oxide	0.11
32	32.71	1655	Bisabolol oxide II	0.54
33	33.45	1684	α-bisabolol	0.97

Note: Compound identification was based on comparison of EI mass spectra with the NIST MS library. Low-abundance peaks with similar library matches were reported as tentative annotations unless confirmed by authentic standards.

Table 2. Identification and quantification of phenolic compounds in the methanolic extract of *Santolina chamaecyparissus* using LC–MS/MS.

Compound	RT	Response	Concentration (µg/g dry extract)
Quinic acid	2.417	17169	6521.3748
Fumaric acid	3.971	92	33.0137
Gallic acid	5.519	26	ND
Pyrogallol	6.928	5	ND
Keracyanin chloride	10.393	21	11.8677
Cyanidin-3-o-glucoside	10.539	3	25.2668
Chlorogenic Acid	10.947	178257	6733.8453
Peonidin-3-o-glucoside	10.973	3	ND
Catechin	10.993	5	ND
4-OH-benzoic acid	11.406	213	ND
Caffeic acid	11.491	324	ND
Epicatechin	11.544	4	ND
Epigallocatechin gallate	11.611	6	ND
Vanillic acid	11.637	21	ND
Vitexin	11.699	11	ND
Hesperidin	11.726	1487	104.1124
Syringic acid	11.823	3	ND
Ellagic acid	11.934	4	ND
Naringin	12.060	113	ND
p-Coumaric acid	12.275	12	ND
Ferulic acid	12.461	5	ND
Rosmarinic acid	12.497	55	25.6033
Vanillin	12.551	15	45.0932
Taxifolin	12.600	137	ND
Myricetin	12.686	15	ND
Sinapic acid	12.808	6	ND
Resveratrol	12.924	4	ND
Luteolin	13.356	2980	<LOQ
Quercetin	13.427	20	ND
Apigenin	13.966	5109	<LOQ
Naringenin	13.994	55	ND
Isorhamnetin	14.180	393	ND
Chrysin	15.228	8	ND
Galangin	15.662	1	ND
Curcumin	16.033	2	ND

RT, retantion time; < LOQ, detected below the limit of quantification; ND, not detected.

Other detected phenolics included hesperidin (104.11 µg/g), vanillin (45.09 µg/g), fumaric acid (33.01 µg/g), rosmarinic acid (25.60 µg/g), and cyanidin-3-O-glucoside (25.27 µg/g). Several other flavonoids and phenolic acids, such as luteolin and apigenin, were detected but remained below the quantification limits in this specific extract.

Antimicrobial activity

The preliminary antimicrobial screening of the SME was evaluated against a panel of seven pathogenic microorganisms using the agar well diffusion method (Table 3). The largest inhibition zones were observed against *S. aureus*, with inhibition zones of 11.66 mm, 11 mm, and 8 mm at concentrations of 20 mg/mL, 10 mg/mL, and 5 mg/mL, respectively. Smaller inhibition zones were recorded against *E. hormaechei* (6.33 mm at 20 mg/mL). For the fungal strains, the extract showed activity against *C. albicans* (5.66 mm at 20 mg/mL), while its effect on *Aspergillus* sp. was equivalent to the minimum measurable zone (5 mm). The extract showed limited or baseline inhibition (5

Table 3. Preliminary agar well diffusion screening of *Santolina chamaecyparissus* methanolic extract against selected microorganisms.

Microorganism	20 mg/mL	10 mg/mL	5 mg/mL	NC	PC
Escherichia coli	5.00 ± 0.00	5.00 ± 0.00	5.00 ± 0.00	NI	17.66 ± 1.15
Pseudomonas aeruginosa	5.00 ± 0.00	5.00 ± 0.00	5.00 ± 0.00	NI	17.00 ± 1.00
Staphylococcus aureus	11.66 ± 0.58[a]	11.00 ± 1[ab]	8.00 ± 1.73[b]	NI	21.00 ± 1.00
VRE	5.00 ± 0.00	5.00 ± 0.00	5.00 ± 0.00	NI	15.33 ± 0.58
Enterobacter hormaechei	6.33 ± 0.58[a]	6.00 ± 0.00[a]	5.66 ± 0.58[a]	NI	17.00 ± 1.00
Candida albicans	5.66 ± 1.15[a]	5.00 ± 0.00[a]	5.00 ± 0.00[a]	NI	15.33 ± 0.58
***Aspergillus* sp.**	5.00 ± 0.00	5.00 ± 0.00	5.00 ± 0.00	NI	16.66 ± 0.58

PC, positive control; gentamicin 10 µg for bacteria and nystatin 100 IU for *Candida albicans;* NC, negative control; NI, no inhibition.
Different superscript letters within the same row indicate statistically significant differences among extract concentrations according to Tukey's HSD test ($p < 0.05$).

mm) against *E. coli*, *P. aeruginosa*, and VRE across the tested concentrations.

Among the microorganisms showing measurable inhibition, a significant concentration-dependent difference was observed only for *S. aureus* (one-way ANOVA, F = 7.923, p = 0.021). Tukey's post-hoc analysis showed that the inhibition zone at 20 mg/mL was significantly greater than that at 5 mg/mL (p = 0.023), whereas the differences between 20 and 10 mg/mL and between 10 and 5 mg/mL were not statistically significant. No significant differences among concentrations were observed for *E. hormaechei* ($p = 0.296$) or *C. albicans* ($p = 0.422$).

DISCUSSION

The present study provides an integrated pharmacognostic and phytochemical evaluation of *S. chamaecyparissus,* showing that its anatomical organization, volatile profile, polar phenolic composition, and antimicrobial behavior are closely interconnected. The anatomical findings indicate that *S. chamaecyparissus* exhibits a pronounced xeromorphic organization, characterized by its greyish-tomentose indumentum and specialized leaf morphology. These features align with the diagnostic descriptions in the Flora of Turkey, which identifies the species by its ± vermiform leaves with numerous oblong, obtuse segments, typically arranged in four ranks. In addition, the taxonomic complexity of the *S. chamaecyparissus* species complex has been emphasized in recent nomenclatural studies, supporting the importance of voucher-based identification and detailed morphological characterization in pharmacognostic investigations.[14] Such structural adaptations, particularly the amphistomatic leaf structure and dense non-glandular indumentum observed here, are consistent with adaptation to dry Mediterranean environments. In pharmacognostic terms, these traits are not only useful for species characterization, distinguishing it from related taxa by its homogamous, discoid capitula and 3–4-angular achenes as noted in regional floristic records,[9] but may also reflect structural strategies that support tolerance to high irradiance and water limitation. This interpretation is in line with previous reports emphasizing the importance of protective and secretory structures in aromatic Asteraceae and in *S. chamaecyparissus* in particular.[8] In aromatic Mediterranean plants, such protective and secretory structures may also contribute to the production and retention of volatile metabolites, which have been proposed to participate in ecological responses to high temperature, intense solar radiation, and other environmental stresses. Accordingly, the anatomical profile observed here provides a relevant structural background for understanding the phytochemical richness of the species.

The volatile profile obtained in the present study further supports this interpretation. The essential oil was clearly dominated by oxygenated monoterpenes, with artemisia ketone (55.96%) and camphor (20.84%) as the principal constituents. This general pattern agrees with previous reports indicating that *S. chamaecyparissus* often produces oils rich in oxygenated monoterpenes, although the relative abundance of the major constituents is highly variable among populations, plant organs, developmental stages, and extraction procedures.[3,4,6,15,16] For example, Indian material analyzed by Garg et al.[15] contained artemisia ketone as the main component, but with lower abundance (approximately 32%), together with substantial levels of 1,8-cineole and myrcene, indicating a related but not identical profile to the present sample. Likewise, cultivated and wild Spanish materials examined by Pérez–Alonso and Velasco–Negueruela[16] showed marked interpopulation heterogeneity and supported the existence of chemically distinct groups within the taxon. More recent work from Serbia also confirmed a chemically variable oil, again with artemisia ketone among the dominant components but accompanied by a different sesquiterpene background.[17] Taken together, these comparisons indicate that the present material can reasonably be interpreted as an artemisia ketone/camphor-dominant chemotype within the known chemical plasticity of the species rather than as an anomalous population.

This variability is also important from a pharmacognostic standpoint. In *S. chamaecyparissus*, literature does not support a single invariant oil profile; instead, it points to a species complex with substantial phytochemical breadth.[3,4,6] Such variation is not unexpected in aromatic plants, where environmental factors, ontogeny, plant part selection, and extraction methodology can alter the balance between monoterpenes and sesquiterpenes.

The non-volatile profile of the methanolic extract adds a second, complementary phytochemical layer to this picture. In

the present study, chlorogenic acid and quinic acid were by far the most abundant quantified constituents, while hesperidin, rosmarinic acid, vanillin, and cyanidin-3-O-glucoside occurred at much lower levels. This pattern suggests that the methanol extract is enriched primarily in polar phenolic acids rather than being dominated by flavonoids alone. Earlier studies on the polar chemistry of *S. chamaecyparissus* likewise showed that the species contains a chemically diverse phenolic fraction, including luteolin derivatives, lonicerin, apigenin glycosides, and other unusual polar constituents, with the butanolic fraction displaying markedly higher total phenolic content and stronger antioxidant activity than the chloroform fraction.[18] By contrast, a recent ethanolic extract study identified ferulic acid and p-coumaric acid as the dominant quantified phenolics.[19] The difference from our results likely reflects differences in extraction solvent, plant material, and analytical target panel rather than contradiction. In other words, the available evidence consistently supports *S. chamaecyparissus* as a phenolic-rich species, but the exact dominant polar metabolites appear to be method- and sample-dependent. The volatile and non-volatile profiles should be interpreted as distinct phytochemical fractions. The essential oil was characterized by artemisia ketone and camphor, whereas the methanolic extract was dominated by chlorogenic acid and quinic acid and contained additional minor phenolic constituents. Because only the methanolic extract was subjected to antimicrobial screening, no inference regarding the antimicrobial contribution of artemisia ketone, camphor, or other essential-oil constituents can be made from the present data. Oxygenated monoterpenes such as camphor are frequently linked to membrane-disruptive effects, whereas chlorogenic-acid-rich polar extracts may contribute to antioxidant and auxiliary antimicrobial actions.[12,13,18,19] Nevertheless, a careful distinction should be maintained between the essential oil and the methanol extract. In the present study, the antimicrobial assay was performed with the methanol extract, not with the isolated essential oil. Therefore, although the essential-oil profile strengthens the phytochemical importance of the species, it should not be used as direct proof of the activity observed in the agar well diffusion test. The observed inhibition-zone responses may reflect contributions from multiple constituents of the methanolic extract; however, the contribution of individual compounds and potential interactions among them were not investigated in the present study.

The agar well diffusion findings should be interpreted as preliminary screening data rather than as quantitative evidence of antimicrobial potency. Within these experimental conditions, the methanol extract produced its largest inhibition zones against *S. aureus*, while the effects against *E. coli*, *P. aeruginosa*, VRE, and *Aspergillus* sp. were weak or close to baseline, and only modest inhibition was recorded for *Enterobacter hormaechei* and *C. albicans*. This trend is biologically plausible and agrees with the broader literature showing that plant-derived phytochemicals often act more efficiently against gram-positive bacteria than against gram-negative bacteria, partly because the outer membrane of gram-negative organisms forms an additional permeability barrier.[2,12,13] The preferential susceptibility of *S. aureus* in the present study is therefore reasonable and suggests a preferential inhibition pattern toward *S. aureus* under the present screening conditions; however, this observation requires confirmation by quantitative broth dilution methods. At the same time, comparison with previous *Santolina* studies shows that the magnitude and spectrum of activity can differ substantially. Djeddi et al.[6] reported strong activity of the essential oil from Algerian material, especially against *Klebsiella pneumoniae* and *C. albicans*, together with camphor/cubenol-rich chemistry and anatomical evidence for oil localization in both endogenous and exogenous secretory sites. Other reports have also described substantial antimicrobial or antifungal effects for *S. chamaecyparissus* essential oils, including activity against *Candida* spp. and other microorganisms.[4,7] Our results are clearly more moderate, but this difference is not surprising because the tested matrix here was a methanolic extract rather than the essential oil, and the applied bioassay was agar well diffusion rather than a broth microdilution design. Accordingly, the lower zones observed in our study should not be interpreted as evidence that the species is weakly bioactive overall; rather, they indicate that under the present extraction and assay conditions, the polar extract expresses selective and limited antibacterial activity, with its clearest effect directed toward *S. aureus*. This distinction between matrices is especially important for future work. The literature suggests that *S. chamaecyparissus* can yield biologically active preparations in both volatile and polar fractions, but the responsible constituents are not necessarily the same. Essential-oil studies emphasize monoterpenes and sesquiterpenes, whereas polar-extract studies highlight phenolic acids, flavonoids, and glycosides.[3,4,6,7,17-19] Our study contributes to this picture by showing, in a single voucher-identified sample, that an artemisia ketone/camphor-rich essential oil coexists with a chlorogenic acid/quinic acid-rich methanolic fraction. That integrated chemical characterization is valuable because it broadens the pharmaceutical-botanical profile of the species beyond the essential-oil literature that has historically dominated the field.

Study limitations

Several limitations, however, should be explicitly acknowledged. First, because antimicrobial testing was carried out only with the methanol extract, no direct correlation can yet be made between the essential-oil constituents and the observed inhibition zones. Second, antimicrobial testing was limited to agar well diffusion, which is suitable for preliminary screening but does not provide quantitative MIC or MBC values. Consequently, the present inhibition-zone findings cannot establish the antimicrobial potency, bacteriostatic, or bactericidal efficacy of the methanolic extract and require confirmation using standardized broth microdilution methods. Finally, although chlorogenic acid and quinic acid were the major quantified phenolics, the observed activity may reflect contributions from multiple constituents; however, potential additive or synergistic interactions were not investigated in the present study.

CONCLUSION

Overall, the present findings strengthen the pharmaceutical-botanical relevance of *S. chamaecyparissus*. The species examined here combines xeromorphic structural adaptation with a chemically layered metabolite profile, consisting of an essential oil dominated by artemisia ketone and camphor and a methanolic extract dominated by chlorogenic and quinic acids. In the preliminary agar well diffusion screening, the methanolic extract produced its largest inhibition zones against *S. aureus*; however, this finding should be considered exploratory and does not establish antimicrobial potency. Quantitative MIC/MBC testing is required before definitive conclusions regarding antimicrobial efficacy can be drawn. Future work should therefore focus on MIC/MBC-based antimicrobial testing, bioactivity-guided fractionation of the methanol extract, separate testing of the essential oil, and direct evaluation of isolated major constituents and defined combinations in order to clarify which fraction best explains the biological potential of this species.

Ethics

Ethics Committee Approval: This study was conducted exclusively using plant material and did not involve humans, human data, human biological materials, or experimental animals. Therefore, ethics committee approval was not required.

Informed Consent: Informed consent was not required because the study did not involve human participants or identifiable personal data.

Footnotes

Authorship Contributions

Concept: Ş.R.O.D., Design: Ş.R.O.D., Data Collection or Processing: Ş.R.O.D., A.D., Analysis or Interpretation: Ş.R.O.D., H.S., Literature Search: Ş.R.O.D., A.D., Writing: Ş.R.O.D., A.D., H.S., T.A.

Conflict of Interest: The authors declare no conflicts of interest.

Financial Disclosure: The authors declared that this study received no financial support.

REFERENCES

1. Fik-Jaskółka M, Mittova V, Motsonelidze C, Vakhania M, Vicidomini C, Roviello GN. Antimicrobial metabolites of Caucasian medicinal plants as alternatives to antibiotics. Antibiotics (Basel). 2024;13:487.
2. Shin J, Prabhakaran VS, Kim KS. The multi-faceted potential of plant-derived metabolites as antimicrobial agents against multidrug-resistant pathogens. Microb Pathog. 2018;116:209-214.
3. Aati HY, Sarawi W, Attia H, Ghazwani R, Aldmaine L. Exploring the phytochemical profile and therapeutic potential of Saudi native *Santolina chamaecyparissus* L. essential oil. Pharmaceutics. 2025;17:830.
4. Bel Hadj Salah-Fatnassi K, Hassayoun F, Cheraif I, Khan S, Jannet HB, Hammami M, Aouni M, Harzallah-Skhiri F. Chemical composition, antibacterial and antifungal activities of flowerhead and root essential oils of *Santolina chamaecyparissus* L., growing wild in Tunisia. Saudi J Biol Sci. 2017;24:875-882.
5. Cavero RY, Akerreta S, Calvo MI. Pharmaceutical ethnobotany in the middle Navarra (Iberian Peninsula). J Ethnopharmacol. 2011;137:844-855.
6. Djeddi S, Djebile K, Hadjbourega G, Achour Z, Argyropoulou C, Skaltsa H. In vitro antimicrobial properties and chemical composition of *Santolina chamaecyparissus* essential oil from Algeria. Nat Prod Commun. 2012;7:937-940.
7. Suresh B, Sriram S, Dhanaraj SA, Elango K, Chinnaswamy K. Anticandidal activity of *Santolina chamaecyparissus* volatile oil. J Ethnopharmacol. 1997;55:151-159.
8. Giuliani C, Milani F, Falsini S, Spada A, Bruschi P, Papini A, Santagostini L, Bottoni M, Fico G. Secretory structures and essential oil composition in *Santolina chamaecyparissus* L. cultivated in Northern Italy. Horticulturae. 2025;11:1184.
9. Grierson AJC. Santolina. In: Davis PH, editor. Flora of Turkey and the East Aegean Islands. Vol. 5. Edinburgh: Edinburgh University Press; 1975. p. 252.
10. Babushok VI, Linstrom PJ, Zenkevich IG. Retention indices for frequently reported compounds of plant essential oils. J Phys Chem Ref Data. 2011;40:043101.
11. Can H, Güven L, Demirkaya Miloğlu F, Abd El-Aty AM. Development and validation of a UHPLC-ESI-MS/MS method for the simultaneous determination of organic acids and phenolic compounds in *Filipendula vulgaris, Polygonum divaricatum, Hypericum linarioides*, and *Rheum ribes*. Microchem J. 2024;201:110683.
12. Angane M, Swift S, Huang K, Butts CA, Quek SY. Essential oils and their major components: an updated review on antimicrobial activities, mechanism of action and their potential application in the food industry. Foods. 2022;11:464.
13. Noui Mehidi I, Ait Ouazzou A, Tachoua W, Hosni K. Investigating the antimicrobial properties of essential oil constituents and their mode of action. Molecules. 2024;29:4119.
14. Giacò A, Astuti G, Peruzzi L. Typification and nomenclature of the names in the *Santolina chamaecyparissus* species complex (Asteraceae). Taxon. 2021;70:189-201.
15. Garg SN, Gupta D, Mehta VK, Kumar S. Volatile constituents of the essential oil of *Santolina chamaecyparissus* Linn. from the southern hills of India. J Essent Oil Res. 2001;13:234-235.
16. Pérez-Alonso MJ, Velasco-Negueruela A. Essential oil components of *Santolina chamaecyparissus* L. Flavour Fragr J. 1992;7:37-41.
17. Lončar B, Cvetković M, Rat M, Stanković Jeremić J, Filipović J, Pezo L, Aćimović M. Chemical composition, chemometric analysis, and sensory profile of *Santolina chamaecyparissus* L. (Asteraceae) essential oil: insights from a case study in Serbia and literature-based review. Separations. 2025;12:115.
18. Labed F, Masullo M, Cerulli A, Benayache F, Benayache S, Piacente S. Chemical constituents of the aerial parts of *Santolina chamaecyparissus* and evaluation of their antioxidant activity. Nat Prod Commun. 2017;12:1605-1608.
19. Radovanović K, Vukić D, Kladar N, Hitl M, Gavarić N, Aćimović M. Chemical analysis and biological potential of cotton lavender ethanolic extract (*Santolina chamaecyparissus* L., Asteraceae). Horticulturae. 2024;10:1247.